Rolle des NF-kappaB Signalweges in zellulärer Seneszenz und Therapie-Effektivität

Dissertation

zur Erlangung des akademischen Grades

doctor rerum naturalium
(Dr. rer. nat.)

im Fach Biologie
eingereicht an der

Mathematisch-Naturwissenschaftlichen Fakultät I
der Humboldt-Universität zu Berlin

von

M. Sc. Hua Jing

Präsident der Humboldt-Universität zu Berlin
Prof. Dr. Jan-Hendrik Olbertz

Dekan der Mathematisch-Naturwissenschaftlichen Fakultät I
Prof. Dr. Stefan Hecht

Gutachter: 1. Prof. Dr. rer. nat. Achim Leutz
2. Prof. Dr. med. Clemens A. Schmitt
3. Prof. Dr. rer. nat. Claus Scheidereit

Tag der mündlichen Prüfung: 8. Mai 2013

Abstract

Cellular senescence is a terminal cell-cycle arrest program that is executed in response to cellular stresses, such as activated oncogenes or DNA-damaging anti-cancer chemotherapy, where it serves as a tumor-suppressive mechanism or contributes to treatment outcome, respectively. Recently, transcription factor NF-kappaB which has long been linked to cancer development primarily through its oncogenic functions, has been postulated to participate in a senescence-associated and possibly senescence-reinforcing cytokine response, thereby suggesting a tumor-restraining role for NF-kappaB.

The aim of my PhD project was to understand the role of the NF-kappaB pathway in senescence and cancer treatment outcome. In this thesis, I show markedly elevated NF-kappaB activity upon therapy-induced senescence (TIS), associated with strong upregulation of NF-kappaB-controlled cytokines. TIS is associated with and depends on hyper-activated NF-kappaB signaling. By characterization and genetic engineering of primary mouse lymphomas according to distinct NF-kappaB-related oncogenic networks reminiscent of diffuse large B-cell lymphoma (DLBCL) subtypes, Bcl2-overexpressing germinal center B-cell-like (GCB) DLBCL were identified as a clinically relevant subgroup with significantly superior outcome when NF-kappaB is hyperactive.

These results demonstrate the context-dependent role of NF-kappaB signaling in cancer therapy and unveil oncogenic scenarios in which NF-kappaB hyperactivity unexpectedly accounts for superior long-term outcome to therapy. This finding has significant ramifications for future clinical trials that aim at inhibiting NF-kappaB activity based on the assumption of its detrimental impact on treatment outcome.

Keywords: NF-kappaB, senescence, cancer therapy, lymphoma, mouse models, DLBCL

Zusammenfassung

Zelluläre Seneszenz beschreibt einen terminalen Zellzyklus-Arrest. Nach zellulärem Stress u. a. durch aktivierte Onkogene oder DNA-schädigende Chemotherapie wird Seneszenz induziert und kann so zur Tumorsuppression bzw. zum Behandlungserfolg beitragen. Vor kurzem wurde gezeigt, dass der Transkriptionsfaktor NF-kappaB – welcher bisher vor allem durch seine onkogenen Funktionen mit Krebs in Verbindung gebracht wurde - bei der Seneszenz-assoziierten Zytokinausschüttung mitwirkt und den seneszenzten Phänotyp möglicherweise sogar verstärkt, wodurch NF-kappaB potentiell eine tumorsuppressive Rolle zukäme.

Ziel dieser Arbeit ist die Untersuchung des NF-kappaB-Signalweges in Seneszenz und Therapie. In der vorliegenden Arbeit zeige ich die deutliche Aktivierung von NF-kappaB nach Therapie-induzierter Seneszenz (therapy-induced senescence, TIS) und erhöhte Expression NF-kappaB-regulierter Zytokine. TIS ist vor allem in vivo mit starker Aktivität des NF-kappaB-Signalweges assoziiert und von selbiger abhängig. Primäre Eμ-myc-transgene Mauslymphome wurden nach ihrer endogenen NF-kappaB-Aktivität klassifiziert bzw. mit inhibierenden und aktivierenden NF-kappaB-Konstrukten modifiziert, welche auch in diffusen großzelligen B-Zell Lymphomen (diffuse large B-cell lymphoma, DLBCL) als natürlich vorkommende Mutationen gefunden wurden. Über einen neuartigen „Cross-Species“-Vergleich wurden Bcl2-hochexprimierende Keimzentrums-B-Zell-DLBCL (germinal center B-cell type, GCB) als klinisch relevante Gruppe identifiziert, welche nach NF-kappaB-Hyperaktivierung signifikant besser auf Therapie ansprach.

Diese Ergebnisse zeigen eine kontextspezifische, d. h. von „onkogenen Netzwerken“ abhängige Rolle des NF-kappaB Signalweges unter Chemotherapie. Diese Information könnte für künftige klinische Studien bedeutsam sein, da sie Bedingungen aufzeigt, unter denen NF-kappaB als Vermittler einer erwünschten Therapie-induzierten Seneszenzantwort eher nicht inhibiert werden sollte.

Schlagwörter: NF-kappaB, Seneszenz, Krebstherapie, Lymphome, Mausmodelle, DLBCL

Table of contents

1 Introduction

The nuclear factor κB (NF-κB) transcriptionally controls a large set of target genes that play important roles in cell survival, inflammation and immune recognition (Bours et al. 2000; Karin et al. 2002; Baeuerle et al. 1994). Aggressive B-cell lymphomas, among other tumor entities, frequently exhibit NF-κB-activating mutations, which are pro-oncogenic by nature, since their targeted inactivation results in selective toxicity to the tumor cells (Shaffer et al. 2012). Contrasting the tumor-promoting pro-survival and pro-inflammatory roles of NF-κB signaling, recently NF-κB has been postulated to participate in a senescence-associated and possibly senescence-reinforcing cytokine response, thereby suggesting a tumor-restraining role for NF-κB (Acosta et al. 2008; Kuilman et al. 2008). This thesis focuses on the function of NF-κB in cellular senescence and lymphoma treatment outcome. Therefore, the NF-κB pathway, cellular senescence, the classification of diffuse large B-cell lymphoma and the Eμ-*myc* mouse lymphoma model will be discussed in the introduction part as important background information.

1.1 The NF-κB signaling pathway

Nuclear factor κB (NF-κB) was described for the first time in 1986 as a nuclear protein binding to the kappa immunoglobulin-light chain enhancer in B cells (Sen et al. 1986). Subsequent studies revealed that NF-κB activity is induced in most cell types in response to a wide variety of stimuli, with major roles in cell survival, inflammation and differentiation. In mammalian cells, there are five NF-κB family members, RelA (p65), RelB, c-Rel, p50/p105 (NF-κB1) and p52/p100 (NF-κB2). NF-κB1 and NF-κB2 are synthesized as large precursors, p105 and p100, that are post-translationally processed to DNA-binding subunits p50 and p52, respectively. All NF-κB family members share a highly conserved Rel homology domain (RHD) that is responsible for DNA binding, dimerization, and interaction with a family of inhibitory proteins

known as inhibitors of NF-κB (IκBs) (Fig. 1).

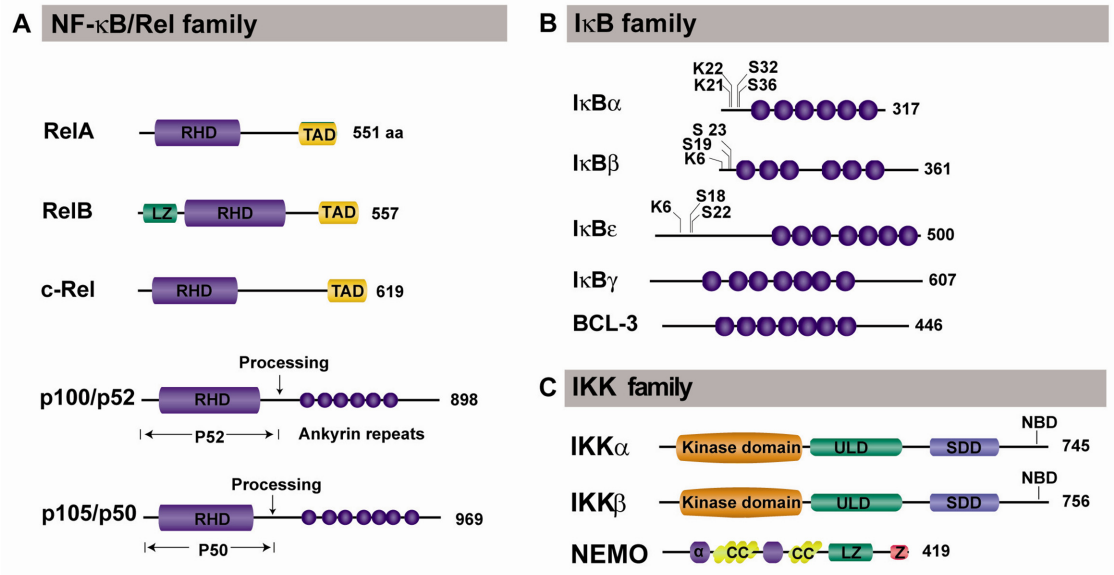

Figure 1: The mammalian members of the NF-κB, IκB and IKK families. (*A*) NF-κB subunits. NF-κB transcription factors share a highly conserved amino-terminal Rel homology domain (RHD), which is responsible for dimerization, nuclear translocation, DNA binding, and interaction with inhibitory IκB proteins. RelA, RelB, and c-Rel additionally possess a carboxy-terminal transactivation domain (TAD) that initiates transcription from NF-κB-binding sites in target genes. The ankyrin repeats containing NF-κB1 and NF-κB2 precursor proteins p105 and p100 can be proteolytically processed to p50 and p52. (*B*) IκB proteins. The IκB proteins are characterized by the presence of 6 or 7 ankyrin repeats to mediate protein-protein interactions. The ankyrin repeat domains bind to regions containing the nuclear localization sequence of NF-κB proteins and are important for the retention of NF-κB in the cytoplasm. Phosphorylation and ubiquitination sites on IκB proteins are indicated. (*C*) IKK proteins. The IKK complex contains the catalytic kinase subunits IKKα and IKKβ, as well as a regulatory subunit IKKγ (NEMO). IKKα and IKKβ contain the kinase domain, a ubiquitin-like domain (ULD) and α-helical scaffold/dimerization domain (SDD). The catalytic subunits interact through their NEMO-binding domain (NBD) with IKKγ, which contains a coiled coil (CC) domain and a leucine zipper (LZ).

NF-κB family members form homo- or heterodimeric complexes, which stay in the

cytoplasm of unstimulated or resting cells in association with IκBs. NF-κB signaling is generally considered to be activated through either the classical or alternative pathway (Bonizzi et al. 2004). In the classical (or canonical) pathway, upon stimulation by proinflammatory cytokines, such as the tumor necrosis factor α (TNFα), signaling leads to the activation of the IκB kinase (IKK) complex. The activated IKK complex, predominantly acting through IKKβ in an IKKγ-dependent manner, catalyzes phosphorylation of IκBs (at sites equivalent to Ser32 and Ser36 of IκBα), followed by polyubiquitination and subsequent degradation by the 26S proteasome. The released NF-κB dimers (in this pathway, most commonly the p50-RelA dimer) translocate to the nucleus, bind DNA and activate gene transcription. The alternative (or non-canonical) pathway is strictly dependent on IKKα. Activated IKKα phosphorylates p100 at two C-terminal sites. Phosphorylation of p100 leads to its ubiquitination and proteasomal processing to p52, creating transcriptionally competent NF-κB p52/RelB complexes that translocate to the nucleus and induce target gene expression (Fig. 2).

A wide array of stimuli, including inflammatory cytokines, bacterial and viral products, results in NF-κB activation by the classical pathway. Beside these, NF-κB also responds to genotoxic agents that cause damage to nuclear DNA. Whereas a majority of the known inducers of classical NF-κB activity function exclusively by transducing cell surface and/or cytoplasmic signals to the cytoplasmic IKKβ:NEMO complexes, the action site of genotoxic agents is located in the nucleus. Due to the spatial separation between the initiating event (DNA damage in the nucleus) and the signal target (inactive NF-κB in the cytoplasm), the concept of a nuclear-to-cytoplasmic NF-κB signaling pathway was proposed; it is now clear that such signaling pathways may be induced by multiple distinct genotoxic agents, resulting in the activation of a cytoplasmic IKK complex, and translocation of NF-κB into the nucleus to modulate the expression of a subset of genes. An example is a pathway that involves the DNA damage-responsive kinase ataxia telangiectasia mutated (ATM), PARP-1 and nuclear IKK (Wu et al. 2006; Stilmann et al. 2009; Hinz et al. 2010) (Fig.2).

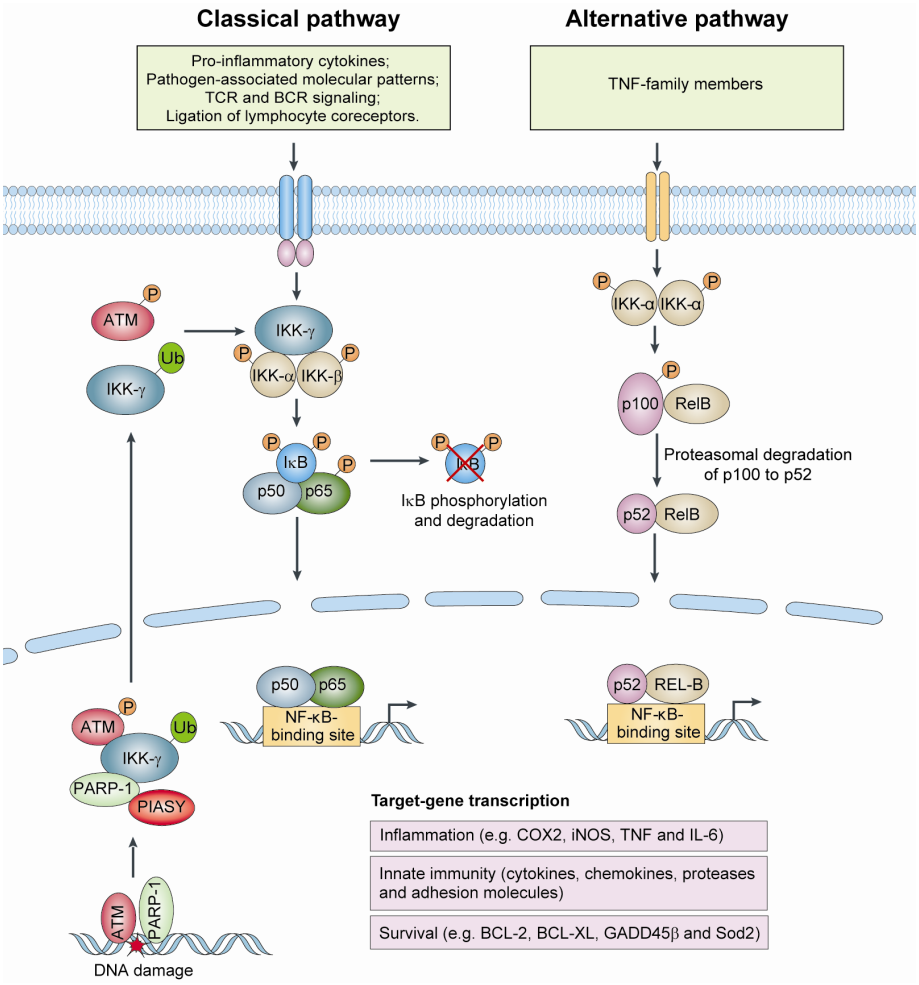

Figure 2: Classical (canonical) and alternative (non-canonical) NF-κB signaling pathways. NF-κB is activated by pro-inflammatory cytokines and DNA damage (leading to IKK-γ activation *via* ATM and PARP-1) and then induces inflammation-, immune- and survival-related target gene transcription upon nuclear translocation of the p50/Rel-A NF-κB dimers in the canonical and the p52/RelB subunits in the alternative pathway (adapted from Karin et al. 2005).

1.2 NF-κB in cancer biology

NF-κB controls gene expression by binding to discrete DNA sequences in promoters and enhancers, thereby orchestrating a plethora of biological functions, including apoptosis, cell adhesion, cellular stress response, inflammation and immunity. Since their discovery, NF-κB transcription factors have been suspected to be involved in cancer development because of their kinship with the v-Rel oncogene product. The

constitutive activation of NF-κB was then observed in different kinds of cancer, including lymphoma, leukemia, breast, colon, liver, pancreas, prostate, and ovarian cancers. Moreover, constitutive activation of NF-κB is associated with recurrence of cancer, poor survival, tumor progression, aggressiveness, and chemoresistance (Arkan et al. 2011; Prasad et al. 2010; Basseres et al. 2006). However, the relationship between NF-κB and cancer is not simple and cannot be reduced to one grand theory. There are also studies that found NF-κB transcription factors or upstream activators rather to act as tumor suppressors (Ben-Neriah et al. 2011), as reviewed in the following (Fig. 3). Given the context dependency of NF-κB's functions, the complexity of NF-κB-governed biological responses, the inducibility of many of these responses by both oncogenes and chemotherapeutic agents, NF-κB effector functions other than anti-apoptosis are likely to impact on treatment efficacy.

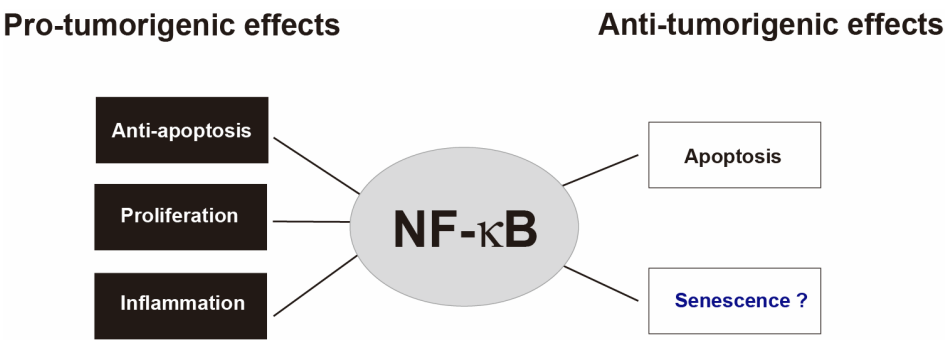

Figure 3: Pro- and anti-cancer roles of NF-κB. The double-edged impact of NF-κB on cancer development underscoring the complexity and potential context dependency of NF-κB network-mediated effector functions. Note that the involvement of NF-κB in some biological responses, like cellular senescence, might be one of the explanations for NF-κB's anti-cancer effect.

1.2.1 Pro-cancer roles of NF-κB

NF-κB controls oncogenic functions that suppress apoptosis or that promote tumor growth and survival. Mutations in genes encoding NF-κB subunits or IκB proteins were identified in a variety of hematological malignancies (Neri et al. 1991; Franzoso

et al. 1992; Compagno et al. 2009). There are now a number of lymphoid malignancies known, where constitutive NF-κB has been implicated as an essential oncogenic lesion. This was first discovered for Hodgkin's lymphoma (Bargou et al. 1996, 1997; Krappmann et al. 1999; Emmerich et al. 1999). Mutations of multiple genes, including IKK, c-Rel, A20, CARD11, Malt1-Bcl10, CD79-ITAM and Myd88, cause deregulation of NF-κB pathway in human lymphomas (Zhou et al, 2004; Ngo et al, 2011; Rosenwald et al. 2001; Sun et al, 2004).

Activating mutations in CARD11 (which encodes Carma-1) have been detected in activated B cell–like diffuse large B cell lymphoma (DLBCL, for more detail, see 2.4). Such mutations generate constitutively active Carma-1 that associates with the Bcl-10–MALT1 complex without antigenic stimulation, which results in persistent activation of NF-κB (Ngo et al. 2006; Lenz et al. 2008a; Staudt et al. 2010). A20 a negative regulator of the NF-κB pathway, prevents excessive activation of NF-κB in response to a variety of external stimuli (Wertz et al. 2004; Heyninck et al. 2005), and is frequently inactivated by somatic mutations and/or deletions in B-cell lymphomas, indicating that uncontrolled signaling of NF-κB caused by loss of A20 function is involved in the pathogenesis of subsets of B-cell lymphomas. Multiple myeloma is also a lymphoid malignancy associated with NF-κB activation. Although no mutations in NF-κB or IκB encoding genes have been discovered in this disease, extensive genetic analysis of primary tumors and multiple myeloma cell lines have revealed a number of mutations in genes encoding upstream signaling molecules that lead to stabilization and accumulation of the NF-κB inducing kinase (NIK) (Annunziata et al. 2007; Keats et al. 2007).

Although oncogenic mutations in NF-κB signal mediators appear to be rare in solid tumors, oncogenic signaling may enhance NF-κB activity in the absence of mutations, as inflammation-associated NF-κB-driven cytokine production promotes carcinogenesis in a noncell- autonomous fashion (Staudt et al 2010; Ben et al. 2011). Accordingly, mouse models demonstrated an oncogenic role for NF-κB in the

development of lymphomas and solid tumors (Basseres et al. 2010; Calado et al. 2010; Yang et al. 2010).

In addition, the number of tumors with activated nuclear NF-κB is much larger than the subfraction of malignancies with confirmed mutations in NF-κB- or IκB-encoding genes. Such observations led to the proposal that some of the NF-κB activation seen in cancer is due to mutations that affect components of signaling pathways that activate NF-κB or is the result of exposure to inflammatory cytokines in the tumor microenvironment.

Production of the cytokines by immune cells that activate the NF-κB pathway in pre-malignant cells to induce genes that stimulate cell proliferation and survival is a major tumor-promoting mechanism (Grivennikov et al. 2010). For example, TNFα and IL-1 secreted by the environmental cells were shown to act on premalignant cells where they activated NF-κB. NF-κB activation further induced expression of genes involved in blockade of apoptosis, promotion of proliferation and angiogenesis, mechanisms collectively enhancing malignant properties (Popivanova et al. 2008; Tu et al. 2008).

The NF-κB pathway also correlates with chemoresistance in cancer treatment. Activation of NF-κB occurs in response to DNA damage, the mode by which most conventional chemotherapeutic agents exert their anti-cancer activity. Activated NF-κB binds to specific DNA sequences in target genes. Among these, a number of NF-κB target genes, including bcl-2 (Catz et al. 2001), bcl-xL (Tamatani et al. 1999), COX-2 (Yamamoto et al. 1995), cyclin D1 (Guttridge et al. 1999), survivin (Zhu et al. 2001), and XIAP (Stehlik et al. 1998) mediate the process of chemoresistance and radioresistance in a wide variety of tumor cells. In activated B-cell-like (ABC) subtypes of diffuse large-B-cell lymphoma (DLBCL), downstream targets of NF-κB are involved in apoptosis inhibition and may thereby block the action of many forms of chemotherapy (Baldwin et al. 2001). The constitutive activation of the NF-κB pathway

may thus contribute to the poor response of the ABC subtype to chemotherapy (Alizadeh et al. 2000; Rosenwald et al. 2002; Lenz et al. 2008a). Moreover, inhibiting NF-κB activation resulted in the reversal of chemoresistance and an enhanced anti-tumor efficacy in a gastric cancer cell line, thereby further supporting the view that NF-κB may indeed mediate resistance to cancer therapy (Uetsuka et al. 2003).

1.2.2 Anti-cancer roles of NF-κB

Although NF-κB transcription factors have an oncogenic role in cancer development and mediate chemoresistance in cancer therapy, other studies found NF-κB transcription factors or upstream activators rather to act as tumor suppressors, thereby underscoring the complexity and potential context dependency of NF-κB network-mediated effector functions.

NF-κB has also been shown to mediate apoptosis (Wang et al. 1998 and Ryan et al. 2000). In contrast to NF-κB's anti-apoptosis function, RelA and c-Rel may have a proapoptotic function in T cells, B cells, fibroblasts, neuronal cells, and HeLa cells. (Kasibhatla et al. 1999; Sheehy et al. 1999; Martin et al. 2009; Schneider et al. 1999; Kaltschmidt et al. 2000). NF-κB can also influence the apoptotic response differently depending on the developmental stage of immune cells. For example, overexpression of RelA caused cell-cycle arrest that is followed by apoptosis in the pro-B cell line 220-8, whereas overexpression of RelA in the WEHI 231 immature B-cell line or in the mature B-cell line M12 did not induce apoptosis (Sheehy et al. 1999). NF-κB factors have double edged-function even in the same cell. Constitutive expression of c-Rel at an early stage imposed a resistance against TNFα-induced apoptosis and later increased the level of spontaneous apoptosis by up-regulation of the manganese superoxide dismutase (MnSOD) in Hela cells (Bernard et al. 2002).

Furthermore, some mouse model-based studies found NF-κB transcription factors or upstream activators to act as tumor suppressors. The first evidence directly linking

NF-κB to tumor suppression was from experiments using murine and human epidermis. Functional blockade of NF-κB in epidermal cells resulted in severe hyperplasia of the skin in transgenic mice, which could be reversed by overexpression of active RelA and p50 subunits of NF-κB, suggesting a tumor-suppressive effect of NF-κB (Seitz et al. 1998). In a diethylnitrosamine-induced hepatocellular carcinoma (HCC) mouse model, hepatocyte-specific ablation of IKK strongly enhanced the development of HCC (Maeda et al. 2005). Hepatocyte-specific ablation of IKKγ or TAK1, which are both required for the activation of IKK and NF-κB, resulted in spontaneous liver damage, hepatocyte death, liver fibrosis and development of HCC (Luedde et al. 2007; Inokuchi et al. 2010; Bettermann et al. 2010). Myc oncoproteins (c-Myc, N-Myc and L-Myc) were activated in ~70% of human malignancies (Dang 1999; Nesbit et al. 1999). In the Eμ-*myc* transgenic mouse model, NF-κB2 loss accelerated lymphoma development by impairing Myc's apoptotic response, suggesting that tumor suppression function of the non-canonical NF-κB pathway (Keller et al. 2010).

1.3 Cellular senescence and cancer

One mechanism that might be related to the anti-cancer function of NF-κB is cellular senescence, which acts as a tumor suppressive mechanism to prevent the proliferation of seriously damaged cells. Silencing of NF-κB transcription factors in senescent human fibroblasts enhanced their proliferative capacity, suggesting that NF-κB signaling may contribute to the senescent growth arrest (Rovillain et al. 2011). NF-κB also triggered a cell-cycle arrest in normal human epidermal cells. IκBα-mediated blockade of NF-κB resulted in the bypass of growth arrest triggered by oncogenic Ras, contributed to the generation of malignant human epidermal tissue resembling squamous cell carcinoma (Dajee et al. 2003). Furthermore, several recent studies demonstrated that senescent cells secreted chemokines, which have NF-κB binding sites in their promoter region and have cellular senescence reinforcing function. Chemokines such as interleukin 8 (IL-8) and other chemokine receptor 2

(CXCR2) ligands reinforce growth arrest of senescent cells in a positive feedback loop through their ability to boost the DNA damaging response (DDR) (Acosta et al. 2008). Other NF-κB targeted genes encoding secreted proteins, such as IL-6 and PAI-1, are involved in the induction of senescence by inhibiting proliferative and mitogenic pathways (Kortlever et al. 2006; Kuilman et al. 2008).

DNA damage induced by anti-cancer therapy (i.e. chemotherapy, radiation) is the common principle by which these moieties act to trigger cellular responses, including programmed cell death (apoptosis) and cellular senescence. Programmed cell death induced by DNA damage is an important mechanism of tumor suppression and benefic for the treatment outcome in cancer chemotherapy. In addition to apoptosis, therapy-induced senescence (TIS) has been identified as another drug-responsive program that impacts the outcome of cancer therapy (Chang et al. 1999; Schmitt et al. 2002a).

1.3.1 Cellular senescence

The evolution of the cellular senescence concept

Fifty years ago, Hayflick and Moorhead described cellular senescence as a terminal cell cycle arrest that reflects the exhaustion of the replicative potential in cultured human fibroblasts (Hayflick et al. 1961). Later, DNA damage signals emanating from eroded telomeres that progressively shorten every time the cell divides, were unveiled as the underlying mechanism of the irreversible block in the G1-phase of the cell-cycle (Harley et al. 1990). Several years later, findings demonstrated that a phenotype indistinguishable from replicative senescence, called premature senescence, can be acutely induced in normal as well as cancer cells by a variety of stresses, including DNA damage and oncogenic signals (Serrano et al. 1997; Jones et al. 2000). Unlike replicative cellular senescence, premature senescence arises independently of telomere shortening. In recent years, evidence for the existence of

premature senescence *in vivo* has been accumulating rapidly and points to a critical role in tumor suppression (Braig et al. 2005; Collado et al. 2005; Michaloglou et al. 2005). Senescence not only stops cell proliferation but also has other functional implication. Over the past several years, senescent cells were found to be cleared by the immune system (Xue et al. 2007) and the importance of secreted factors in senescence was realized (Kuilman et al. 2008; Coppé et al. 2008; Wajapeyee et al. 2008).

Features of senescent cells

Cellular senescence is a growth-arrest program that limits the lifespan of mammalian cells and prevents unlimited cell proliferation. Senescent cells are viable, remain metabolically active and undergo characteristic changes in morphology. They flatten out and display a vacuole-rich cytoplasm. Lysosomal activity of the cytoplasmic β-galactosidase enzyme is increased in senescent cells, which can be detected by a colorimetric assay using X-gal as a substrate (Dimri et al. 1995). Senescent cells reorganize their chromatin in specific domains and accumulate senescence-associated heterochromatic foci (SAHFs) (Narita et al. 2003). These SAHF are specifically enriched in methylated Lysine 9 of histone H3 (a modification catalyzed by the histone methyltransferase Suv39h1). Senescent cells show an altered gene and protein expression pattern compared to normal cycling or quiescent cells (Dimri et al. 1995; Shelton et al. 1999). Upregulation of proteins like p53 (Serrano et al. 1997; Harvey et al. 1993), ARF (Dimri et al. 2000; Kamijo et al. 1997), or $p16^{INK4a}$ are cardinal features of a senescent cell. Furthermore, cells undergoing senescence exhibit profound changes in their transcriptomes. A major consequence of this is the secretion of many dozens of factors, including cytokines and chemokines, termed the “senescence-associated secretory phenotype (SASP).

1.3.2 Pathways controlling cellular senescence

DNA damage response

Cellular senescence is, at least in part, triggered by a DNA damage response (DDR) initiated by increased production of reactive oxygen species and replication stress as a result of unscheduled S-phase entry in response to activated oncogenes or due to chemo-therapeutic agent (Bartkova et al. 2006; Di Micco et al. 2006; Mallette et al. 2007). When a eukaryotic cell is exposed to stimuli like oxidative stress, oncogenic stress, chemotherapy or ionizing radiation, the cell mounts the orchestrated and conserved signaling response - DNA damage response (Ciccia et al. 2010; Reinhardt et al. 2009; Derheimer et al. 2010; Bakkenist et al. 2004; Jackson et al. 2009). As a whole, the DDR involves the detection of specific DNA damage, the activation of DNA damage repair mechanisms, cell cycle checkpoints, transcriptional responses and post-translational kinase kinases. The outcome of the DDR may consist of satisfactory lesion repair and cell survival, while excessive damage may result in persistent DNA damage, which activates the checkpoint kinases ATM/ATR and CHK1/2, and leads to p53 accumulation. The accumulation of p53 allows the activation of downstream genes such as p21, and the induction of cellular senescence.

RB and p53 tumor suppressor pathways

The retinoblastoma protein (pRb) and p53 tumor suppressor pathways represent the core signaling pathways involved in the induction of cellular senescence (Fig. 4) (Lowe et al. 2003; Narita et al. 2003 and Collado et al. 2010). The tumor suppressive p53 transcription factor is required for cellular senescence. Mutation or deletion of the TP53 gene occurs in more than half of human cancers (Hollstein et al. 1994). p53 accumulates in response to cellular stresses, activates a specific program of target genes to restrict the growth of abnormal or damaged cells by inducing

apoptosis or cellular senescence. The outcome reached is thought to depend on the type and level of stress signal involved, and the cellular context (Riley et al. 2008, Vousden et al. 2009). Transcriptional target genes of p53 include the cyclin-dependent kinase (CDK) inhibitor p21, the proapoptotic genes BAX and APAF1, and the E3 ubiquitin ligase MDM2 (Vousden et al. 2002, Riley et al. 2008). The upstream $p14^{Arf}$ protein ($p19^{Arf}$ in mice) prevents the degradation of p53 (Sherr et al. 2006). It is not fully understood how p53 plays a role in cellular senescence, but its ability to transactivate the p21 promoter, leading to the accumulation of p21 protein, is well established as a means by which p53 can induce growth arrest (Levine et al. 1997, Vousden et al. 2009). The p21 protein primarily acts by the inhibition of cyclin/CDK complexes upstream of pRb. This inhibition leads to a reduction in pRb phosphorylation, increased association of pRb with E2F and repression of E2F target genes (Fig. 4).

In addition to p53, senescence is linked to the RB tumor suppressor and its signaling partners, including p16INK4A (a cyclin-dependent kinase inhibitor acting upstream of RB).The tumor suppressor activity of the pRb protein is mainly attributed to its ability to bind and inactivate the E2F family of transcription factors, which transactivate genes encoding cell cycle proteins and DNA replication factors required for cell growth (Bracken et al. 2004; Blais et al. 2007). In stressed cells, the transcriptionally upregulated 16INK4a inhibits cyclin D-dependent kinases, thereby preventing the phosphorylation and inactivation of the retinoblastoma protein (Collado et al. 2006) (Fig. 4). This promotes the repressive association between pRb and the E2F pro-proliferative transcriptional activators, preventing progression through the cell cycle, and permitting the formation of a repressive or ‘closed’ chromatin structure around E2F target gene promoters, known as senescence-associated heterochromatin foci (SAHF). In SAHF, explicitly methylation of the lysine 9 residue at histone H3 (H3K9) mediated the stable epigenetic silencing of E2F-responsive genes. Suv39h1, a heterochromatic histone methyltransferases (HMT), bound to the hypophosphorylated Rb protein, and, thus, was recruited into a multimeric complex

with E2F transcription factors. The formation of HMT/Rb/E2F complex repressed the expression of E2F-regulated genes (Schmitt. 2006).

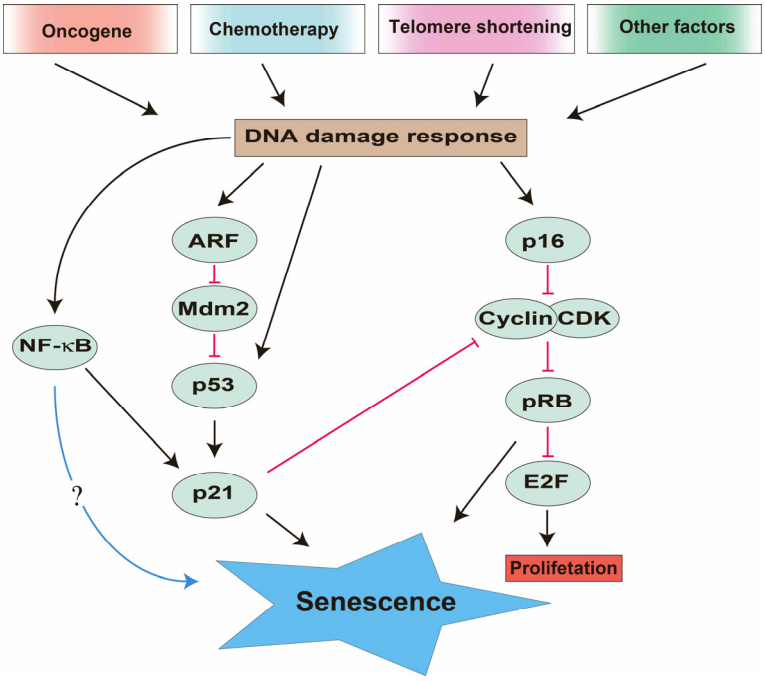

Figure 4: Molecular mechanisms of cellular senescence. The p53 and pRb pathways are central to cellular senescence control. Oncogene activation, cytotoxic drugs, telomere attrition and radiation have all been shown to induce the DNA damage response (DDR). DDR and senescence signals change the cellular phenotype through activation of the p53-p21 and p16-pRB pathway. NF-κB pathway is activated upon DNA damage. Some studies indicated that p21 is a NF-κB target gene (Hinata et al. 2003; Krappmann et al. 2004). Whether NF-κB plays a positive role in cellular senescence is addressed in this thesis.

1.3.3 Senescence-associated secretory phenotype (SASP)

Since 1999, it has been known that the establishment of replicative senescence in human skin fibroblasts leads to a strong inflammatory response involving the transcriptional upregulation of cytokines (Shelton et al. 1999). These results were initially interpreted as idiosyncratic of dermal fibroblasts and the recapitulation of the inflammatory process associated with wound healing in vitro, a suspicion

strengthened by the observation that such a response was augmented by high concentrations of serum, since the transcriptional program of fibroblasts in response to serum appeared to be related to the physiology of wound repair (Iyer et al. 1999). We now know that senescence leads to a coordinated secretion of a large number of factors (Krtolica et al. 2001; Coppé et al. 2006) - the so-called senescence-associated secretory phenotype (SASP) – and this occurs in different cell types following different stresses (Kuilman et al. 2008).

SASP is composed of pro-inflammatory cytokines such as IL-1α, IL-1β, IL-6, IL-8, bFGF, TGF-β (in some settings), or GM-CSF, as well as inflammation-related chemokines such as CXCL-1/-2/-3/-5/-7, MIP-1α, or MCP-1 (a.k.a. CCL2), but also contains secretable factors with, at least in some contexts, anti-proliferative activity such as IGFBPs or PAI-1, as well as factors like the MMPs that remodel the extracellular matrix (Acosta et al. 2008; Kortlever et al. 2006; Kuilman et al. 2009). Moreover, SASP is not restricted to secretable factors, but also includes cell surface molecules serving as ligands and receptors, for instance TNF receptors, CXCR2 or the IL-6R, thereby creating potential autocrine loops (e.g. CXCL-1/-5/-7 or IL-8 with CXCR2) (Acosta et al. 2008) or even, as claimed, intra-cellular short cuts (e.g. IL-6 and the IL-6R) (Kuilman et al. 2008), and self-amplifying cascades (e.g. NF-κB signaling via TNF-R).

Proinflammatory cytokines secreted by senescent cells trigger a variety of cellular responses. In certain settings, they have pro-oncogenic effects: the proliferative rate, migration, and invasion of premalignant cells are enhanced when they are cocultured with, or grown in medium conditioned by senescent fibroblasts (Krtolica et al. 2001; Dilley et al. 2003; Parrinello et al. 2005). Intriguingly, in addition to influencing their microenvironment, some inflammatory cytokines reinforce the arrest status in a cell-autonomous and/or paracrine fashion by enhancing expression levels of the p15INK4b CDK inhibitor, and, probably, additional effector principles. For example, signaling through the IL-6 and IL-8 (CXCR2) receptors is essential, in a cell

autonomous fashion, for cells to enter senescence in response to oncogenic BRAF or replicative exhaustion, respectively (Acosta et al. 2008; Kuilman et al. 2008). This is relayed by the C/EBPβ and NF-κB transcription factors and is associated with the activation of an inflammatory transcriptome.

The mechanistic basis of SASP is unclear. Given the fact that many of these senescence-associated cytokine, chemokine and receptor genes bear NF-κB- and/or C/EBPβ-binding sites in their promoters (Kuilman et al. 2008; Adams et al. 2009), a prediction is that the DNA damage response components NBS1, ATM and CHK2 activate NF-κB and C/EBP, which further mediate the expression of the SASP factors. Indeed, NF-κB is a downstream target of ATM (Li et al. 2001; Stilmann et al. 2009; Hinz et al. 2010), although the impact of DDR factors on C/EBP is less clear.

As discussed in 2.3.2, Cellular senescence is, at least in part, triggered by the DNA damage response (DDR). Meanwhile, the IKK/NF-κB pathway, a potential key regulator of numerous SASP factors, is a recognized downstream target of ATM, which is a key component of the DDR. Therefore, it is reasonable to hypothesize that NF-κB may be involved in the process of senescence and SASP.

1.3.4 Cellular senescence and cancer treatment outcome

Premature senescence is a stress-inducible fail-safe mechanism initiated via DNA damage response signaling evoked by oncogenic activation or anti-cancer chemotherapy (Schmitt et al. 2007; Kuilman et al. 2010). Moreover, cellular senescence is increasingly recognized as a possible outcome for the treatment because it can be executed by cells in response to therapeutic drugs and irradiation (Chang et al. 1999). Indeed, therapy-induced senescence (TIS) is detectable in human tumor biopsies after exposure to neoadjuvant chemotherapy (te Poele et al. 2002) and has also been shown to improve the long-term outcome of cancer therapy (Schmitt et al. 2002a).

Therapy-induced senescence as an alternative to apoptosis

Chemotherapy is still the most important treatment method for many types of cancer. The possible outcomes of chemotherapeutic treatments reach from apoptosis, mitotic catastrophe to cellular senescence. Most of the chemotherapeutic agents used in the clinic are assumed to exert their anti-tumor effect through the induction of apoptosis. However, an intact apoptotic machinery is often unavailable in malignant cells. For example, high expression of Bcl2, an antiapototic moiety, in lymphomas prevents cells from undergoing apoptosis. In tumor cells with an apoptotic defect, senescence could be activated as an alternative treatment response and contribute to the outcome (Fig.5).

It is not well understood what defines the choice of a cell to respond to the treatment either with apoptosis or senescence. It could depend on the dosage of the chemotherapeutic agents with low doses inducing senescence and high doses apoptosis (Rebbaa et al. 2003). Moreover, the fact that anticancer therapy *in vivo* induced a rapid apoptosis response and a delayed senescence status suggest that the senescence machinery may act as a back-up program to substitute for or to reinforce an insufficient apoptotic response (Lee et al. 2003). In addition, specific genetic defects that have been accumulated in cancer cells during tumorigenesis are strong determinants of a possible treatment outcome. In tumors with apoptosis defects, promoting senescence may improve the treatment outcome.

Therapy-induced senescence and tumor microenvironment

As with many drug treatment responses, TIS may appear in a heterogeneous degree in tumors. In other words, not all the cells may respond with senescence to chemotherapeutics. As mentioned before, the expression of cytokines and secreted factors by senescent cancer cells may have an inhibitory effect on the growth of surrounding bystander cells. Alternatively, this heterogeneous response may have a

growth-promoting effect in some situations. Moreover, factors secreted by senescent cells can also act on macrophages, neutrophils, and NK cells, thereby promoting immune responses that, on one hand, may ultimately lead to the clearance of senescent tumor cells (Xue et al, 2007), but, on the other hand, might also create a microenvironment that fosters tumor progression (Coppé et al, 2010). Thus, the outcome of anticancer therapy is not only determined by a quantitative effect on cancer cells forced to irreversibly exit the cell cycle but may also depend on novel capabilities acquired by senescent cells that can impact on their malignant and non-malignant neighbors in different ways (Fig. 5). With further identification of precise pathways that regulate senescence and additional specific senescence-inducing agents, there will be a wider exploitation of this approach in cancer treatment.

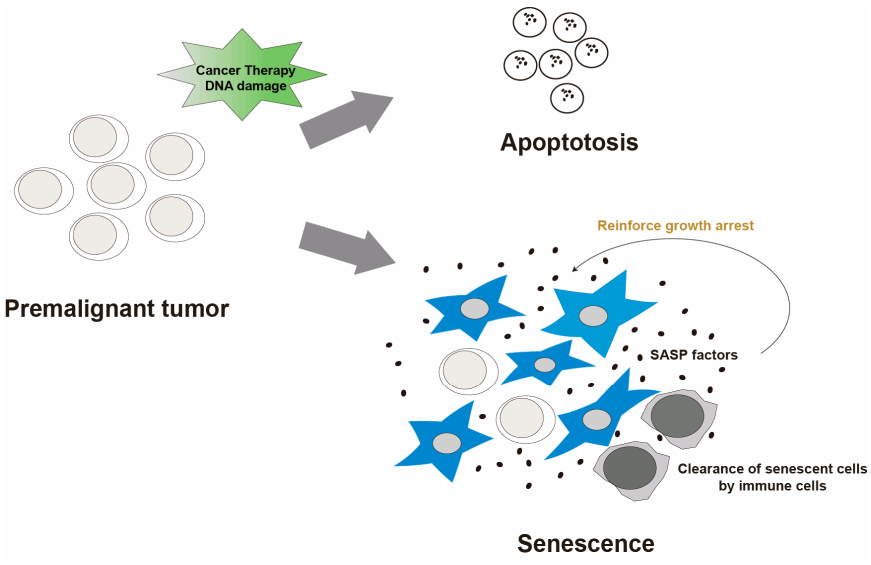

Figure 5: Therapy-induced senescence as an alternative to apoptosis in cancer treatment. In response to DNA-damaging agents, cancer cells can rapidly undergo apoptosis or may enter premature senescence as a potential back-up mechanism. In addition to the tumor suppressive function, senescence induction is accompanied by the secretion of SASP factors, which may further reinforce the growth arrest or induce senescence in surrounding cells. With increased expression of immune cell-interacting molecules, senescence cells can be cleared by immune cells.

1.4 Diffuse large B-cell lymphoma

Diffuse large B-cell lymphoma (DLBCL) is a heterogeneous disorder that shows a diffuse architecture, a mature B cell phenotype and large cell morphology. It is a type of aggressive B-cell non-Hodgkin's lymphoma and accounts for approximately 30-40% of all lymphomas among adults (Shaffer et al. 2002). DLBCL can be subdivided into subtypes based on many different criteria such as morphology, viral association or underlying genetic abnormalities. Clinicians have difficulties in choosing appropriate therapies for treating diffuse large B-cell lymphoma because patients present apparently similar diagnoses, but markedly different clinical outcomes. The heterogeneity of DLBCL in genetic features might be one reason for the differences in treatment outcome. With the development of the microarray technology for gene expression profiling (GEP), it has been demonstrated that different gene expression profiles indicate biologically distinct subtypes of lymphoma, with functional studies leading to an improved understanding of the pathogenetic mechanisms in lymphoma and a better classification system.

1.4.1 Classification of diffuse large B-cell lymphoma

According to their gene expression profiling (GEP), DLBCL can be divided into at least three histologically indistinguishable molecular subtypes: the activated B-cell-like (ABC) subtype, the germinal-center B-cell-like (GCB) subtype, and primary mediastinal B-cell lymphoma (PMBL) (Alizadeh et al. 2000; Rosenwald et al. 2002; Rosenwald et al. 2003). While PMBL is distinct from other DLBCLs, GCB and ABC present as the clinically most relevant subtypes.

GCB and ABC subtypes apparently arise from different stages of normal B-cell differentiation, differ in the expression of thousands of genes and utilize distinct oncogenic pathways (Staudt et al. 2005). GCB and ABC subtypes also differ in their clinical presentation, in cure rates after chemotherapy, and in responsiveness to

targeted therapies (Fig 6).

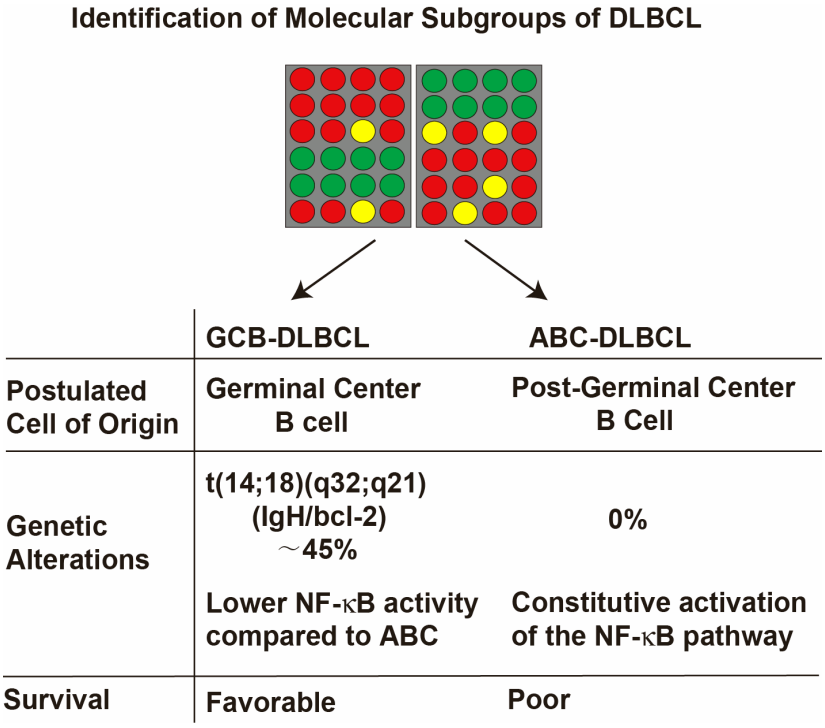

Figure 6: Gene expression profiling identified molecular subgroups of diffuse large B-cell lymphoma (DLBCL). GCB and ABC DLBCL differ in their presumed cell of origin, in underlying genetic alterations and in their clinical behavior.

ABC DLBCL

The activated B-cell like (ABC) subtype DLBCL highly expresses genes otherwise found in normal activated B-cells, such as cyclin D2, FOX-p1 and NUM1/IRF-4 (Rosenwald et al. 2003). The hallmark of ABC DLBCL is constitutive activation of the NF-κB pathway. Analysis of the gene expression signature in the ABC-DLBCL subtype revealed preferential expression of a large number of classical NF-κB target genes, including Bcl-2 family members, c-FLIP, and cyclin D2, compared with GCB DLBCL. Moreover, in cell line models of DLBCL, constitutive IKK activity, rapid IκBα degradation and high nuclear NF-κB DNA binding activity were found in ABC-DLBCL but not in the GCB-DLBCL subtype (Davis et al. 2001).

NF-κB is activated in ABC DLBCL by a variety of mechanisms including oncogenic mutations and a chronic active form of B-cell receptor signaling. Recent mutation analyses demonstrated that mutations of the NF-κB pathway regulators are, at least partly, responsible for a substantial fraction of cases with NF-κB activation in ABC-DLBCL. These include mutations of the coiled-coil domain of CARD11 in about 10% of ABC DLBCL cases leading to increased oligomerization of CARD11 and subsequently, NF-κB activation (Lenz et al. 2008). Other studies confirmed the presence of CARD11 mutations in DLBCL and identified additional mutations affecting TNFAIP3 (A20), MYD88, CD19-ITAM, C-Rel, MAP3K7 (TAK1), TNFRSF11A (RANK), TRAF5 and TRAF2 (Compagno et al. 2009; Honma et al. 2009). CARD11 is a multi-domain signaling adapter that contains an amino-terminal CARD and coiled-coil domains, an intervening linker domain, and a C-terminal MAGUK domain. Prior to activation, CARD11 is located in the cytosol, where it is presumably kept in an inactive conformation through an intramolecular interaction between its coiled-coil and linker domains. PKCβ-dependent serine phosphorylation within the CARD11 linker domain is thought to relieve this intramolecular association. CARD11 is then able to translocate to the plasma membrane, where it binds BCL10 and MALT1. Subsequently, MALT1 recruits TRAF6, which ubiquitinates MALT1, TAB2, and IKKγ. Ubiquitinated TAB2 activates the kinase TAK1, which can then phosphorylate IKKβ in its activation loop. Full activation of IKK requires both phosphorylation and ubiquitination of IKKγ (Shaffer et al. 2012). MYD88 is an adapter protein that couples TIR-containing receptors, such as the TLRs, to a variety of downstream signaling circuits, including the NF-κB, p38MAP kinase, and type I interferon pathways. Another mutation found in ABC-DLBCL affects A20. A20 is a deubiquitinating enzyme and inactivates IKKβ by removing regulatory K63- linked polyubiquitin chains from IKKγ. These gene products are positive or negative regulators of the NF-κB pathway and their alterations promote abnormal activation of the pathway (Fig. 7).

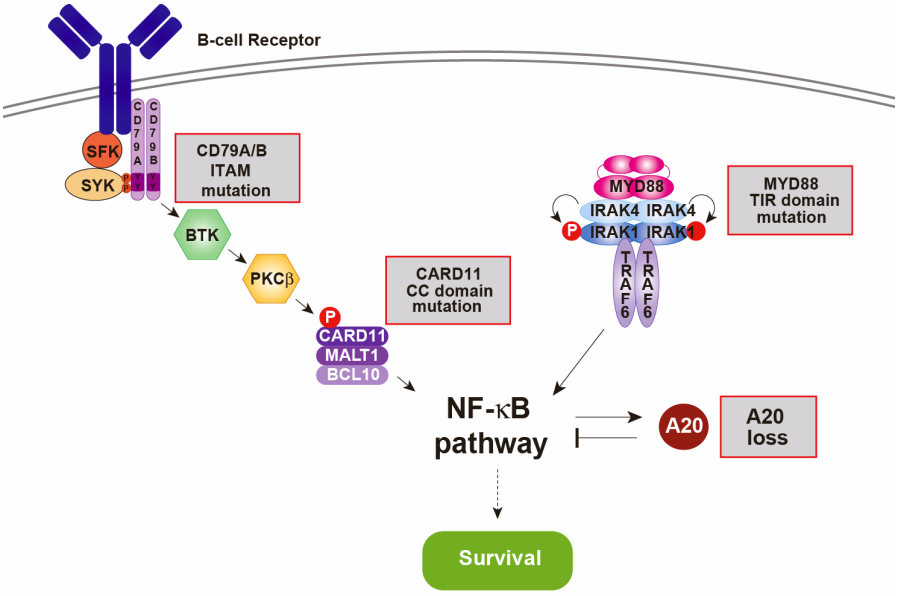

Figure 7: Mutations of regulators of the NF-κB pathway in ABC DLBCL. Constitutive activation of the NF-κB pathway promotes survival in ABC DLBCL and can be achieved by several oncogenic mechanisms, including mutations in CD79A/B/ITAM, CARD11, MYD88 and A20 (adapted from Shaffer et al. 2012).

GCB DLBCL

The germinal-center B-cell like (GCB) subtype DLBCL is characterized by high expression of the "signature" genes of normal germinal center B-cells, including CD10 and CD38, the nuclear factor A-myb, as well as BCL-6 (Alizadeh et al. 2000; Nyman et al. 2007). GCB DLBCL is likely derived from rapidly proliferating centroblasts within the germinal center of a lymph node. In particular, the NF-κB pathway is essentially silent in germinal center B cells, as measured by expression of NF-κB target genes and by nuclear accumulation of NF-κB heterodimers (Shaffer et al. 2006)

GCB-DLBCL frequently present with a genomic translocation t(14;18) that puts Bcl2 in the vicinity of the immunoglobulin heavy chain locus. This oncogenic event was found to be common in GCB DLBCL, occurring in 45% (29/65) of cases analyzed, and also was detected in 18% (2/11) of PMBL cases (Huang et al. 2002; Rosenwald et al. 2002). By contrast, BCL-2 translocation is virtually absent in ABC DLBCL.

Nonetheless, the majority of ABC DLBCLs express Bcl-2 mRNA at high levels, presumably due to transcriptional activation of Bcl-2 as an NF-κB target (Rosenwald et al. 2002; Wright et al. 2003).

1.4.2 NF-κB and clinical outcome in diffuse large B-cell lymphoma

In general, a 5-year survival rate of 60% can be achieved in DLBCL; however, patients with an ABC subtype have a significantly shorter survival than those with GCB DLBCL when treated with standard doxorubicin-based chemotherapy such as CHOP (cyclophosphamide, doxorubicin, vincristine, and prednisone), with or without rituximab (Rosenwald et al. 2002; Lenz et al. 2008; Wilson et al. 2008). To date, no therapy has shown greater benefit in ABC DLBCL.

The hypothesis that the constitutively active NF-κB pathway in ABC DLBCL is linked with inferior treatment outcome is supported by several in vitro experiments. Introduction of the IκBα super repressor to inhibit NF-κB in distinct DLBCL cell lines resulted in rapid apoptosis and cell-cycle arrest, selectively in ABC-DLBCL cells (Davis et al, 2001), while the GCB DLBCL cells were not affected, indicating that the constitutive NF-κB activity is specifically required for the survival and proliferation of ABC-DLBCL cells. Furthermore, the IKKβ inhibitors PS-1145 and MLX105 were selectively toxic for ABC-DLBCL cells but not for GCB DLBCL cells. Cell death was accompanied by decrease in the expression of NF-κB target genes and an activation of the proapoptotic caspases 3 and 7. Introduction of an estrogen-inducible RelA fusion protein into ABC-DLBCL restored NF-κB activity even in the presence of IKK inhibition. The active forms of RelA also stopped apoptosis induction by the kinase inhibitors PS-1145 and MLX105, demonstrating that the NF-κB inhibition is directly responsible for tumor cell death (Lam et al. 2005).

Taken together, gene expression profiling of DLBCL has revealed distinct molecular

subtypes that include germinal center B-cell like and activated B cell–like DLBCL. ABC DLBCL present with an inferior prognosis after chemotherapy and are characterized by constitutive activation of the NF-κB pathway, which appears to confer treatment resistance. In vitro analyses demonstrated that inhibition of NF-κB can sensitize ABC but not GCB DLBCL. Although NF-κB's function in GCB is not clear, the NF-κB pathway is central to the pathogenesis of ABC DLBCL and is a potential treatment target in this subgroup.

1.5 Eμ-*myc* mouse lymphoma model

Transgenic mice bearing the cellular *myc* oncogene coupled to the lymphoid-specific IgH enhancer (μ) develop with high incidence a fatal lymphoma within a few months after birth. The prototype Eμ-*myc* mice succumb to pre-B and B-cell lymphomas, following a preneoplastic phase in which cycling pre-B cells massively expanded. The hallmark of the disease in Eμ-*myc* mice is a profound enlargement of the lymph nodes. The onset of tumor occurs around 3 and 18 weeks of age (Adams et al. 1885).

The Eμ-*myc* transgenic mouse serves as a useful model to study genetic mechanisms of tumor development and treatment sensitivity in spontaneous B-cell malignancies for several reasons. Firstly, the genetics and histopathology of Eμ-*myc* lymphomas resemble human non-Hodgkin's lymphomas. Secondly, the tumor burden can be easily monitored by lymph-node palpation or blood smears. Thirdly, large numbers of pure tumor cells can be isolated, cultured, transduced and transplanted into syngeneic, non-transgenic mice. When Eμ-*myc* transgenic lymphoma cells were transplanted into normal, immunocompetent recipient mice, the recipient mice developed systemic lymphomas indistinguishable from the primary transgenic host they were initially derived from (Schmitt et al. 1999, 2000).

In the Eμ-*myc* mouse lymphoma model, both senescence and apoptosis were contributing to the *in vivo* response to chemotherapy (Schmitt et al. 2002b). When

apoptosis was blocked in Eμ-*myc* lymphomas, senescence became the principal tumor response to chemotherapy. Eμ-*myc* tumors harboring a Bcl2-mediated apoptotic block underwent drug-induced senescence involving the accumulation of p53 and p16INK4a *in vivo* (Schmitt et al. 2002a). Likewise, primary Eμ-*myc* transgenic, retrovirally bcl2-infected lymphoma cells can enter senescence in response to the treatment of DNA-damaging drugs *in vitro* (therapy-induced senescence, “TIS”).

To sum up, the NF-κB pathway transcriptionally controls a large set of target genes that play multiple roles in cell survival, inflammation and immune recognition. In ABC-DLBCL, constitutively active NF-κB signaling prevents apoptosis and thereby blocks the action of many forms of chemotherapy. In addition to apoptosis, senescence is another drug-responsive effector program of cancer therapy. Recent evidence points to a potentially tumor-suppressive function of NF-κB as a mediator of the senescence-associated secretory phenotype. SASP, reflecting a broad array of cytokines and chemokines, are produced in a predominantly NF-κB-dependent fashion during cellular senescence, presumably related to oncogene- or chemotherapy-induced DNA damage that is considered to initiate cellular signaling ultimately leading to the terminal, senescent cell-cycle arrest. Given the context dependency of NF-κB’s functions and the complexity of NF-κB-governed biological responses, NF-κB’s perspective function in senescence are likely to impact on treatment efficacy.

2 Scientific aims of this PhD thesis

The general objective of this PhD project is to elucidate the role of the NF-κB pathway in senescence and cancer treatment outcome. Therefore, the following specific aims will be addressed:

- Is the NF-κB pathway activated in therapy-induced senescence?
- Is therapy-induced senescence dependent on the NF-κB pathway?
- Does hyperactive NF-κB contribute to treatment outcome in human lymphoma patients?

3 Material and Methods

3.1 Material

3.1.1 Chemicals and reagents

ABT-263	Selleck
ABT-737	Selleck
Adriamycin (Doxorubicin)	Sigma
Agar	Roth
Agarose	Serva Electrophoresis
Albumin Fraktion V	Roth
Ammoniumpersulfate (APS)	Roth
Ampicillin sodium salt	Roth
Bay11-7082	Sigma-Aldrich
Blasticidin	Invitrogen
Bradford reagent (RotiQuant)	Roth
Bromophenolblue powder	Eurobio
Calciumchloride ($CaCl_2$)	Roth
Chloroform	Merck
Dual Endogenous Enzyme Block	DAKO
Dako REAL™ Antibody Diluent	DAKO
DAPI	Sigma
Diethyl pyrocarbonate (DEPC)	Sigma
di-Sodium hydrogenphosphate dihydrate	Merck
dNTPs	Roth
DTT	Fluka
Ethanol absolute	Roth
Ethidium bromide powder	Roth
Ethylenediaminetetraacetate (EDTA)	Roth
Fetal Calf Serum (FCS)	Biochrom
Formaldehyde	Roth
Glacial acetic acid	Merck

Glucose	Roth
α-D(+) Glucose (Dextrose)	Roth
Glutaraldehyde	Roth
Glycerin	Merck
Glycine	Serva Electrophoresis
HCl	Merck
HEPES	Roth
Hexademethrinebromide (Polybrene)	Sigma
Hygromycin B	Roche
KINK-1	provided by M. Schmidt Supprian (Schon et al. 2008)
L-Glutamine	Biochrom
Magnesiumchloride for PCR	Roche Applied Biosystems
Magnesiumchloride-hexahydrate ($MgCl_2$)	Roth
Methanol	J.T.Baker
Milk powder	Roth
Mowiol 4-88	Calbiochem
N,N,N´,N´-Tetramethylethylenediamine (TEMED)	Sigma
N,N-dimethylformamide (DMFO)	Roth
N,N-dimethylsulfoxide (DMSO)	Roth
Na-Desoxycholate	Sigma
NH_4Cl	Merck
Nonident 40 (NP-40)	Merck
Paraformaldehyde (PFA)	Sigma
PBS Dulbecco	Biochrom
PCR buffer	Applied Biosystems
Penicillin-streptomycin	Biochrom
PMSF	Sigma
Potassium ferricyanide ($K_3Fe(CN)_6$)	Sigma
Potassium ferrocyanide ($K_4Fe(CN)_6$ x 3 H_2O)	Sigma
Potassiumchloride (KCl)	Merck
Potassiunacetate (KAc)	Roth
2-propanol	Sigma
Protease inhibitors (Complete protease inhibitor)	Roche

Puromycin dihydrochloride	Calbiochem
SDS (Sodiumdodecylsulfat)	Roth
Sodiumchloride (NaCl)	Merck
Sodium desoxycholate	Sigma
Sodiumfluoride	Sigma
Sodiumhydroxide (NaOH)	Roth
Sodiumorthovanadate	Sigma
β-mercaptoethanol	Roth
Taq polymerase	Applied Biosystems
TaqMan® Gene Expression Master Mix	Applied Biosystems
TNF-α	Sigma-Aldrich
TPCA-1	Merck
Tris (hydroxymethyl) aminomethane	Merck
Triton X-100	Merck
TRIZOL reagent Gibco	Invitrogen
Trypan blue solution	Sigma
Trypsin-EDTA	Biochrom
Trypton/Pepton from casein	Roth
Tween 20	Roth
X-Gal	Roth
Yeast extract	Roth

3.1.2 Enzymes

Klenow	Promega
Pfu DNA polymerase	Agilent
Proteinase K	Merck
Restriction enzymes	NEB Biolabs
RNase A	Fluka
RNasin Plus RNase Inhibitor	Invitrogen
T4 DNA ligase	NEB Biolabs

3.1.3 Kits

Kits	Company
Reverse Transcription Kit	Invitrogen
Dako REAL™ Detection System, Alkaline Phosphatase_RED, Rabbit_Mouse	DAKO
Luciferase Reporter Gene Detection Kit	Sigma
Nuclear Extract Kit	Active motif
TransAM® NFκB Family	Active motif
Immobilon Western Chemiluminescent AP Substrate	Millipore

3.1.4 Oligonucleotides

Oligo	Sequence
IκBα forward	5'-ATAAGATCTGCCACCATGACCGAGGACGGGGACTCGT-3'
IκBα reverse	5'-AGCGAATTCTCATAACGTCAGACGCTGGC-3'
Luc forward	5'-AGGAACCAGGGCGTATCTCT-3'
Luc reverse	5'-CGTCGCCAGTCAAGTAACAA-3'

3.1.5 Expression vectors for retroviral transduction

Plasmids used in this study are ecotropic vectors based on the Moloney Murine Leukemia Virus (MMLV) and taken for retroviral transduction of rodent cells. The MSCV (Murine Stem Cell Virus) vector contains the packaging sequence (ψ^+), gene of interest, the PKG (Phosphoglycerate kinase) promoter and a selectable marker (antibiotic resistance) /or IRES-GFP between the 5´ and 3´LTR (Figure 8). For further details see www.clonetech.com.

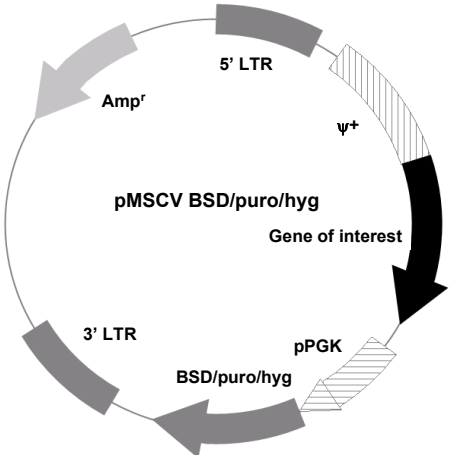

Figure 8: MSCV BSD/puro/hyg plasmid map

Vectors based on the pMSCV are listed below:

Plasmid Name	**Backbone**	**Insert**
MSCV-SR-BSD (SR = IκBα-ΔN)	MSCV-BSD	Part of the human IκB-alpha cDNA (amino-acid residues 71–317)
MSCV-SR-IRES-GFP	MSCV-IRES-GFP	Part of the human IκB-alpha cDNA (amino-acid residues 71–317)
MSCV-CARD11L251P-puro	MSCV-puro	Mouse CARD11 cDNA with L251P mutation

pMSCV(SIN) vector

The U3 region of the 3' LTR (sequence between restriction sites NheI and XbaI) in the MSCV-hyg vector was cut off. Therefore, the MSCV-SIN vector lacks the enhancer region of the 3' LTR, introducing the need of using an internal promoter to drive the expression of the reporter gene.

pMSCV(SIN)-NF-κB-Luc vector

The pMSCV(SIN)-NF-κB-Luc vector was constructed based on the self-inactivating (SIN) MSCV vector. A fragment containing six NF-κB-binding DNA consensus sites (GGGGACTTTCCCT) linked to a luciferase reporter gene (6×NF-κB-Luc) was cloned into the multi cloning site of the MSCV-SIN vector to get the pMSCV(SIN)-NF-κB-Luc vector (Figure 9).

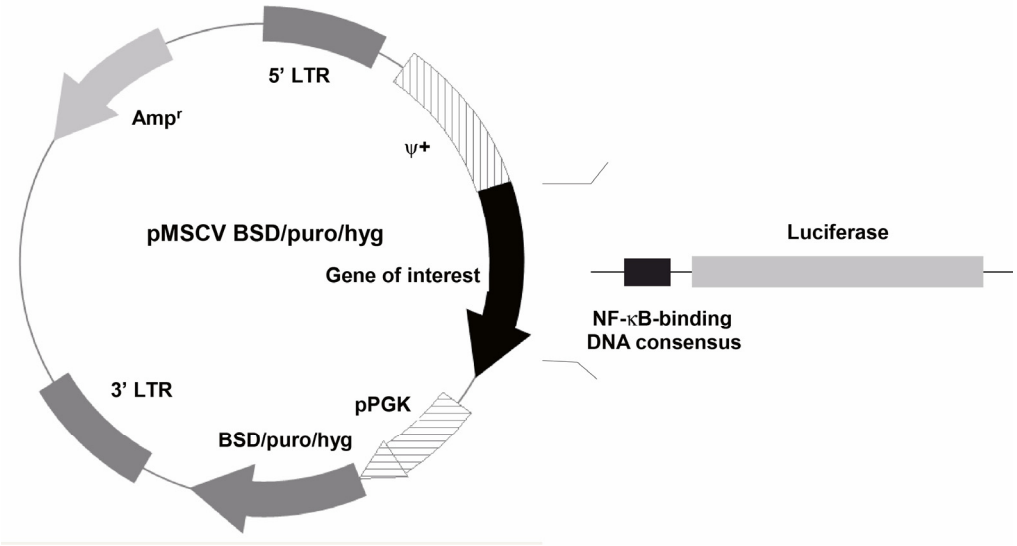

Figure 9: pMSCV(SIN)-NF-κB-Luc plasmid map

3.1.6 Bacteria strains

E. coli DH5α	Invitrogen
	Genotype: F-φ80*dlc*ZΔM15Δ(*lac*ZYA-*arg*F)U169 *deo*R, *rec*A1 *end*A1*hsd*R17 $r_k^- m_k^+$ *pho*A *sup*E44λ-*thi*-1*gyr*A96 *rel*A1

3.1.7 Markers

Marker	**Company**
Protein	
PageRuler™ Plus Prestained Protein Ladder	Roth
DNA	
pBR Mix 328	Roth
GeneRuler™ 1 kb Plus DNA Ladder	Thermo

3.1.8 Antibodies

Antibody	Host / Conjugate	Used for	Dilution	Company
Anti-α-tubulin (T5168)	mouse	WB	1:2000	Sigma
Anti-H3K9me3 (ab8898)	rabbit	WB	1:1000	Abcam
Anti- IκBα (Sc-371)	rabbit	WB	1:250	Santa cruz
Anti-Ki67 (M7249)	rat	ICC	1:25	DAKO
Anti-phospho-p65 (Ser536)	rabbit	WB	1:1000	Cell signaling
Anti-p65 (C-20)	rabbit	IF	1:250	Santa cruz
Anti-p65 (#3034)	rabbit	WB	1:1000	Cell signaling
Anti-IgG AlexaFluor 488	rabbit	IF	1:400	Invitrogen
Anti-rabbit IgG	HRP	WB	1:1000	Amersham
Anti-mouse IgG	HRP	WB	1:1000	Amersham

3.1.9 Cells

Cell type	Medium	Source
NIH 3T3 Adherent mouse embryonic fibroblast cell line, Cytogenetics: hypertriploid karyotype and 3% polyploidy; deleted in the Ink4Arf locus. ATCC number: CRL-1658	DMEM medium	Cell line
Phoenix Eco φ $^{-}$ Adherent human embryonic kidney cell line 293T, adenovirus-transformed and stably transfected with two plasmids encoding the MML virus sequences “gag”, “pol”, “env”. www.standford.edu/group/nolan.html	DMEM medium	Cell line

MEF	DMEM medium	Primary
Primary mouse embrionic fibroblasts, isolated from E12.5 mice; adherent cells.		
B-Lymphoma cells	B cell medium	Primary
Primary murine Myc-driven B-cell lymphoma cells isolated from the spleen or lymphnode of a terminally sick Eμ-*myc* transgenic mouse; suspension cells, culture with feeder cell.		

3.1.10 Buffers and solutions

Solutions for Immunofluorescence	**Reagents**
Fixation solution	4% paraformaldehyde in 1x PBS *prepare freshly*
Blocking solution	1% BSA in 1x PBS
Permeabilization buffer	0.1%Triton X-100 in 1x PBS
Detergent buffer	0.01% Tween 20 in 1x PBS

Solutions for Plasmid Mini-Preparation	**Reagents**
Solution I	50 mM Glucose 25 mM Tris pH 8.0 10 mM EDTA pH 8.0 *store at 4°C*
Solution II	0.2 N NaOH 0.5% SDS *prepare freshly*
Solution III	25% 5 M KAc 15% Acetic acid

	adjust to 100 ml with distilled water *store at 4°C*
Solutions for PCR / RT-PCR	**Reagents**
50x TAE	242 g Tris base 57.1 ml Glacial acetic acid 100 ml 0.5 M EDTA (pH 8.0) *store at RT*
DEPC water	0.1% DEPC in distilled water incubate at 37°C for 1 hour, autoclave *store at RT*
Solutions for Retroviral Transduction	**Reagents**
2 M $CaCl_2$	5.88 g $CaCl_2$ adjust to 20 ml with distilled water filter (0.2 µm) *store at -20°C*
2x HBS (Hepes buffered saline)	280 mM NaCl 10 mM KCl 1.5 mM Na_2HPO_4 x $2H_2O$ 12 mM dextrose 50 mM HEPES adjust pH to 7.05 adjust to 100 ml with distilled water, filter *store at -20°C*
100 mM Chloroquine	0.516 g Chloroquine diphosphate adjust to 10 ml with distilled water filter (0.2 µm)

	store at -20°C

Solutions for SA-β-gal assay	**Reagents**
PBS/$MgCl_2$	1 mM $MgCl_2$ in 1x PBS
	store at RT
Fixation solution	0.25% Glutaraldehyde/ 2%
	paraformaldehyde, in PBS/$MgCl_2$
	PH 5.5 solution
	prepare freshly
Staining solution	9.25 ml PBS/ $MgCl_2$
	0.5 ml 20x KC solution
	0.25 ml 40x X-Gal solution
	prepare freshly
20x Potassium cyanide (KC) stock	20 mg $K_3Fe(CN)_6$
	1.050 mg $K_4Fe(CN)_6x\ 3H_2O$
	in 25 ml 1x PBS
	store at 4°C in the dark
40x X-Gal solution	40 mg X-Gal in 1 ml DMFO
	store at -20°C

Solutions for Western Blot	**Reagents**
Protein lysis buffer (Lämmli)	1 ml of 0.5 M Tris-HCl, pH 6.8
	0.8 ml Glycerol
	1.6 ml of 10% SDS
	0.4 ml of 14.3M β-mercaptoethanol
	3.8 ml distilled water
	store at RT
SDS sample buffer	1 ml 0.5 M Tris-HCl (pH 6.8)
	0.8 ml Glycerol

	1.6 ml 10% SDS
	0.4 ml 14.3 M β-mercaptoethanol
	0.4 ml of 1% bromophenol blue
	store at -20°C
0.5 M Tris-HCl pH 6.8	6 g Tris base
	60 ml dH_2O
	adjust to pH 6.8, adjust with distilled water to 100 ml
	store at RT
1.5 M Tris-HCl, pH 8.8	27.23 g Tris base
	80 ml dH_2O
	adjust to pH 8.8, adjust with distilled water to 100 ml
	store at RT
10x Electrode running buffer (pH 8.3)	30 g Tris base
	144 g Glycin
	10 g SDS
	adjust with distilled water to 1 L
	store at RT
Transfer buffer	2.9 g Tris base
	14.5 g glycine
	200 ml methanol
	Adjust with distilled water to 1 L
	Store at 4°C
25x TBS	60 g Tris base
	200 g NaCl
	9.5 ml 10 N HCl
	adjust with distilled water to 1 L
	store at RT

1x TBS-Tween (TBS-T)	0.2% Tween 20 in 1x TBS *store at RT*
Blocking buffer	5% dry milk in 1x TBS-T prepare freshly or *store at 4°C (1 day)*

3.1.11 Media

Medium	**Component**
DMEM medium	DMEM + 10% FCS + Penicillin-streptomycin (100 U/ml) s*tore at 4°C*
B cell medium	DMEM+ IMDM (1:1) + 10% FCS + Penicillin-streptomycin (100 U/ml) + 4 mM L-Glutamine + 25 µM β-mercaptoethanol *store at 4°C*
Freezing medium	FCS + 10% DMSO s*tore at 4°C*
LB-Medium (Luria-Bertani)	10 g Trypton 5 g Yeast Extract 10 g NaCl adjust to 1 L with distilled water (pH 7.2-7.5) *store at 4°C*
LB-bacteria plates	10 g Trypton 5 g Yeast Extract

	10 g NaCl 15 g Agar adjust to 1 L with distilled water (pH 7.2-7.5) *store at 4°C*

3.1.12 Equipment

Plastic-ware and other dispensable materials	**Company**
Cell culture dishes, sterile (different sizes)	TPP
Centrifuge tubes, sterile (different sizes)	TPP
Serological pipettes, sterile (different sizes)	Falcon Becton Dickinson
“Mr. Frosty” Freezing box	Nalgene Cryo 1°C Freezing Container
Syringes for single-use, sterile (different sizes)	Braun, Omnifix, BS Plastic
Neubauer cell-counter chamber (Improved 0.025 mm, Depth 0.1mm)	Superior Marienfeld
Needles for single-use, sterile (different sizes)	Neoject
Disposable scalpel for single-use, sterile	Feather
Cryotubes, sterile PK-100 (1.2 ml)	Simport Plastics
Nylon Mesh (35 µm)	Sefar
Rotilabo Filter sterile (0.45 µM PVDF)	Roth
Rotilabo Filter sterile (0.22 µM PVDF)	Roth
Microscopy Immersion Oil	Merck

Cytospin Equipment	**Company**
- Centrifuge (Rotina 35R)	Hettich
- Inserts (1670) and Plastics (1668)	Hettich

Western Blot Equipment	**Company**
Western blot chamber for SDS-PAGE	C.S.B. Scientific CO
Western blot semidry blotting apparatus (Transblot Semidry Transfer Cell)	BIORAD
PVDF membrane (Immobilon-P)	Millipore
Whatman paper (3 MM)	Schleicher-Schuell
ChemoCam Imager	INTAS

Standard Equipment	**Company**
Centrifuges	Eppendorf Centrifuge 5417R Eppendorf Megafuge 1.0 R
PCR machine	Mastercycler Eppendorf
Photometer	Eppendorf BioPhotometer 8.5 mm
Microscope	Zeiss Telaval 31
Fluorescence microscope	Zeiss Axioplan
Flow Hood	Typ UVF 6.18S BDK
Incubator	Heraeus cytoperm 2
Real-time PCR system	Applied Biosystems StepOnePlus™ Systems
UV detection system	Biometra T13 UV table and BioDoc CCD-Camera + Software
VICTOR™ X Multilabel Plate Reader	PerkinElmer

All instrumentation/material not listed in detail is standard lab equipment

3.2 Methods

3.2.1 Cell culture

3.2.1.1 Thawing of cells

Reagents, solutions and material

- *Frozen cells in -80°C or LN_2*
- *Pre-warmed DMEM culture medium or B cell medium*
- *Feeder cells (for lymphoma cells) in conditioned B cell medium*

Cells were thawed quickly at 37°C in a water bath and transferred dropwise to 5 ml of the respective medium. After centrifugation (1200 rpm, 5´, RT), supernatant was removeded and pellet was resuspended in 1 ml of the respective medium. Cells were seeded in an appropriate cell number on culture dishes or feeder cells.

3.2.1.2 Freezing of cells

Reagents, solutions and material

- *Cells*
- *Freezing medium (4°C)*
- *1x PBS*
- *1x Trypsin*
- *DMEM culture medium or B cell medium*
- *Cryotubes*
- *"Mr. Frosty" freezing box (stepwise cool down of cells; 1°C in 1´)*

Adherent cells:

Medium was removed from the culture plate. Cells were washed with 1x PBS, detached with Trypsin (37°C; 1´), resuspend in fresh DMEM medium, and centrifuged

(1200 rpm, 5',RT).

Suspension cells:
Cells were directly harvested from the culture plate and centrifuged (1200 rpm, 5',RT).

After centrifugation, supernatant was removed and pellet was resuspended in ice-cold freezing medium. Cells were frozen in the density of 1-2x10^6 cells/ml freezing medium. Cryotubes were put into "Mr. Frosty" box and immediately transferred to -80°C (4h). For long-term storage, cells were transferred to LN_2.

3.2.1.3 Culture of adherent cells

Reagents, solutions and material

- *NIH 3T3 fibroblasts, Phoenix cells or mouse embryonic fibroblast (MEF)*
- *Pre-warmed DMEM culture medium*
- *1x PBS*
- *1x Trypsin*

NIH 3T3 fibroblasts, Phoenix cells or MEF were seeded 30-50% confluent in DMEM medium and cultivated under standard conditions (37°C, 5% CO_2, 20% O_2, 95% humidity) until they reached confluency. Cells were split by the following procedure: medium was removed and cells were washed with 1x PBS. 1 ml of Trypsin was added until cells detached (37°C). Cells were resuspended in culture medium and re-seeded in the desired density (1:2 – 1:20) onto new cell culture plates containing fresh medium.

Mouse embryonic fibroblast were plated in DMEM medium and cultivated in low O_2 conditions (37°C, 5% CO_2, 3% O_2, 95% humidity). The following procedures are similar to the culture methods of NIH 3T3 fibroblasts or Phoenix cells.

3.2.1.4 Preparation of feeder cells

Reagents, solutions and material

- *NIH 3T3 fibroblasts*
- *Pre-warmed DMEM medium*
- *1x PBS*
- *1x Trypsin*
- *Pre-warmed B cell medium*

NIH 3T3 fibroblasts were seeded in DMEM medium. When they reached 70-80% confluency, cells were irradiated with 20 Gy (3000 rad). 12 hours post irradiation cells were split according to standard procedures and resuspended in fresh B cell medium. Cell number and viability was assessed by trypan blue exclusion. Cells were re-seeded at a density of 0.5 x 10^5 cells per well in 6-well plates. Medium was changed every 2-3 days. Feeder plates were not used when feeder cells got flattened or vacuole rich. Medium enriched with growth promoting factors of irradiated 3T3 cells (12 to 24 hours after plating feeder cells) was used as “conditioned medium” for lymphoma cells culture.

3.2.1.5 Culture of primary lymphoma cells

Reagents, solutions and material

- *Freshly isolated / thawed lymphoma cells (low passage)*
- *Feeder cells (irradiated NIH 3T3 feeder layer)*
- *B cell medium*

Lymphoma cells were seeded at a subconfluent density (~70%) on a feeder plate and cultivated under standard conditions (37°C, 5% CO_2, 20% O_2, 95% humidity). Cells were grown until their density reached 5 x 10^6 cells/ ml or medium turned too acidic. For splitting, about 1/3 of the cell suspension was removed (cultivated on new feeder plates with fresh medium, frozen or discarded). Feeder cell plates were changed after ~1 week of culture or when feeder turned too old. For this, the plate was gently rinsed

to remove lymphoma cells sticking on the feeders. Suspension was centrifuged at 1200 rpm for 5´ (4°C). A few ml of the supernatant were retained to resuspend the cell pellet and cell suspension was subsequently transferred to a new plate of feeders with conditioned B-cell medium. Splitting was considered as one passage.

Lymphomas cells were only used at a viability of more than 50 % and at low passages (to prevent selection for clones that have gained mutations by long-term culture).

3.2.2 Animal procedures

The main part of the animal experiments was conducted by Drs. Soyoung Lee and Julia Kase.

3.2.2.1 Dissection of mice

Reagents, solutions and material

- *Tumor-bearing mouse*
- *Small box with dry ice, filled with a few ml of H_2O*
- *70% Ethanol*
- *Mouse preparation equipment*
- *Cold 1x PBS*
- *4% Formaldehyde in 1x PBS*

After CO_2-euthanizing the Eμ-*myc* transgenic mouse at the time a well-palpable lymphadenopathy became detectable, animal was rinsed with ethanol and pinned down on a dissecting board with the belly facing up. Mouse was opened using an inversed “T”-cut: skin anterior to the urethral tract was held with forceps and the skin along the ventral midline was cut from the groin to the chin (careful not to damage the muscle wall underneath). Next, incision was made down near the knee on both sides of the animal and skin was reflected back. Transparent peritoneal wall was cut carefully. Body cavity was opened up and reflected back to have access to the

structures underneath. After removing the diaphragm on the bottom of the breast, the sternum was opened by lifting it up with forceps and cutting along each side up to the girdle to have access to the thoracic organs. Before cutting the peritoneum, lymphnodes that are located subcutaneously or in the connective tissue between muscles were checked. After opening the peritoneum, abdominal organs were checked for any anatomical abnormalities (right place of the organ, size and color). To open the sternum, diaphragm was punctured and cut along each side up through the cervical girdle, avoiding any damage to the thoracic organs underneath. Organs in the thorax were checked intensely. If at any time point organs were enlarged or showed abnormal features, they were cut with scissors and forceps, released from the connected tissue and rinsed in cold 1x PBS. After measuring the size, parts of the organ and the mouse body were conserved and single-cell suspensions were prepared for cell culture assays.

3.2.2.2 Preparation of lymphoma cells

Reagents, solutions and material

- *Freshly prepared organs of the respective mouse*
- *Mouse preparation equipment*
- *Cold 1x PBS*
- *Sterile frosted glass slides*
- *Sterile nylon mesh (35 µm)*
- *ACK red blood cells lysis buffer*
- *25 gauge needle and syringe*
- *Anticoagulant (7.5 % K3-EDTA)*

Lymph nodes were washed, placed into cold 1x PBS and gently minced between two glass slides using the frosted side of the slides. Mixture was resuspended by repeated pipetting. To obtain a single-cell suspension, mixture was filtered through a sterile membrane and centrifuged at 1200 rpm for 5´ (RT). To get rid of red blood cells, pellet was resuspended in 3 ml of ACK lysis buffer and incubated at RT for 5´. Before

centrifugation (1200 rpm, 5´, RT), 27 ml of B cell medium were added for neutralization. Procedure was repeated if red blood cells remained. Cells were frozen or immediately used for further experiments.

Importantly, primary Eμ-*myc* lymphomas used for drug assays in this study were checked for a proper p53 pathway response (i.e. induction of total p53, phospho-p53-Ser18 and $p21^{cip1}$) after γ-irradiation (4Gy) in vitro (after 4 hours). Only p53-pathway-intact lymphomas were included in experience +/- the SR moiety.

3.2.2.3 Lymphoma transplantation and *in vivo* treatment

- *Lymphoma cells*
- *PBS*
- *Syringe*
- *Needle**
- *Mouse restrainer*
- *Cyclophosphamide (CTX)*

Lymphoma cells were isolated, retrovirally infected and transplanted by tail vein injection into normal, immunocompetent recipient mice, where they formed systemic lymphomas indistinguishable from the primary transgenic host they were initially derived from. At the moment lymph nodes became palpable in recipient animals, mice were exposed to a single intraperitoneal dose of the DNA-damaging anti-cancer agent cyclophosphamide (CTX) (300 mg/kg body weight), and responses were monitored by lymph node palpation or in lymphoma material isolated at day 5 after therapy.

3.2.3 Molecular biology

3.2.3.1 Polymerase chain reaction

Reagents, solutions and material

- *Genomic DNA, plasmid or cDNA (100-500 ng/µl)*
- *10x PCR buffer incl 15 mM $MgCl_2$*
- *dNTP mix (10 mM each)*
- *Respective primer (stock 10 pM)*
- *Taq Polymerase (5 U/µl)*
- *dH_2O*

A PCR reaction mixture was prepared according to the following protocols:

Component	**Amount**
Template DNA	1 µl (5-500 ng/µl)
10x PCR buffer with $MgCl_2$	2 µl
dNTP mix	1 µl
Primer forward	1 µl (10 pM)
Primer reverse	1 µl (10 pM)
Taq Polymerase	1 µl
dH_2O	Add 13 µl of dH_2O to the total volume of 20 µl.

The following cycling conditions were used for PCR product amplification:

Steps	**Temperature**	**Time**
1 Denaturation	95°C	5 min
2 Denaturation	95°C	30 sec
3 Annealing	According to the annealing temperature of specific primers	30 sec
4 Elongation	72°C	1 min / 1kb product
repeat steps 2-4 34 x		
5 Elongation	72°C	7 min
6 Hold	4°C	∞

3.2.3.2 Agarose gel electrophoresis

Reagents, solutions and material

- *DNA in 6x DNA loading buffer*
- *1 kb ladder or pBR marker*
- *Agarose*
- *1x TAE*
- *1% Ethidium bromide*
- *Equipment for gel electrophoresis*

Agarose gels were prepared according to the following procedure: agarose was dissolved in 1x TAE at the desired concentration and melted in a microwave until the solution became clear. When the solution cooled to about 50-55°C, ethidium brodmide was added in the appropriate concentration. After casting the gel, hardening occurred within 10-15´. Gel chamber was filled with 1x TAE. The aliquots of the DNA samples including the corresponding amount of loading buffer were loaded into separate wells in the gel. To determine DNA length of the fragments, an appropriate DNA ladder standard was used. Depending on the size of the supposed bands, gel was run 30-60´ (120V). DNA was visualized by UV-light.

3.2.3.3 Preparation of RNA

Reagents, solutions and material

- *Cells*
- *TRIZOL reagent*
- *Chloroform*
- *Isopropanol*
- *75% Ethanol*
- *DEPC H_2O*
- *Photometer*

Cells were harvested and centrifuged at 1200 rpm for 5´ (RT). Medium was removed and pellet was resuspended by gently pipetting in 1 ml of TRIZOL reagent. Suspension was homogenized by shaking moderately for several seconds. After

incubation (2´-3´ at RT), 200 µl of chloroform were added to separate RNA from proteins and DNA. Suspension was vortexed for 15´´ and incubated for additional 2´-3´ at RT. After centrifugation, (12 000 g for 10´, 4°C), the colorless aqueous phase was transferred to a new effendorf tube. To precipitate RNA, 500 µl of isopropanol were added to the samples, incubated for 10´ at RT and centrifuged again at 12 000 g for 10´ (4°C). Supernatant was removed and pellet was washed with 1 ml of 75% Ethanol. After centrifugation at 7500 g for 5´ (4°C), supernatant was removed and pellet was dried in air until ethanol was evaporated. RNA was re-dissolved in DEPC H_2O and incubated for 10´ at 55°C before measuring RNA in a photometer (260/280nm) using DEPC H_2O as a reference. RNA is pure at a 260/280 ratio of ≤ 1.8. In general, RNA was stored at -20°C and for long-term storage at -80°C. All buffers, solutions, tips and other equipment were RNase free.

3.2.3.4 First strand cDNA synthesis

Reagents, solutions and material

- *Extracted RNA*
- *Oligo (dT) primer (500 ng/µl)*
- *DEPC dH_2O*
- *5x first strand buffer*
- *0.1 M DTT*
- *dNTP mix (10 mM each)*
- *1 U RNasin enzyme*
- *200 U SuperScript Reverse Transcriptase*

1µg of RNA, 1µl dNTP mix and 1µl of Oligo (dT) primer were mixed and adjusted with dH_2O to 13µl. Samples were incubated for 5´ at 65°C to destroy RNA secondary structures and incubate on ice for at least 1´. The following mix was prepared for each sample: 4µl first strand buffer, each 1µl DTT, dNTPs and RNasin. Mix was incubated for 60´ at 50°C. Reaction was inactivated by hearting at 70°C (15´). The cDNA product was stored at -20°C and for long-term storage at -80°C.

3.2.3.5 Real-time PCR

Reagents, solutions and material

- *cDNA product*
- *TaqMan® Gene Expression primers*
- *TaqMan® Gene Expression Master Mix*
- *dH_2O*

The RQ-PCR reaction mixture was prepared according to the following protocols:

Component	**Amount**
cDNA	2 µl (50 ng/µl)
TaqMan® Gene Expression Master Mix	5 µl
TaqMan® Gene Expression primers	1 µl
dH_2O	2.5 µl

RQ-PCR was carried out on the StepOnePlus™ Real-Time PCR Systems (Applied Biosystems). Primers were ordered as TaqMan® Gene Expression Assays from Applied Biosystems. Real-time PCR amplification reactions were performed using the TaqMan® Gene Expression Master Mix. Thermal cycling conditions were as follows:

Steps	**Temputer**	**Time**
1 Anealing	50°C	2 min
2 Denaturing	95°C	10 min
3 Denaturing	95°C	15 sec
4 Extention	60°C	1 min
repeat steps 3-4 40 x		

Data were collected and analyzed with the Sequence Detection System 1.2 or 2.2 software (Applied Biosystems). For every given sample, ΔCt values were determined as the difference between the Ct value of a specific transcript and the Ct value of

GAPDH, serving as the housekeeping control mRNA, and relative transcript levels (e.g., treated vs. untreated) were then produced based on $2^{\{-\Delta\Delta Ct\}}$ with $\Delta\Delta Ct = \Delta Ct_{treated} - \Delta Ct_{untreated}$.

3.2.4 Protein biochemistry

3.2.4.1 Western Blot

Western Blotting was performed using a 10% or 12% SDS-PAGE-system and a semi-dry blotting technique.

Reagents, solutions and material

- *Cell pellets for protein lysis (freshly prepared or frozen)*
- *Protein lysis buffer (Triton X-100)*
- *Protease inhibitors*
- *Rotimark Bradford Reagent*
- *BSA (stock 1 µg/µl in dH_2O)*
- *Tris-HCl pH 6.8 and pH 8.0*
- *30% Acrylamide*
- *10% SDS*
- *TEMED and 10% APS*
- *dH_2O*
- *Isopropanol*
- *Sample buffer (SDS reducing buffer)*
- *10x electrode running buffer*
- *Western Blot equipment*
- *Low or high molecular weight standards (Roti Prestained Marker)*
- *PVDF-membrane (Immobilon-P)*
- *Methanol*
- *Whatman paper*

- *Transfer buffer*
- *Semi-dry blotting apparatus*
- *1x TBS-T (TBS-Tween 20)*
- *5 % non-fat milk (in 1x TBS-T)*
- *Washing buffer*
- *First and corresponding secondary antibody*
- *Immobilon Western Chemiluminescent AP Substrate*

Protein extraction from cultured cells

Cells were washed once in 1x PBS and centrifuged at 1200 rpm for 5´ (RT). Cell pellet was resuspended in ice-cold protein lysis buffer (Volume = 3x volume of cell pellet) and incubated in a shaker at 4°C for 60´. To remove cell debris, lysates were centrifuged (14000 rpm, 10´, 4°C) and supernatant containing the proteins was transferred to a new tube. Protein concentration was determined by a standard Bradford assay and lysates were kept at -20°C or -80°C for long term storage.

Protein measurement (Bradford´s protein micro assay)

A ready-to-use Bradford solution was prepared by diluting 1 volume of 5x Bradford reagent with 4 volumes dH_2O. A BSA standard curve was set up using 0, 1, 2, 4, 6, 8 and 10 µg BSA including 1 µl of the protein lysis buffer each (corresponding to the volume of the protein lysate that is measured afterwards). To create a standard curve, the absorbance of the individual standard solutions was determined in a photometer at a wavelength of 595 nm against the no BSA-control. The curve was depicted in a linear regression (R^2 values close to 1.0). For the individual protein lysates, each 1 µl was pipetted into 1 ml of the prediluted Bradford solution. The protein concentration was determined by the standard curve. To improve accuracy each sample was measured in triplicates.

Preparation of the protein samples

Protein samples were thawed on ice. Volume for the desired protein amount was

calculated and the respective volume of loading buffer was added to the samples. The mixtures were then boiled for 5´ at 95°C.

Preparation of SDS-PAGE gel

Gel plates were cleaned with 70% Ethanol and wipe clean with sterile Kimwipe before they were set in the casting apparatus. Separating gels (10ml) was set up mixing the following solutions:

Compound	**10 % SDS-PAGE**	**12% SDS-PAGE**
Distilled water	4 ml	3.3 ml
30% Acrylamide mix	3.3 ml	4.0 ml
1.5 M Tris pH 8.8	2.5 ml	2.5 ml
10% SDS	0.1 ml	0.1 ml

100 µl APS and 4 µl TEMED were added to the gel mixture, vortexed and promptly casted between the spacers of the prepared glass plates from side to side. To prevent evaporation, a small layer of isopropanol was carefully added on top. Once the gel has polymerized (about 10-15 min´), isopropanol was removed from the separating gel and rinsed with water. The excess water was carefully blotted off with a filter paper. Meanwhile, a stacking gel was prepared (5 ml):

Compound	**Stacking gel**
Distilled water	3.4 ml
30% Acrylamide mix	0.83ml
1.5 M Tris pH 6.8	0.63 ml
20% SDS	0.05 ml

50 µl APS and 5 µl TEMED were added to the stacking gel mixture, vortexed and pipetted on top of the separating gel. A comb with the desired number of slots was inserted. Once the gel has polymerized, the comb was slowly removed under running

water.

Gel electrophoresis (SDS-PAGE)

Chambers were filled with 1x electrode running buffer. Protein samples were loaded into the slots. A lane with 8 µl of a molecular weight standard (Rotimark Prestained) as a marker was inculeded. Gel was started at a constant voltage of 70-90 V until the blue dye front reached the front of the separating gel. Gel was run at a voltage of 120-180 V until the blue dye front has nearly run out of the gel. After disassembling the gel apparatus, stacking gel was carefully removed. Separating gel was rinsed in dH_2O and equilibrated in transfer buffer.

Semi-dry blotting procedure

Six pieces of Whatman paper and an Immobilon blot membrane were cut in the size of the gel and semi-dry blotting chamber was cleaned. Membrane was activated with methanol for a few seconds, rinsed with dH_2O and soaked in transfer buffer. Whatman paper was soaked in transfer buffer. A semidry blotting “sandwich” was set up in the following order onto the anode platform:

• 3 Whatman papers
• Activated Immobilon blot membrane
• Gel
• 3 Whatman papers

Air bubbles were rolled out and sandwich was blotted for 60´ at 1.2 mA per cm^2 gel. Afterwards, blotting apparatus was disassembled and membrane was used for further immnmoblot.

Antibody incubation

Membrane was blocked for 60´ at RT in freshly prepared blocking solution with constant agitation. Meanwhile, the first antibody was diluted to an appropriate concentration in blocking solution. Membrane was incubated 1 hours at room temperature or overnight at 4°C with gentle agitation. Afterwards, antibody solution

was saved (and reused when stored at -20°C) and membrane was washed 3x 10´ in washing buffer. Subsequently, the membrane was incubated with the corresponding secondary antibody (RT) for 60´ under gentle agitation followed by three washing steps (3x 10´). Next, the two Immobilon Western Chemiluminescent AP Substrates were mixed 1:1 and transferred onto the protein-covered side of the wet membrane. After 1-2´ incubation, membrane was imaged using the INTAS ChemoCam Imager.

3.2.4.2 Immunofluorescence

Reagents, solutions and material

- Cells
- *Cytospin equipment*
- *Freshly prepared fixation solution (4% paraformaldehyde)*
- *0.1% Triton X-100/PBS*
- *PBS*
- *Blocking solution (1% BSA in PBS)*
- *Primary antibodies and respective secondary antibody (in blocking solution)*
- *DAPI*
- *Mowiol 4-88*

For lymphoma cells:

Cells were harvested at the appropriate time point. After centrifugation (1200 rpm, 5´, RT), cells were washed in 1x PBS. Cell number and viability were assessed by trypan blue exclusion. 100,000 cells were transferred to a slot of the cytospin plastic and centrifuged at 700 rpm for 8´ (4°C). Supernatant was carefully removed by aspiration.

For mouse embryonic fibroblasts:

24 hours before harvest, cells were detached with trypsin, resuspended in culture medium, and re-seeded in 12-well plates with glass cover slips on the bottom. Cells were cultivated in low O_2 conditions (37°C, 5% CO_2, 3% O_2, 95% humidity). Before

harvest, medium was removed from the plates and cells were washed in 1x PBS.

Afterwards, lymphoma cells or MEF were fixed by a freshly prepared fixation solution. After incubation (15´, RT), slides were washed three times in 1x PBS and then permeabilized in 0.1% Triton X-100/PBS for 10´ (RT). After the incubation in the first antibody over night (4°C), cells were incubated with 0.01% Tween 20 as detergent buffer. Slides were washed in PBS (3x 5´) and subsequently incubated with the corresponding secondary antibody for 60´ (RT). After extensive washing in PBS (3x 5´), slides were stained with DAPI as a nuclear counterstain, mounted with Mowiol 4-88 and fluorescence was detected under the microscope. Slides were stored in the dark at 4°C.

3.2.4.3 Immunohistochemistry

Reagents, solutions and material

- Cells or tissue cryosections
- *Cytospin equipment*
- *Freshly prepared fixation solution (2% paraformaldehyde)*
- *0.1% Triton X-100/PBS*
- *PBS*
- *Dako REAL™ Antibody Diluent*
- *Dako REAL™ Detection System, Alkaline Phosphatase_RED, Rabbit_Mouse*
- *DAKO Dual Endogenous Enzyme Block*
- *Ki67 antibodies*
- *Mowiol 4-88*

Cytospin preparations or tissue cryosections were fixed with 2% paraformaldehyde, washed with 1x PBS and permeabilized in 0.1% Triton X-100/PBS for 10´ (RT). After another PBS washing cycle, slides were incubated with the primary antibody against Ki67 (1:25; M7249, Dako, diluted in Dako REAL™ Antibody Diluent), followed by a

streptavidin - biotin complex peroxidase kit (Dako REAL™ Detection System, Alkaline Phosphatase_RED, Rabbit_Mouse), used according to the manufacturer's instructions.

3.2.5 Luciferase assay

Reagents, solutions and material

- Lymphoma cells
- *PBS*
- Luciferase Reporter Gene Detection Kit

Lymphoma cells were washed once in 1x PBS and centrifuged at 1200 rpm for 5´ (RT). Cell pellet was resuspended in 50-100 µl of 1x Cell Culture Lysis Reagent, incubated at room temperature for 10 minutes and centrifuged at 12000´ g for 1 minute (4 °C). The supernatant was removed to a new tube and stored on ice. 5 µl of the cell lysate was added to 25 µl of the luciferase substrate. After a fully mixing, the light emission was read in the VICTOR™ X Multilabel Plate Reader. Protein concentration was mensured by BioRad assay and used to normalize luciferase values (calculate RLU/µg protein by dividing luminometer reading by protein concentration).

3.2.6 Measurement of NF-κB DNA binding activity

- *Lymphoma cells*
- *PBS*
- *Nuclear Extract Kit*
- *TransAM® NFκB Family Kit*

Lymphoma cells were harvested and washed once in ice-cold PBS/Phosphatase Inhibitors. Nuclear protein was extracted using Nuclear Extract Kit according to the manufacturer's instructions and stored at –80°C. Nuclear extracts were assayed at 5 µg/ well to determine DNA binding activity of NF-κB p65, p50, c-Rel, Rel-B or p52

subunits using TransAM NF-κB p65 kit (Active Motif). Absorbance was read at 450 nm in the VICTOR™ X Multilabel Plate Reader.

3.2.7 Retroviral transduction

Reagents, solutions and material

- *Low passage Phoenix cells (<20)*
- *Low passage lymphoma cells or mouse embryonic fibroblasts*
- *Retroviral plasmid DNA (including an appropriate marker)*
- *Ecotropic helper plasmid DNA*
- *dH_2O*
- *2M $CaCl_2$*
- *2x HBS pH 7.05*
- *Chloroquine (stock 100 mM)*
- *1x PBS*
- *Polybrene (stock 4 mg/ml), an transduction enhancer*
- *Conditioned B cell medium (filtered to prevent contamination with feeder cells) or DMEM medium*
- *FACS equipment, puromycin (stock 300 µg/ml, final 2.5 µg/ml), Blasticidin (stock 10 mg/ml, final 10 µg/ml-20 µg/ml)) or hygromycin (stock 50 mg/ml, final 50 µg/ml)*

Transfection of Phoenix cells

Low passage Phoenix cells were grown in a 10 cm plate to a maximal density of 70%. 20µg retroviral plasmid DNA, 15µg helper plasmid DNA and 62.5µl $CaCl_2$ were mixed in a FACS tube and adjusted with sterile water to 500µl. After adding 500µl 2x HBS dropwise under constant agitation (air bubbles), DNA precipitation occurred within 5´ at RT. Meanwhile, old medium of Phoenix cells was exchanged for 9 ml DMEM medium containing 25 mM Chloroquine. Subsequently, the precipitate (1 ml) was added dropwise. Cells were cultured under the standard conditions (37°C, 5% CO_2, 20% O_2, 95% humidity). 12 hours after transfection, medium including the precipitate was removed from the Phoenix cells. Cells were washed carefully with 1x PBS and 4

ml of conditioned B cell medium (for lymphomas) or DMEM medium (for MEF) were added to collect the first virus supernatant in 24 hours.

Retroviral transduction procedure

For lymphoma cells:

The first virus supernatant was harvested after 24 hours by aspiration and filtered through a 0.45 µm filter. A well growing cell population was pelleted by centrifugation (1200 rpm, 5´, RT) and resuspended in the virus supernatant including 4 µg/ml polybrene. New medium (4 ml) was added to the Phoenix cells for the next round of transduction. Afterwards, cells were incubated and grown under standard conditions.

After 8-12 hours of incubation, the second virus supernatant was harvested and added according to the procedure above, supplemented with polybrene was added to the lymphoma culture. After spinoculation of the plates (1500 rpm, 10´, 32°), cells were incubated and grown until the next round of transduction. In addition, new medium (4 ml) was added to the Phoenix cells for the next round of transduction. The third and fourth virus supernatants were collected 12 hours and 24 hours later according to the procedure above.

12 hours after the last transduction, medium was removed from the cells by centrifugation and cell pellet was resuspended in fresh conditioned B cell medium. Lymphomas were grown for an additional 24 hours to allow cells to express the gene of interest. For cells transduced with GFP-plasmids, percentage of positive cells was determined by flow cytometry (FACS) using a non-transduced control. For cells transduced with an antibiotic marker, cell population was selected with puromycin (~3 day), blasticidin (~5 day) or hygromycin (~5 day) until non-transduced cells were completely dead.

For mouse embryonic fibroblasts:

MEF were seeded at subconfluent density 12 hours after Phoenix cells transfection. The first virus supernatant was harvested 24 hours after transfection by aspiration

and filtered through a 0.45 µm filter. Medium was removed from the MEF and virus supernatant including 4 µg/ml polybrene was added. New medium (4 ml) was added to the Phoenix cells for the next round of transduction. Afterwards, cells were incubated and grown under standard conditions.

After 12 hours of incubation, the second virus supernatant was harvested according to the procedure above, supplemented with polybrene and added to the MEF culture. After spinoculation of the plates (1500 rpm, 10´, 32°C), cells were incubated and grown until the next round of transduction. In addition, new medium (4 ml) was added to the Phoenix cells for the next round of transduction. The third and fourth virus supernatants were collected 12 hours and 24 hours later according to the procedure of the first two rounds transduction.

12 hours after the last transduction, medium was removed from the cells and fresh DMEM medium was added to the MEF. MEF were grown for approximately 24 hours to allow cells to express the gene of interest. Cell population was selected with puromycin (~3 day) or blasticidin (~5 day) until non-transduced cells were completely dead.

3.2.8 Cell viability assays, apoptosis and senescence

3.2.8.1 Assessment of cell number and cellular viability

Reagents, solutions and material

- *All cell types*
- *Trypan blue solution (diluted in 1x PBS)*
- *Neubauer counting chamber*

Cells were harvested, centrifuged (1200 rpm, 5´, RT) and resuspended in an appropriate volume of 1x PBS. A 1:1 mixture of the cell suspension and the trypan blue solution was made and incubated for 1´. Cell suspension was applied to the

edge of the Neubauer chamber and checked for equal distribution of the cells in all four big quadrants. Non-viable cells were blue, viable cells were unstained. If more samples were counted, the trypan blue solution was added shortly before counting and cells were placed on ice.

For viability assessment and cytotoxicity assays, at least 200 cells were counted in total (dead and alive). Percentage of viability was indicated as the ratio of living cells to the whole cell number. For total cell number and growth analysis, all viable cells in 16 quadrants of the big 4-square-field were counted and number of living cells in culture was assessed by the following calculation: cell number / ml = total number of cells alive in 16 quadrants x dilution factor x 10^4.

3.2.8.2 *In vitro* drug assays

Reagents, solutions and material

- *Low passage lymphoma cells*
- *Conditioned B cell medium*
- *Adriamycin ADR (= Doxorubicin)*
- *ABT-263*
- *ABT-737*
- *Trypan blue solution (diluted in 1x PBS)*
- *Neubauer counting chamber*

A well growing lymphoma cells population was harvested and a small aliquot was taken to check viability. 1 x 10^5 lymphoma cells were seeded in duplicates onto a 24-well plate with feeder cells. The following adriamycin concentrations were used: 0.005 µl/ml, 0.05 µl/ml, 0.5 µl/ml. Cells were incubated with/without indicated concentration of ADR for 24 hours under standard culture conditions. In the inhibitors treatment setting, lymphoma cells were pre-exposed for 30 min to the Bcl-2 inhibitors prior to the subsequent ADR treatment. After centrifugation (1200 rpm, 5´, RT), cell viability was assessed using trypan blue exclusion.

3.2.8.3 Chemotherapy-induced senescence

Reagents, solutions and material

- *Low passage Bcl-2-overexpressing lymphoma cells or MEF (myc - bcl2)*
- *B-cell medium or DMEM medium*
- *Adriamycin (ADR, Doxorubicin)*
- *Various NF-κB inhibitors (Bay11-7082, TPCA-1 and KINK-1)*
- *1x PBS*
- *1x Trypsin*

For lymphoma cells:

Lymphoma cells retrovirally transduced with Bcl2 were harvested and a small aliquot was taken to check cell concentration. 1 x 10^6 – 2 x 10^6 lymphoma cells were seeded onto a 6-well plate with feeder cells. Adriamycin was added to the final concentration of 0.05 µl/ml. After 3 days of culture, the plate was gently rinsed to remove lymphoma cells sticking to the feeder cells and the suspension was centrifuged at 1200 rpm for 5´ (4°C). Cells were resuspended in 4 ml fresh B-cell medium without ADR and seeded in another 6-well plate with new feeder cells. After another 2 days of culture, treated lymphoma cells were tested for their senescent status and used for future experiment.

In the inhibitors treatment setting, lymphoma cells were pre-exposed for 30´ to the indicated inhibitors prior to a subsequent ADR treatment. At day 3, fresh inhibitors were added again into the medium.

For MEF (*myc - bcl2*):

MEF retrovirally transduced with Bcl2 and myc were seeded at subconfluent density (~7.5 × 10^5) in 10 cm plate and incubated for 12 hours until all the cells were attached to the plate. Adriamycin was added to the medium to the final concentration of 0.05 µl/ml. Medium was changed every three days over the experimental period. Fresh adriamycin was added when the medium was changed. Cells were harvested at

different time points for further experiments.

3.2.8.4 Radiation-induced senescence

Reagents, solutions and material

- *Low passage mouse embryonic fibroblasts*
- *DMEM medium*
- *1x PBS*
- *1x Trypsin*

Mouse embryonic fibroblasts were seeded in DMEM culture medium and grown for 12-24 hours. When they reached 60-70% confluency, cells were irradiated with 15 Gy γ-ray and cultivated in low O_2 conditions. Medium was changed every 3 days and cells were harvest at different time points for further experiments.

3.2.8.5 Growth curve analysis

Reagents, solutions and material

- *Low passage lymphoma cells*
- *Conditioned B cell medium*
- *Trypan blue solution (diluted in 1x PBS)*
- *Neubauer counting chamber*

A small aliquot of lymphoma cells was taken to check cell viability and concentration. Equal amounts of lymphoma cells (1x 10^4) were seeded in well-conditioned B cell medium onto a 24-well plate. Cell growth is determined over a defined period and viable cell number was estimated by trypan blue exclusion. To set equal conditions, the same feeder cells and the same conditioned medium were used. Cells were split onto a bigger plate when necessary.

3.2.8.6 SA-β-galactosidase assay

Reagents, solutions and material

- *Senescent lymphoma cells or senescent* mouse embryonic fibroblasts *and their corresponding controls*
- *Cytospin equipment*
- *PBS with 1 mM $MgCl_2$ (pH 5.5)*
- *Freshly prepared fixation solution*
- *Staining solution*
- *DAPI (1 mg/ml stock solution, final 1 µg/ml)*
- *Mowiol 4-88*

For lymphoma cells:

Cells were harvested at the indicated time point. After centrifugation (1200 rpm, 5´, RT), cells were washed in 1x PBS. Cell number and viability were assessed by trypan blue exclusion. 100,000 cells were transferred to a slot of the cytospin plastic and centrifuged at 700 rpm for 8´ (4°C). Supernatant was carefully removed by aspiration.

For mouse embryonic fibroblasts:

24 hours before harvest, cells were detached with Trypsin. After resuspended in culture medium, cells were re-seeded in 12-well plates on glass cover slips and allowed to grow. Before harvest, medium was removed from the plates and cells were washed in 1x PBS.

Afterwards, lymphoma cells or MEF were fixed immediately in freshly prepared fixation solution in order to avoid drying of the slide. After incubation (15´, RT), fixation solution was removed and cells were washed twice in PBS/$MgCl_2$. Staining solution was added dropwise and slides were incubated in the dark in a 37°C incubator (10-16 hours depending on the experiment). Afterwards, the staining solution was removed by aspiration. Cells were gently washed with 1x PBS and mounted while still wet. Slides were analyzed under the microscope and stored at 4°C.

3.2.9 Bacteriological work

3.2.9.1 Transformation of bacteria

Reagents, solutions and material

- *Competent E. coli (DH5α)*
- *Plasmid DNA (500 ng-1 µg)*
- *LB medium*
- *Pre-warmed LB plates (Ampicillin)*

Competent bacteria were thawed on ice. The desired plasmid DNA was added and mixed by gentle flicking of the tube. The mixture was incubated on ice for 30´. Bacteria were heat shocked at 42°C for 1´ and immediately transferred to ice (5´). 1ml LB medium without antibiotic was added and bacteria were incubated at 37°C under gentle agitation for 60´. Bacteria were centrifuged (3000 rpm, 5´, RT) and pellet was carefully resuspended in ~100 µl LB. Suspension was plated on an agar plates containing the right antibiotic and incubated over night at 37°C. Colonies were monitored and picked within one week when stored at 4°C.

3.2.9.2 Plasmid DNA Mini-Preparation of bacterial culture

Reagents, solutions and material

- *Bacteria plate from the transformed DH5α with the plasmid of interest*
- *Pre-warmed LB medium including ampicillin (1 µg/ml)*
- *Ice-cold Solution I including 100 µg/ml RNase A*
- *Freshly prepared solution II*
- *Ice-cold Solution III*
- 2-propanol
- *70% Ethanol*
- *dH_2O*

A single colony of transformed bacteria was incubated in 2 ml LB medium with the

required antibiotic over night (37°C). Bacteria suspension was transferred to an Eppendorf tube, centrifuged at 3000 rpm (5´, 4°C). Medium was removed by aspiration and pellet was lysed by adding 100 µl ice-cold Solution I. Afterwards, 200 µl of freshly prepared Solution II were added and mixed by inverting the tube several times. After 5´ of incubation on ice, 150 µl of ice-cold Solution III were added and dispersed through the viscous bacterial lysate by inverting the tube several times. After centrifugation (14000 rpm, 10´, 4°C), supernatant was transferred to a new Eppendorf tube and 0.4 ml of 2-propanol was added to precipitate DNA. After vortexing and centrifugation (14000 rpm, 10´, 4°C) the pellet was washed with 1 ml of 70% Ethanol and centrifuged again (7500 rpm, 5´, 4°C). Pellet was air-dried and DNA was dissolved in ~30 µl dH_2O. The solution was gently vortexed for a few seconds. DNA concentration was measured with the Nanodrop Spectrophotometer.

3.2.10 Transcriptome and clinical data analysis

*Microarray-based gene expression profiling of mouse lymphomas was conducted by Jan Dö*rr*, Drs. Maja Milanovic, Julia Kase and Dido Lenze.*

For microarray-based gene expression profiling, RNA was isolated from untreated or 5-day ADR-treated control;bcl2 Eμ-*myc* lymphomas using the RNeasy minikit (Qiagen) and hybridized to Affymetrix Mouse Genome 430 2.0 microarrays (Affymetrix) according to the manufacturer's instructions. The arrays were hybridized and washed in the GeneChip Fluidics Station 450, and signals were detected on an Affymetrix GeneChip Scanner 3000. Affymetrix files were imported into Partek Genomic Suite software (version 6.4, Partek, Inc.) and processed by the implemented robust multiarray (RMA) work flow (consisting of median polish probe set summarization, RMA background correction, and quantile normalization). The raw microarray data were deposited at the Gene Expression Omnibus (GEO) repository of the National Center for Biotechnology Information under the accession number GSE31099 (http://www.ncbi.nlm.nih.gov/geo/query/acc.cgi?acc=GSE31099). For

further analysis of mouse microarray data, genetic signatures of NF-κB activation were taken without further change from the Thomas Gilmore laboratoryWeb site (a complete list of genes and related references is available at http://www.bu.edu/nf-kb/gene-resources/target-genes). The enrichment of NF-κB target gene sets within the global transcript signals from matched pairs of untreated versus ADR-treated control;bcl2 lymphoma cells was analyzed by applying the GSEA version 2.0 software (Broad Institute of the Massachusetts Institute of Technology and Harvard, http://www.broad.mit.edu/gsea). Normalized enrichment scores (NES) reflect a statistically significant enrichment for P-values <0.05 and FDR (false discovery rate) values <0.25 (Subramanian et al. 2005).

Clinical data analysis was done in cooperation with the lab of Prof. Georg Lenz.

Gene expression data of lymphoma biopsies from 233 patients, who were treated with R-CHOP-like immunochemotherapy and profiled using Affymetrix HG-U133 Plus 2.0 microarrays (Lenz et al. 2008b), were obtained from the NCBI GEO (GSE10846). Patients were classified into ABC DLBCL, GCB DLBCL, and unclassified DLBCL according to Lenz et al (2008b). The 100 GCB DLBCL patient samples, for which clinical follow up information for progression-free survival was available, were equally divided into groups of high and low Bcl2 expression, based on the median expression. Within these two cohorts, patients were subsequently divided into high and low NF-κB groups according to the median expression of a previously described NF-κB gene expression signature consisting of 63 known NF-κB target genes (http://lymphochip.nih.gov/cgi-bin/signaturedb/signatureDB_DisplayGenes.cgi?signatureID=83; Shaffer et al. 2006).

3.3 Experimental setting

To elucidate the function of the NF-κB pathway in senescence, primary Eμ-*myc* transgenic mouse lymphomas, a well-established model for human aggressive B-cell non-Hodgkin's lymphomas (B-NHL) were stably transduced with the NF-κB SR (or an empty vector as a control) as well as Bcl2 to prevent drug-induced apoptosis. After inhibition of the NF-κB pathway and the induction of senescence by chemotherapy, growth effect and NF-κB activity as well as SASP were measured *in vitro* (Fig. 10A).

To further investigate the function of the NF-κB pathway in senescence *in vivo*, Bcl2 overexpressing lymphomas with/without NF-κB inhibition were transplanted into syngeneic recipients by tail vein injection. When lymph nodes became palpable in recipient animals, mice were exposed to chemotherapy and lymphoma senescent ability was measured in situ (Fig. 10B).

Additionally, to find out the subgroup of human lymphoma patients in which hyperactive NF-κB contributes to treatment outcome, we applied a novel method- "cross-species investigations" in cooperation with the group of Prof. Georg Lenz (Charité). First, primary mouse lymphomas were characterized and genetically engineered according to distinct NF-κB related oncogenic networks reminiscent of diffuse large B-cell lymphoma (DLBCL). Suggested by the results in the mouse lymphoma model, gene expression profiling of human diffuse large B-cell lymphoma samples at diagnosis were analyzed to identify the clinically relevant subgroup (Fig. 10C).

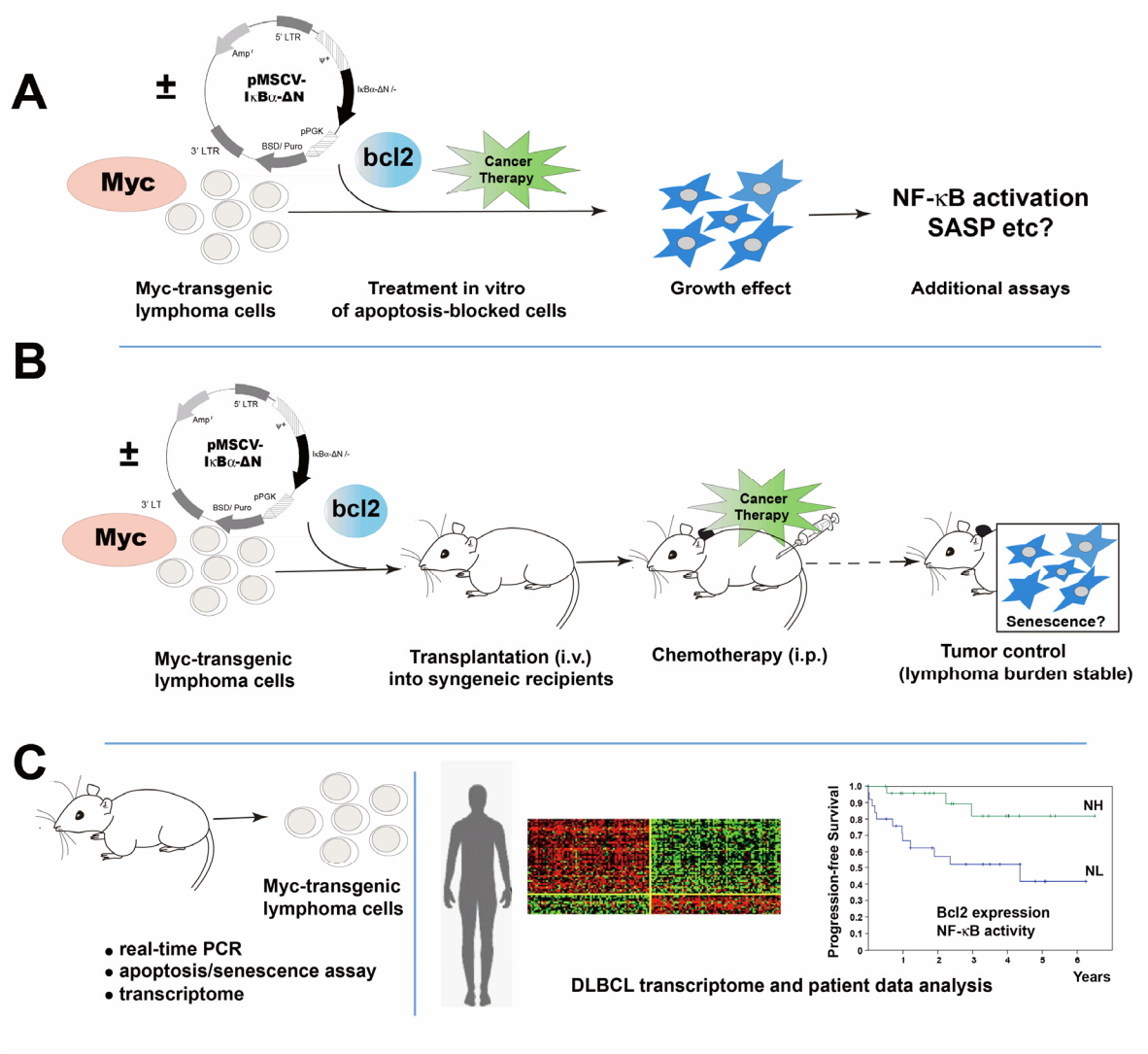

Fig 10: Experimental outline. (A) *In vitro* investigation of NF-κB's function in senescence. (B) *In vivo* investigation of NF-κB's function in senescence. (C) "Cross-species investigations" to identify a clinical relevant subgroup.

4 Results

The experiments finished by collaborations are listed here:

- *Microarray-based gene expression analysis of mouse lymphomas was done by Jan Dö*rr*, Drs. Maja Milanovic, Julia Kase and Dido Lenze.*

- *Animal experiments were done by Drs. Soyoung Lee and Julia Kase.*

- *Clinical data analysis was done in cooperation with the laboratory of Prof. Georg Lenz.*

4.1 NF-κB activity is increased in therapy-induced senescence

4.1.1 Therapy-induced senescence in lymphoma cells

To assess the role of NF-κB in senescence, an *in vitro* TIS model was established using primary *Myc*-driven B-cell lymphomas (referred to as ‘‘control’’ lymphomas) isolated from Eμ-*myc* transgenic mice (Schmitt et al. 2002 a). Although senescence can be induced by conventional chemotherapy in *Myc*-driven B-cell lymphomas, it is often masked by a faster apoptotic response. Therefore, primary lymphomas were stably transduced with bcl2 to prevent drug-induced apoptosis, and exposed to the DNA-damaging chemotherapeutic agent adriamycin (ADR). At day 5, ADR-treated control;bcl2 lymphomas were fully growth-arrested (Fig. 11A), stained negative for the proliferation marker Ki67, and uniformly exhibited senescence-associated β-galactosidase activity (SA-β-gal) (Fig. 11B).

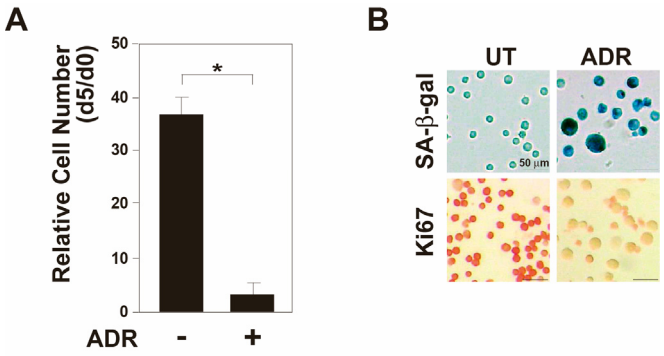

Figure 11: Features of ADR-induced senescence in Eμ-*myc* transgenic control lymphomas *in vitro*. (*A*) Growth curve analysis of ADR (50 ng/ml) treated-senescent *vs.* untreated (ut) control;bcl2 lymphomas presented as relative growth at day 5/day 0 (*n* = 5 samples each; histogram bars indicate mean values ± SDEV; * indicates P<0.05). (*B*) Representative photomicrographs of lymphoma samples as in *A* stained for SA-β-gal (*top*) or Ki67 (*bottom*); *n* > 25 samples, scale bars indicate 50 μm.

4.1.2 Therapy-induced senescence is accompanied by NF-κB activation

Senescent cells are characterized by altered pattern of gene expression. To unveil TIS-related changes on the transcriptome level, genome-wide microarray gene expression profiles (GEPs) were generated from 12 matched pairs of primary control;bcl2 lymphomas that were either drug-senescent or untreated. Gene set enrichment analysis (GSEA) demonstrated that NF-κB target genes as a whole, and NF-κB-controlled cytokines in particular, were strongly skewed toward the TIS group (Fig. 12).

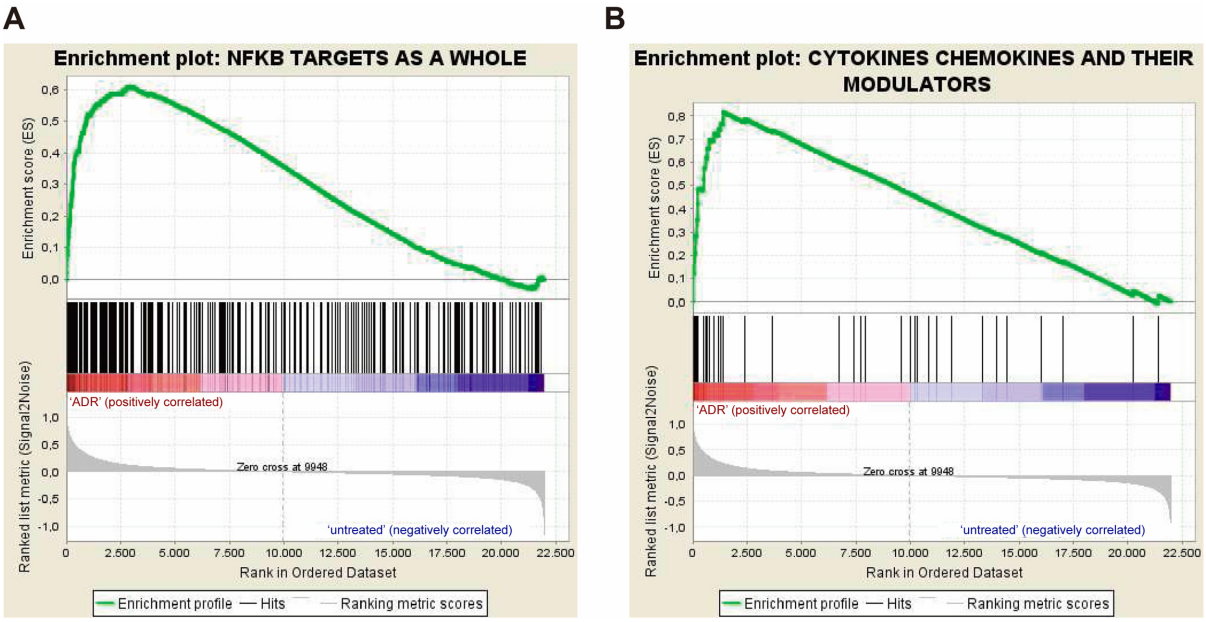

Figure 12: Gene set enrichment analysis of ADR-senescent *vs.* untreated (ut) Eμ-*myc* control;bcl2 lymphomas. Gene set enrichment analyses of NF-κB targets (*A*) and the subset of cytokines and their modulators therein (*B*) in the GEP of ADR-senescent (ADR) *vs.* untreated (ut) Eμ-*myc* control;bcl2 lymphomas (*n* = 12 matched pairs).

In line with the increased transcription of NF-κB target genes, the activation of the NF-κB pathway is also characterized by enhanced DNA-binding activity. In matched

pairs of untreated versus senescent lymphomas, endogenous NF-κB-DNA binding activity was analyzed in nuclear extract from lymphomas. Using a multiplex DNA-binding ELISA-based analysis, significantly higher DNA-binding activities for the four NF-κB family subunits p50, p52, p65 (RelA), and RelB in senescent cells were detected, indicating that both the classical and the alternative NF-κB pathways are activated in TIS (Fig. 13A). Matched-pair analyses of the p65 DNA binding activity in the same individual lymphomas are highlighted in Fig.13B.

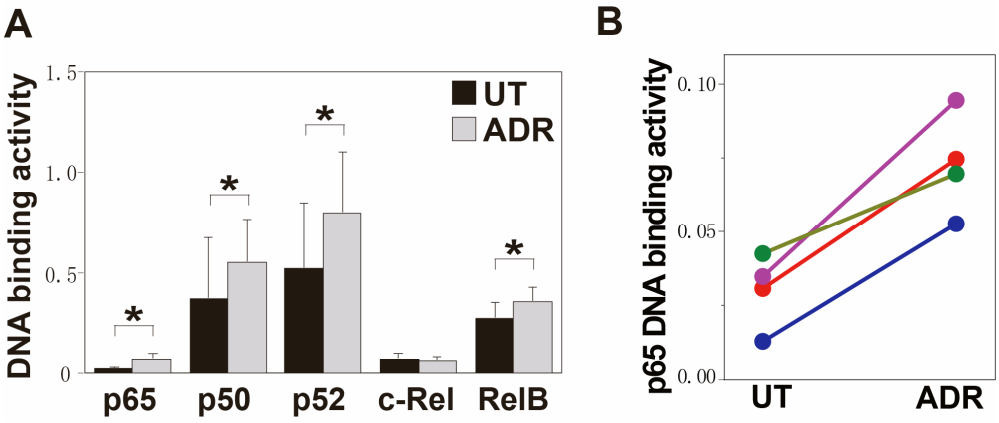

Figure 13: DNA binding activity of ADR-senescent *vs.* untreated (ut) Eμ-*myc* control;bcl2 lymphomas. (*A*) DNA binding activity of the indicated NF-κB subunits in ADR-senescent and untreated (ut) Eμ-*myc* control;bcl2 lymphomas ($n \geq 3$ matched pairs per subunit; * indicates $P<0.05$). (*B*) Matched untreated/ADR-senescent lymphoma pairs for the p65 DNA binding activity. NF-κB DNA binding activity was determined using TransAM™ NF-κB Family ELISA Kit.

Furthermore, a lunciferase-based assay also confirmed the higher DNA-binding and transcriptional activation of NF-κB in senescent lymphomas. Primary control;bcl2 lymphomas were stably transfected with the NF-κB-luciferase reporter. After 5-day-treatment with ADR, luciferase activity was measured in matched pairs of untreated versus senescent lymphomas. As shown in Figure 14, luciferase activity in senescent lymphoma was significantly higher than untreated lymphoma, indicating higher NF-κB DNA binding and transcriptional activity in senescent cells.

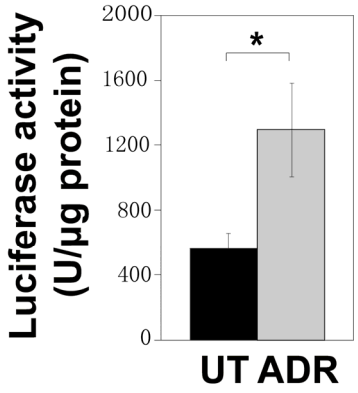

Figure 14: Luciferase activity of an NF-κB-luciferase reporter in ADR-senescent *vs.* untreated (ut) Eμ-*myc* control;bcl2 lymphomas. Eμ-*myc* control;bcl2 lymphomas were stably transfected with NF-κB luciferase reporter plasmid, and exposed to ADR to induce senescence. The NF-κB activity in lymphomas was measured by the luciferase activity assay. Firefly-luciferase activity was normalized to the amount of protein (n = 4; the data represent mean values ± SDEV; * indicates $P<0.05$).

In accordance with the increased DNA binding activity of NF-κB in senescent cells, immunofluorescence stained p65 in TIS lymphomas predominantly in the nucleus, while nonsenescent cells displayed a preferentially cytoplasmic localization (Fig.15A). In addition to nuclear translocation and enhanced DNA-binding activity of NF-κB, optimal induction of NF-κB target genes also requires phosphorylation of NF-κB proteins, such as p65, within their transactivation domain by a variety of kinases in response to distinct stimuli. DNA-damaging agents, in addition to their ability to target IκBα degradation via an IKK-independent pathway, also lead to p65 phosphorylation at Ser536 (Viatour et al, 2005), which can be observed by immunoblot analysis. As expected, TIS lymphomas presented with induced expression levels of Ser536-phosphorylated p65 (p65-P-S536), indicating increased p65 transactivation capacity in senescent cells (Fig. 15B).

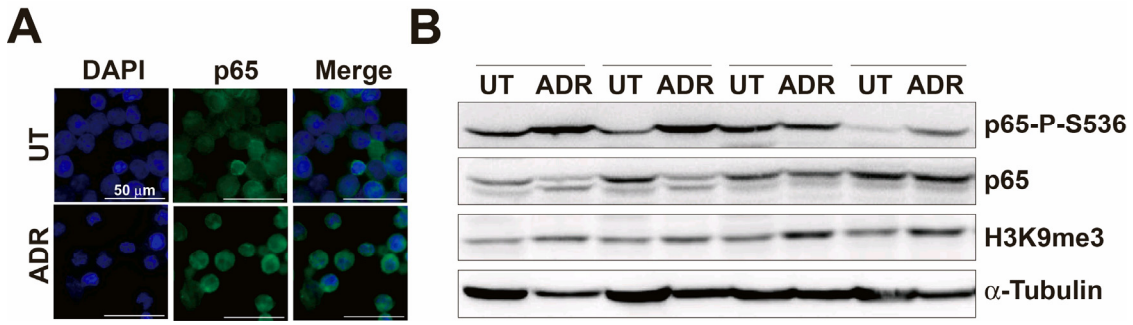

Figure 15: (A) Immunofluorescence of the NF-κB subunit p65 in cytospin preparations of ADR-senescent *vs.* untreated (ut) Eμ-*myc* control;bcl2 lymphomas (representative example of three cases analyzed; scale bars indicate 50 µm). (B) Immunoblot analyses of the indicated proteins in cell lysates from four matched lymphoma pairs. Whole cell lysates from lymphomas were evaluated by immunoblotting using antibodies specific for total p65, phospho-p65 (p65-p-S536), H3K9me3 and α-Tubulin. H3K9me3 serves as a senescence marker and α-Tubulin serves as a loading control.

To confirm NF-κB activity at the level of individual target genes, the expression of transcripts that were among the differentially regulated gene products in the microarray analysis was measured by quantitative real-time PCR (RQ-PCR). For instance, *IκBα*, *CycD2*, *c-Flip*, *Irf4* and *Ccr7* are literature-defined NF-κB signature genes for mouse and human lymphoma characterization (Davis et al. 2001). *Il1α*, *Il6*, *Cxcl1*, *CCL2* and *Igfbp6* contain NF-κB binding sites in their promoter region and belong to the SASP factors (Acosta et al. 2008; Kuilman et al. 2009). *CXCR2* (chemokine receptor 2), which is an NF-κB target gene, reinforces the growth arrest of senescent cells in a positive feedback loop through its ability to boost the DNA damage response (Acosta et al. 2008). *Igfbp7* is one of the secreted factors from senescent cells, but there is no NF-κB binding site in its promoter region. As shown in Fig. 16, all NF-κB target genes tested—non-secreted genes and SASP factors in particular—were expressed at higher levels in TIS compared with non-senescent lymphoma cells.

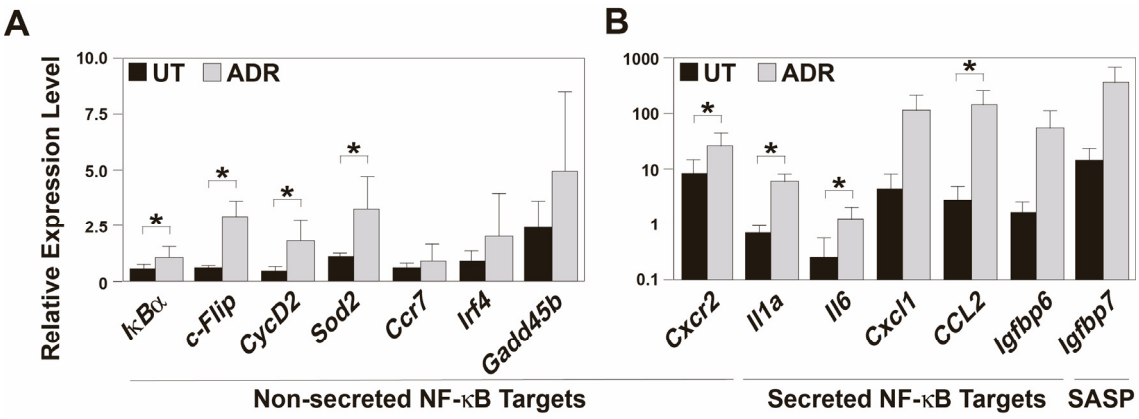

Figure 16: Quantitative real-time RT-PCR (RQ-PCR) analyses of the indicated non-secreted (A) and secreted transcripts (B) in lymphomas as in *Figure 12* (*n* = 5 samples each). Total RNA was extracted and analyzed by RT-PCR with primer sets specific for the indicated transcripts. Shown are relative expression levels, normalized to an internal control (*GAPDH*), that are comparable throughout all data sets (note the log-scaled presentation in the cytokine panel). All histogram bars indicate mean values ± SDEV; * indicates P<0.05.

Taken together, therapy-induced senescence exhibits a senescence-associated secretory phenotype. Activated NF-κB signaling is a prominent feature of chemotherapy-related senescence in full-blown tumor cells.

4.1.3 NF-κB activity is increased in senescent mouse embryonic fibroblasts

Using a simplified TIS model based on mouse embryonic fibroblasts (MEF), we further confirmed that the NF-κB pathway is activated during the process of senescence. Mouse embryonic fibroblasts were first stably transduced with *myc* and *bcl2* to mimic the bcl2 overexpressing Eμ-*myc* transgenic lymphomas model, and then exposed to the DNA damaging chemotherapeutic agent adriamycin (ADR). MEF were harvested at the indicated time. The senescence phenotype, the NF-κB pathway status and the SASP were tested in ADR-treated and untreated cells. As shown in Fig. 17, SA-β-gal-positive cells were detectable two days after ADR

treatment. Meanwhile, immunofluorescence staining of p65 in nuclei increased in ADR treated cells, indicating the nuclear translocation and also the increased expression of p65 in senescent cells. Four days after ADR treatment, with a persistent p65 nuclear localization, MEF uniformly exhibited SA-β-gal activity.

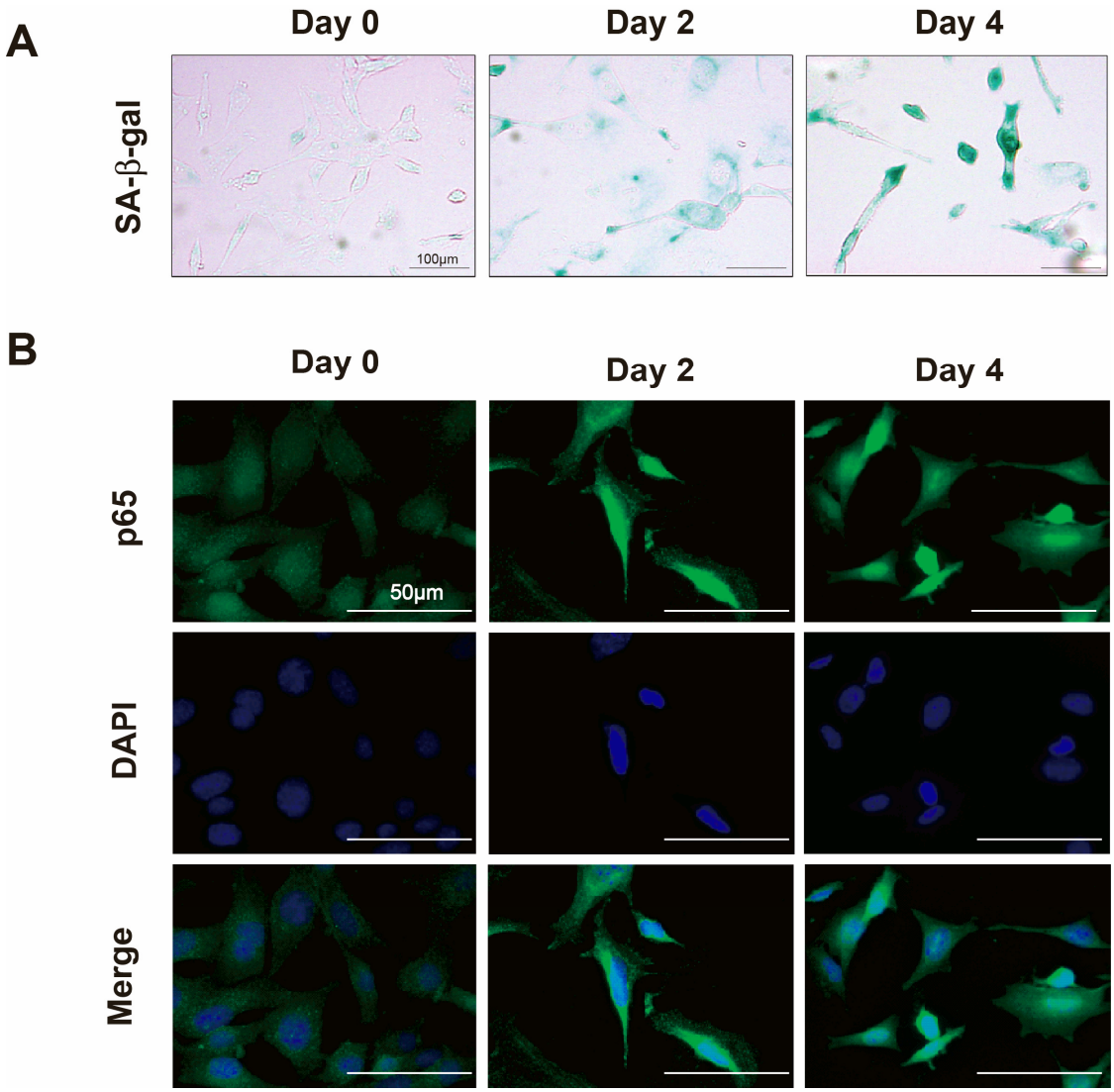

Figure 17: ADR-induced senescence in MEF (*myc* - *bcl2*). (*A*) Photomicrographs of MEF stained for SA-β-gal at different time points (scale bars indicate 100 µm). (*B*) Nuclear translocation of p65 coincides with senescence. MEF overexpressing myc and bcl2 were treated with ADR (0.05 µl/ml) for the indicated time. Cells were stained with fluorescence-conjugated anti-p65 antibodies and counterstained with DAPI (representative example of three cases analyzed; scale bars indicate 50 µm).

Furthermore, the expression of NF-κB target genes, *Ccl20*, *Mcp1*, *Il7* and *Ptgs2* was detected by RQ-PCR at different time points. As show in Fig. 18, a higher expression level of the respective genes was detected two days after ADR treatment. Four days after treatment, all NF-κB target genes tested were expressed at higher levels in senescent MEF compared with non-senescent cells. The high expression of *Ccl20*, *Mcp1* and *Il7*, which encode NF-κB target SASP factors, not only confirmed the activation of NF-κB in senescent cells, but also indicated that SASP appear as a common feature of senescent cells.

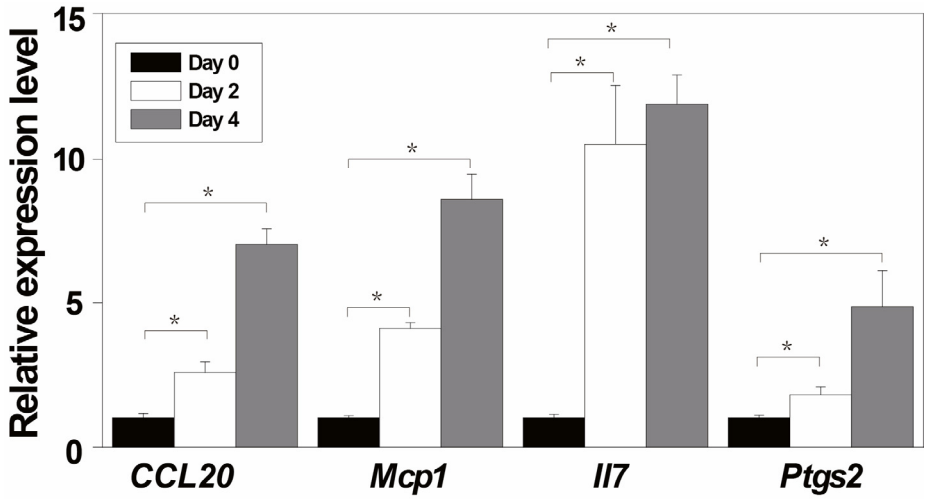

Figure 18: Quantitative real-time RT-PCR (RQ-PCR) analyses of the indicated NF-κB target genes in MEF (*myc* - *bcl2*). Shown are relative expression levels, normalized to an internal control (*GAPDH*). All histogram bars indicate mean values ± SDEV; * indicates P<0.05.

Taken together, the results in the simplified MEF model confirmed that NF-κB signaling is activated in the process of therapy-induced senescence.

4.2 TIS depends on intact NF-κB function *in vivo*

4.2.1 Inhibition of the NF-κB pathway ablates the SASP in TIS

The data presented in 5.1. demonstrated that TIS cells display a senescence-associated secretory phenotype, and, in addition, are characterized by NF-κB activation. Given the fact that many SASP factors contain NF-κB binding sites in their promoter region, we predicted that the senescence-associated secretory phenotype is, at least partly regulated by the NF-κB pathway.

To address whether SASP depends on enhanced NF-κB activity, a NF-κB super repressor IκBα-ΔN (SR) - a nondegradable IκBα moiety, containing amino-acid residues 71–317 of IκB-alpha (Krappmann et al. 1996) - was used to inhibit the NF-κB pathway. Eμ-*myc* control;bcl2 lymphomas were stably transfected with the SR or an empty vector as control and the expression of IκBα-ΔN was detected by immunoblot analyses. As shown in Fig. 19A, IκBα-ΔN was only detected in lymphomas transfected with the SR, but not in the control setting.

Next, proper functionality of the SR was tested in a TNF-α treatment setting. Lymphoma cells were treated with TNF-α at 50 μM for 24 hours and the expression levels of NF-κB target genes were detected by RQ-PCR. In response to TNF-α, NF-κB target genes in lymphomas were induced and then further inhibited by SR (Fig.19B). Meanwhile, cells expressing the SR showed lower p65 signaling and no p65 nuclear translocation upon short-term TNF-α treatment (Fig. 19C). To address the question whether the SR affects the proliferating character of lymphoma cells, proliferation of the lymphomas transduced with Vector or SR was assessed by a 6-day growth curve under standard culture conditions as described in the Materials and methods section. The result suggests that SR has little impact on proliferation in

untreated lymphoma cells (Fig. 19D).

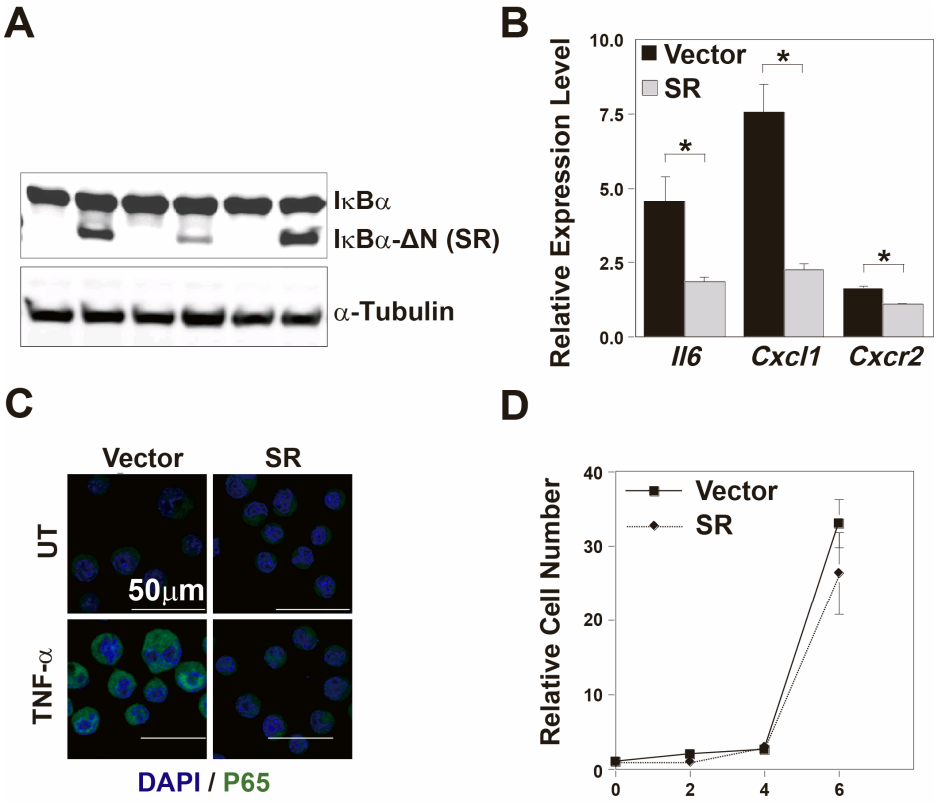

Figure 19: Inactivation of NF-κB by stable expression of IκBα-ΔN (SR). (*A*) Expression of NF-κB super repressor IkBa-ΔN (SR) in three matched lymphoma pairs detected by Immunoblot analyses. Thirty micrograms of whole cell lysate from lymphomas stably transfected with empty vector (Vector) or IκBα-ΔN (SR) were evaluated by immunoblotting using antibodies specific for IκBα and α-Tubulin. (*B*) RQ-PCR analyses of the indicated transcripts after 24 hours of TNF-α treatment (*n* = 5 samples each). (*C*) Proper functionality of the NF-κB super repressor IκBα-ΔN (SR) in TNF-α-exposed Eμ-*myc* lymphoma cells, as demonstrated by the inhibition of nuclear translocation of the NF-κB subunit p65 after 30 minutes (anti-p65 immunofluorescence with DAPI as nuclear counterstaining; representative example of three independent cases, scale bars indicate 50 μm). (*D*) Growth curve analysis of untreated control lymphomas stably expressing the SR or vector-infected (representative comparison of one individual lymphoma ± SR shown; *n* = 5 samples).

Then the SR was further used to investigate the function of NF-κB regarding the

senescence-associated secretory phenotype. Control;bcl2 lymphomas stably expressing the SR or the empty vector were treated with ADR for 5 days to induce senescence. Gene expression was determined by real-time PCR and normalized by the level of *GAPDH* as an internal control. Because the initial fold induction after ADR treatment varied in such a large scale, to facilitate easy comparison, the relative expression levels of ADR-treated cells compared to UT cells (ADR/UT) was calculated first and this value of SR cells was compared to that of vector control, to get the fold reduction. In treatment induced senescence, the expression of most NF-κB target genes—both SASP and nonsecreted genes—was sharply reduced in the ADR-exposed SR engineered control;bcl2 lymphoma group, as further highlighted in matched-pair analyses of the same individual lymphomas with or without the SR moiety for representative NF-κB-controlled SASP factors (Fig. 20).

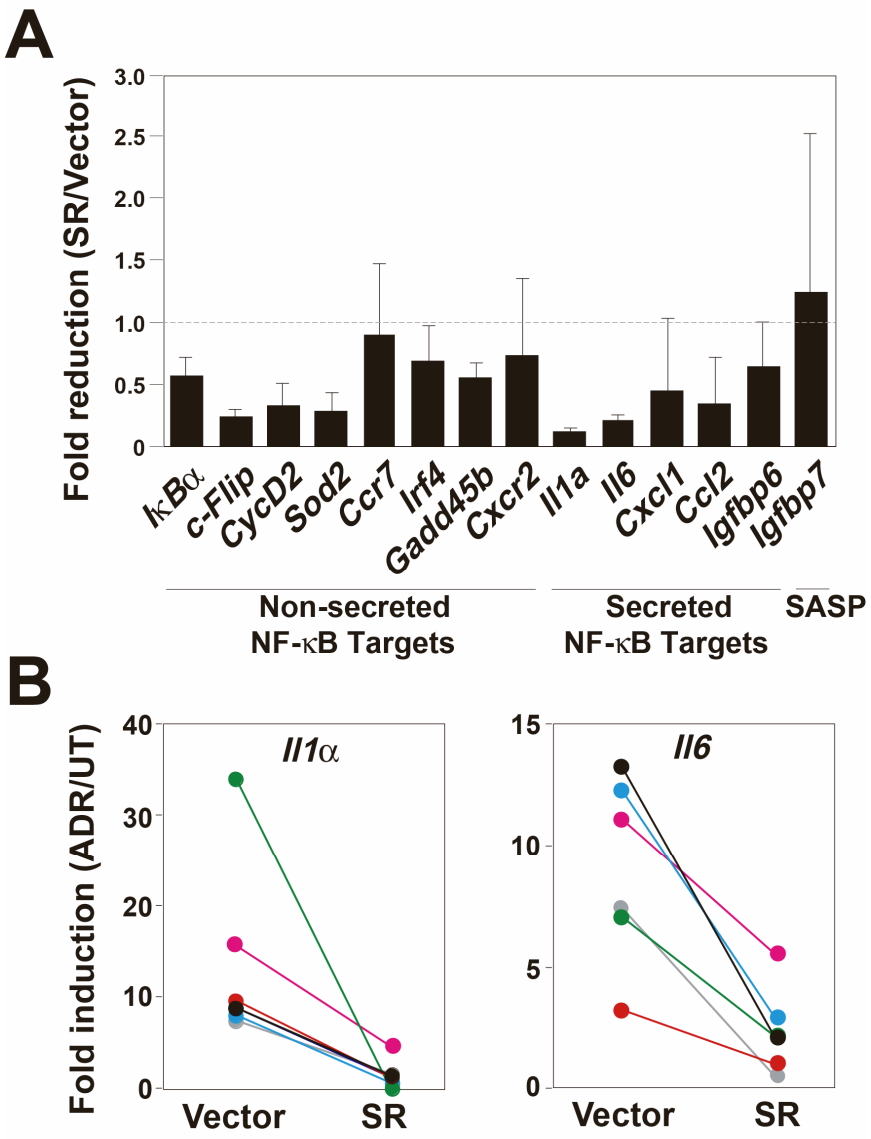

Figure 20: The expression of NF-κB target genes in the ADR-exposed SR/empty engineered control;bcl2 lymphoma group. (*A*) RQ-PCR analyses of the indicated transcripts in lymphomas presented as the ratio of the relative values for ADR-exposed *vs.* untreated control;bcl2 lymphomas stably expressing the NF-κB super-repressor IκBα-ΔN (SR) or being empty vector-infected as a control (at least five samples each). (*B*) Matched ADR-exposed control;bcl2 lymphoma pairs ± SR shown for the relative expression levels of two representative SASP factors.

Likewise, NF-κB inhibitors also prevent the induction of SASP factors in senescent cells. Control;bcl2 lymphoma cells were treated with ADR in combination with a

variety of pharmacological NF-κB inhibitors and the expression levels of NF-κB targets were measured. As shown in Fig. 21, Bay11-7082, an IκBα phosphorylation inhibitor, suppressed the expression of *Il1α*, *Il6*, *Cxcl1*, *Cxcr2*, *Ccl2* and *Gm-csf* in senescent cells. TPCA-1 and KINK-1, both are IKK-2 inhibitors, suppressed the expression of *Il1α*, *Il6* and *Gm-csf*, but not other genes tested in senescent cells, suggesting that Bay11-7082 is a more efficient NF-κB inhibitor.

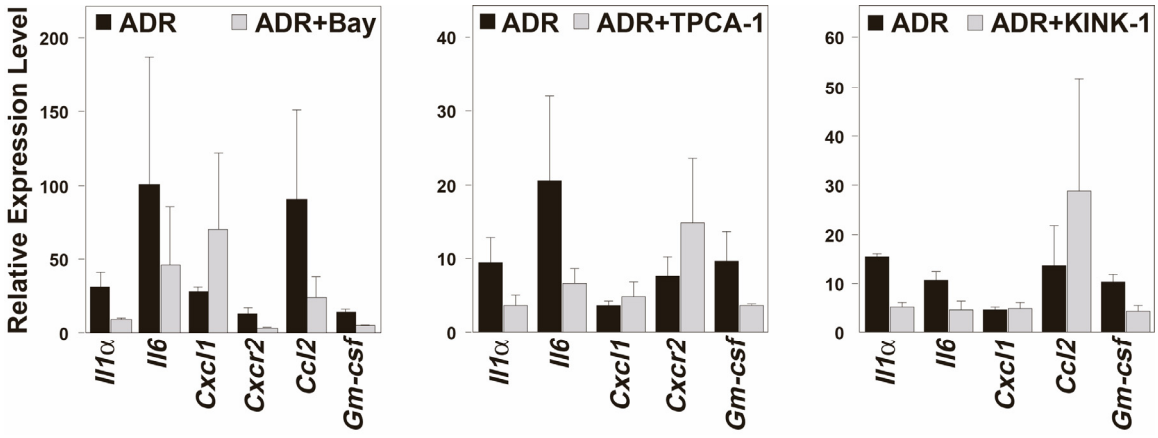

Fig. 21: RQ-PCR analyses of the indicated transcripts in lymphomas presented as the ratio of the relative values for ADR-exposed *vs.* untreated control;bcl2 lymphomas, with or without preceding exposure to the indicated pharmacological NF-κB inhibitors (*i.e.* Bay11-7082 [Bay; *left*], TPCA-1 [*center*], and KINK-1 [*right*]; at least five samples each). Note that values are not comparable between inhibitor panels, because different individual lymphomas were used. All histogram bars indicate mean values ± SDEV.

In summary, NF-κB acts as a master regulator of the SASP in therapy-induced senescence, as revealed by genetic and pharmacological inhibition of the NF-κB pathway.

4.2.2 Inhibition of the NF-κB pathway ablates the SASP in radiation-induced senescence

In addition to chemotherapy, senescence can also be induced by radiation therapy.

The results in primary lymphoma cells demonstrate that the senescence-associated secretory phenotype depends on NF-κB activation. To address the question whether the dependency of the SASP on NF-κB signaling is a common mechanism or a context-dependent phenomenon, mouse embryonic fibroblasts were subjected to ionizing radiation to induce senescence. Ten days after irradiation, MEF were fully growth-arrested and exhibited senescence-associated β-galactosidase activity. Meanwhile, senescent MEF showed the senescence-associated secretory phenotype Fig. 22A and C).

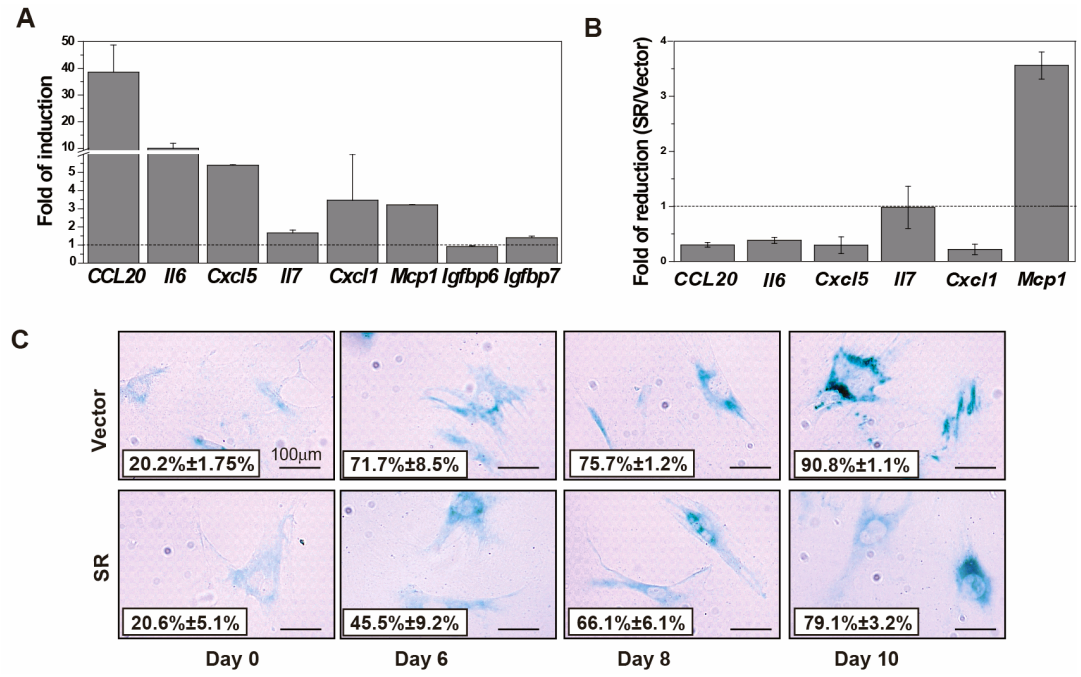

Figure 22: The SASP depends on NF-κB signaling in irradiation-induced senescence. *(A)* RQ-PCR analyses of the indicated transcripts in MEF ten days after irradiation *vs.* untreated MEF. Changes are expressed as fold of induction relative to untreated MEF. (*B*) Ten days after irradiation, RQ-PCR analyses of the indicated transcripts in MEF presented as the ratio of the relative values for radiation-exposed *vs.* untreated MEF stably expressing the NF-κB super-repressor IκBα-ΔN (SR) or being empty vector-infected as a control. Shown are relative expression levels, normalized to an internal control (*GAPDH*). All histogram bars indicate mean values ± SDEV. (*E*) Photomicrographs of MEF stained for SA-β-gal at the indicated days (scale bars indicate 100 μm). Note that the gene expression pattern of SASP in MEF and lymphomas is slightly different.

To understand the function of NF-κB in SASP in the radiation-induced senescence model, the stably expressed NF-κB super repressor IkBa-ΔN (SR) was used to inhibit the NF-κB pathway. The expression of SASP factors was tested in irradiated and untreated MEF at different time points. The real-time PCR results demonstrate that NF-κB inhibition sharply reduced the expression levels of NF-κB targeted SASP factors (Fig. 22B). Meanwhile, the percentage of SA-β-gal positive cells is slightly lower in the irradiated SR engineered MEF (Fig 22C). These findings suggest that NF-κB activation is necessary for secretion of at least some SASP components in MEF. These data, together with previous results on lymphomas, indicate that the dependency of SASP on the NF-κB pathway is a common mechanism.

4.2.3 TIS depends on intact NF-κB function

The obvious next question was whether TIS not only presents with enhanced NF-κB activity, but also depends on it. The senescence capability of lymphomas expressing the NF-κB superrepressor IκBa-ΔN (SR) was tested *in vitro*. SA-β-gal-based analyses of matched pairs differing only in their SR status revealed a spectrum that reached from a substantial decline in the percentage of SA-β-gal-positive cells in some to an uncompromised TIS phenotype in other lymphomas of the SR cohort, reflecting a mean reduction of SA-β-gal reactivity by >30% (Fig. 23A). Collectively, these data suggest a modest contribution of putative pro-senescent NF-κB-governed functions in a homotypic tumor cell population—Irrespective of their intracellular, autocrine, or paracrine modes of action (Acosta et al. 2008; Kuilman et al. 2008) - at least in a subset of genetically susceptible primary tumors. Rather than functioning as a linear and essential component of the DDR-initiated senescence pathway, it is very well conceivable that the NF-κB network operates as a corroborating, collateral relay of the prosenescent DDR. In such a scenario, the uniform exposure of all cells to a chemotherapeutic agent in culture would probably launch such a strong DDR cascade in every given cell that a quantitative reduction of a senescence-reinforcing principle by the SR will not instantly translate into a senescence-defective phenotype

—except collateral prosenescent pathways became dysfunctional, thereby making the contribution of NF-κB signaling to TIS critical.

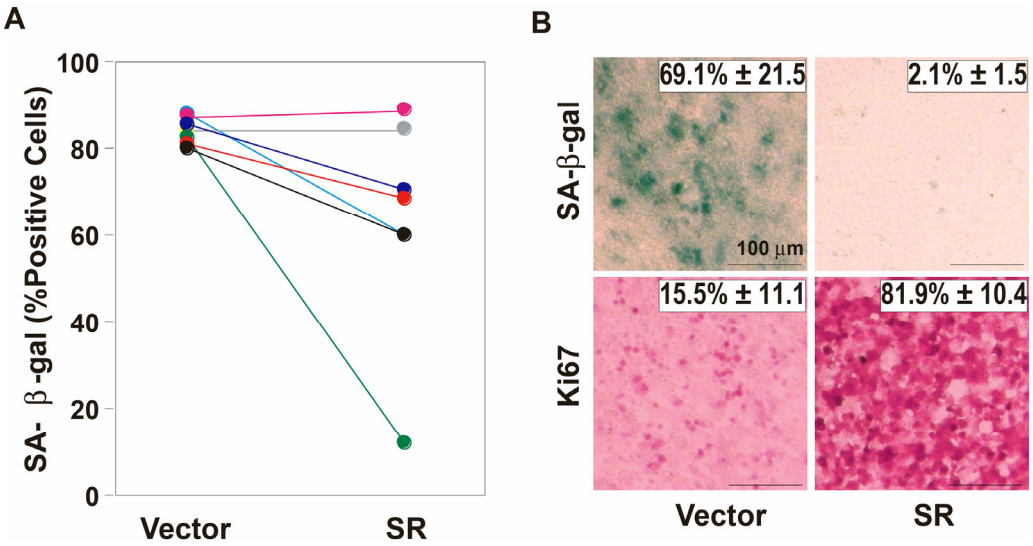

Figure 23: TIS depends on intact NF-κB function. (*A*) Frequencies of SA-β-gal-positive cells from matched lymphoma pairs ± SR, exposed to ADR *in vitro* (*n* = 7 pairs). (*B*) *In situ*-frequencies of SA-β-gal-positive as well as Ki67-positive cells in matched-pair (± SR) lymphoma sections, exposed to CTX *in vivo* (*n* = 3 pairs; representative photomicrographs shown, scale bars reflect 100 μm). All histogram bars or numbers indicate mean values ± SDEV.

The *in vivo* situation is by far more complex, including aspects such as inhomogeneous drug delivery and heterotypic cell–cell interactions that were not covered by *in vitro* analyses. To address the potential contribution of NF-κB activity to a drug-inducible senescence phenotype in a scenario most closely recapitulating the natural tumor situation, genetically compatible transplant lymphomas were investigated *in vivo*. Control;bcl2 lymphomas retrovirally infected with the SR construct or an empty vector for comparison were transplanted into normal, immunocompetent recipient mice, where they formed systemic lymphomas indistinguishable from the primary transgenic host they were initially derived from. At the time a peripheral lymphadenopathy became palpable, mice harboring a

comparable tumor burden were treated once with the DNA-damaging anti-cancer agent cyclophosphamide (CTX), and lymphomas were analyzed for in situ signs of TIS 5 days later. Intriguingly, while control lymphomas showed a strong SA-β-gal reactivity and less than 20% Ki67-positive cells, TIS-competent SR lymphomas presented with virtually no SA-β-gal reactivity and >80% Ki67-positive cells following CTX exposure *in vivo* (Fig. 23B).

Therefore, SR-expressing lymphomas displayed a much more profound TIS defect *in vivo*, even if they exhibited only some reduction of their SA-β-gal reactivity *in vitro*, indicating a critical, NF-κB-dependent prosenescent contribution of bystander cells within the tumor microenvironment. Of note, senescence-associated interaction with host immune cells is cocontrolled by NF-κB activity as well (Chien et al. 2011; Xue et al. 2007), thereby suggesting immune-mediated clearance of senescent cells as another link by which NF-κB may control tumor growth. Taken together, the NF-κB network operates as a critical component of the drug-inducible senescence response, whereby the actual quantitative impact of its interference with cell-autonomous and non-cell-autonomous senescence-relevant processes can only be appreciated *in vivo*.

4.3 Oncogenic networks determine opposing roles of NF-κB on treatment outcome

In human diffuse large B-cell lymphoma, the ABC subgroup is associated with constitutive activation of NF-κB and has poor treatment outcome. It is reported that the ability of NF-κB to inhibit responses to cancer therapeutic agents may contribute to the refractory clinical behavior of ABC DLBCL (Baldwin et al. 2001). Our data in mouse lymphoma model unveiled that the NF-κB network operates as a critical component of the drug-inducible senescence response. Since senescence contributes to the outcome of cancer therapy, we asked the question whether hyperactive NF-κB contributes to treatment outcome in human lymphoma patients. To find the subgroup in which hyperactive NF-κB benefits the treatment outcome, primary mouse lymphomas were characterized and genetically engineered according to distinct NF-κB-related oncogenic networks reminiscent of diffuse large B-cell lymphoma.

4.3.1 NF-κB-mediated chemoresistance results in poor treatment outcome in ABC-reminiscent lymphomas

To quantify and dissect the contribution of NF-κB signaling to the long-term outcome of naturally formed B-cell lymphomas prior to any therapy, twelve primary Eμ-*myc* lymphomas were grouped according to endogenous NF-κB activation assessed by nuclear p65 DNA-binding ELISA. Accordingly, lymphomas were grouped as an ‘‘NF-κB low’’ (NL, the four lowest cases) and an ‘‘NF-κB high’’ (NH, the four highest cases) cohort (Fig. 24).

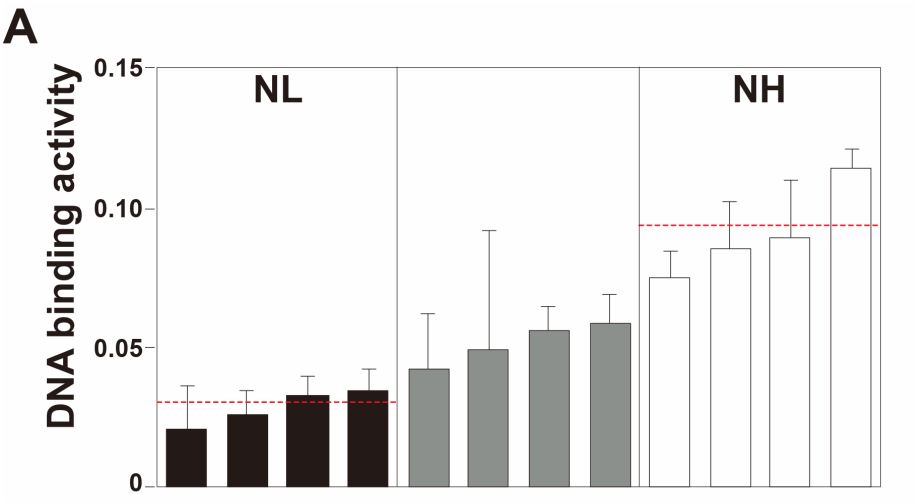

Figure 24: Classification of primary control lymphomas by the NF-κB status. Stratification of twelve primary control lymphomas in an "NF-κB low" (NL; black bars), an intermediate (grey bars), and an "NF-κB high" (NH; white bars) group according to their NF-κB p65 DNA binding activities at diagnosis. Primary lymphoma cells were cultured for 24 hours *in vitro* to eliminate normal cell contamination. Nuclear extracts were prepared, and 5 µg of the nuclear extract protein was used for ELISA-based DNA binding assay (measured in triplicate; horizontal lines indicate mean activity within the respective group).

Constitutive activation of NF-κB is an important anti-apoptotic mechanism in B-cell lymphomas with poor prognosis. Therefore, the apoptotic potential of these lymphomas was detected by their short-term drug sensitivity. Lymphomas were treated *in vitro* with 5 ng/ml of ADR for 24 hours and cell viability was measured by trypan blue. Expectedly, the NH group was virtually resistant to ADR, while lymphoma cells of the NL group quantitatively died at the same dose level (Fig. 25A).

Since Bcl2 is frequently detected at overexpressed levels in human B-cell lymphomas and a *bona fide* NF-κB target, we reasoned that chemoresistance in NH lymphomas might be mediated, at least in part, via induction of Bcl2 (Schmitt et al. 2000; Feuerhake et al. 2005). Indeed, Bcl2 transcript levels, measured by RQ-PCR, were significantly higher in the NH compared with the NL group (Fig. 25B).

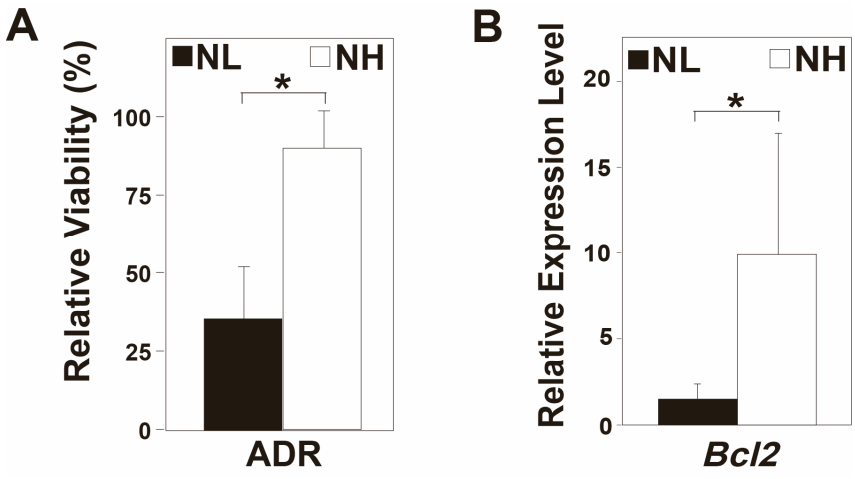

Figure 25: Bcl2 mediates treatment resistance in lymphomas. (*A*) Viability analysis by trypan blue dye exclusion of the NL *vs.* NH lymphoma cell populations exposed *in vitro* for 24 hours to 5 ng/ml of ADR relative to untreated cells of the same group (*n* = 4 each group). (*B*) RQ-PCR analyses of the transcript levels of the NF-κB target *bcl2* in the NH and NL lymphoma groups (Histogram bars indicate mean values ± SDEV; * indicates P<0.05).

Accordingly, when lymphoma cells were co-treated with ADR and Abt-737 (a BH3 mimetic small-molecule inhibitor that binds with high affinity to Bcl-2 and Bcl-xL), The NH group regained chemo-sensitivity, while the NL group did not significantly change (Fig. 26A). Likewise, at the dose level that NL group showed no significant difference in cell viability, cell viability of NH group decreased significantly under the co-treatment of ADR and Abt-263 (structurally related to ABT-737, a disruptor of Bcl-2/Bcl-xL interactions) (Fig. 26B).

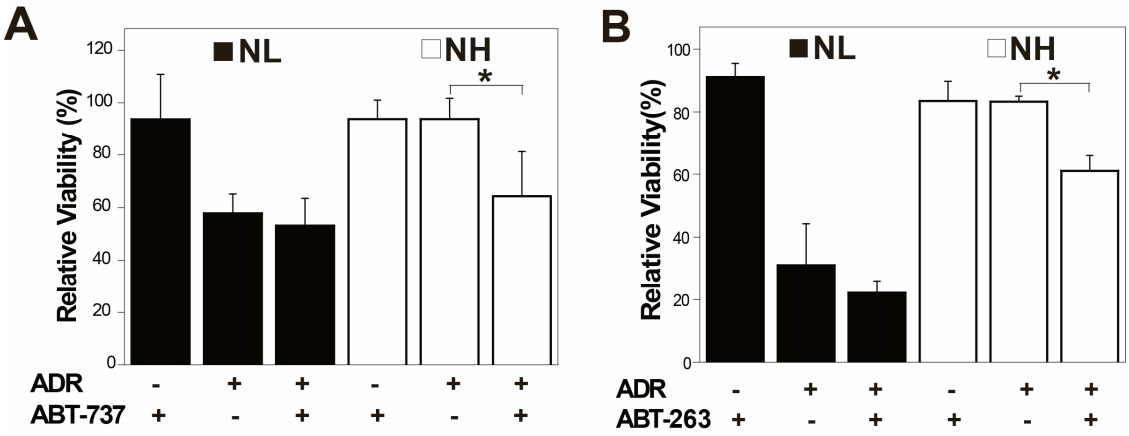

Figure 26: NF-κB high lymphomas (NH) are more sensitive to Bcl2 inhibition. (*A*) Viability analysis by trypan blue dye exclusion of the NL (n = 4) *vs.* NH (n = 3) lymphoma cell populations exposed *in vitro* for 24 hours to 5 ng/ml of ADR, 0.1 µM ABT-737, or 5 ng/ml of ADR and 0.1 µM ABT-737 relative to untreated cells of the same group. (*B*) Viability analysis by trypan blue dye exclusion of the NL (n = 4) *vs.* NH (n = 3) lymphoma cell populations exposed *in vitro* for 24 hours to 5 ng/ml of ADR, 0.5 µM ABT-263, or 5 ng/ml of ADR and 0.1 µM ABT-263 relative to untreated cells of the same group.

Moreover, retroviral overexpression of Bcl2 rendered NL lymphomas as chemoresistant as NH lymphomas (Fig. 27A). Conversely, we asked whether inhibition of NF-κB activity might overcome the short-term drug resistance in the NH group. While inactivation of NF-κB function by the SR moiety had little impact in the NL group, it restored chemosensitivity in the NH group, thereby uncovering highly active NF-κB signaling as an ‘‘Achilles’ heel’’ of this group during chemotherapy (Fig. 27B).

Taken together, a proportion of primary Myc-driven lymphomas presents with high-level NF-κB activity at diagnosis, suggestive for an oncogenic function of the NF-κB pathway selected for during lymphoma development that simultaneously anticipates primary drug resistance.

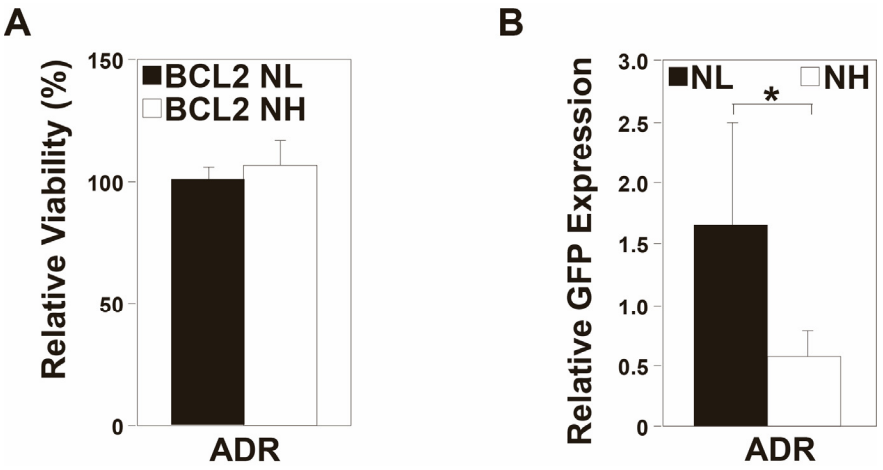

Fig 27: NF-κB-driven, high Bcl2 expression mediates treatment resistance in lymphomas. (*A*) Viability analysis as in Figure 25*A* and with the same lymphoma samples, now overexpressing Bcl2 from retroviral alleles in both groups. (*B*) GFP enrichment analysis of MSCV-SR-IRES-GFP-expressing cells treated as in Figure 25*A*, but for 48 hours; selective drop of GFP-positive cells in the NH group indicating their increased chemosensitivity upon NF-κB inhibition (*n* = 3 each group). All histogram bars indicate mean values ± SDEV.

Recapitulating the clinical outcome of patients suffering from DLBCL, ~60% of the mice harboring Eμ-*myc* control lymphomas achieve long-term remissions (reflecting cure), while the remaining 40% encounter a relapse after cyclophosphamide (CTX) induction therapy (Schmitt et al. 1999, 2000; Lenz et al. 2008). To generate ‘‘time-to-relapse’’ data, 13 primary (not *bcl2*-infected) Eμ-*myc* lymphomas were transplanted into recipient mice and exposed to CTX at the time of lymphoma manifestation. While all animals entered a remission, seven lymphomas relapsed within the 100-day observation period. Therefore, the 13 lymphomas at diagnosis were grouped as either ‘‘never relapse’’ (NR) or ‘‘relapse prone’’ (RP). Based on the previous results, we assessed basal NF-κB activity by the expression of two NF-κB targets, *IκBα* and *Bcl2* in untreated lymphomas of these two groups (Fig. 28). Strikingly, RP lymphomas were found to exhibit significantly higher *IκBα* expression levels, further accompanied by substantially higher *bcl2* expression levels, thus reminiscent of the NF-κB/Bcl2 network analyzed before and of the genetic hallmark

lesions detectable in activated B-cell like (ABC) DLBCL, the prognostically inferior DLBCL subtype characterized by constitutively active NF-κB signaling due to a variety of activating mutations in the NF-κB pathway and by very high *Bcl2* transcript levels (Iqbal et al. 2006; Lenz et al. 2008b; Compagno et al. 2009; Staudt 2010; Nogai et al. 2011).

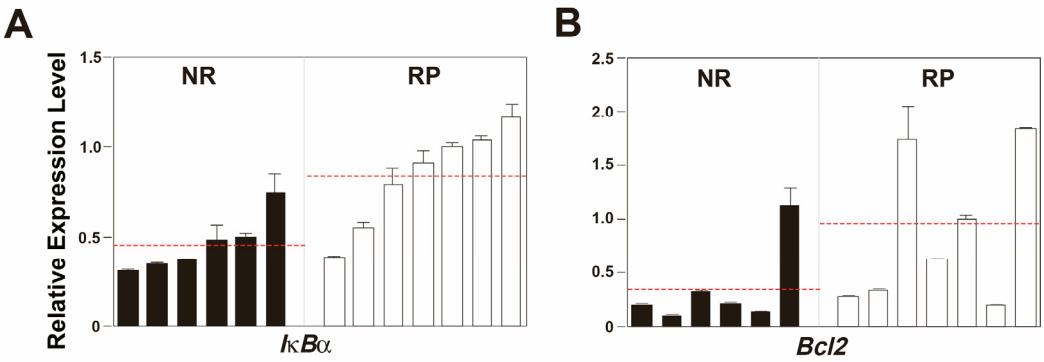

Figure 28: Grouping of 13 primary control lymphomas according to the long-term responses to CTX therapy following transplant tumor formation *in vivo* as either "never relapse" (NR) or "relapse prone" (RP) lymphomas. RQ-PCR analyses of their *IκBα* transcript levels at diagnosis (*i.e.* prior to any therapy) as a representative *bona fide* NF-κB target (*A*), and of *bcl2* levels of the same samples (*B)*; presented in the same order); horizontal lines indicate mean activity within the respective groups.

4.3.2 ABC-reminiscent lymphomas show a senescence defect

In addition to apoptosis, senescence is another drug-responsive effector program of cancer therapy. Since NF-κB-driven-high Bcl2 expression blocks apoptosis in ABC-reminiscent lymphomas, we asked whether high NF-κB activity contribute to senescence in this group. To address this question, Bcl2-overexpressing NL lymphomas, NH lymphomas and p53 null lymphomas were treated with ADR. At day 5, senescence was analyzed by SA-β-gal and Ki67 staining. Unlike the expectation that high NF-κB activity would lead to more TIS, NH lymphomas displayed less

SA-β-gal positive cells and a high Ki67 index after ADR treatment in comparison with NL lymphomas (Fig. 29), which suggest that NH lymphomas are, at least partly, deficient to enter senescence upon cancer therapeutic agent treatment.

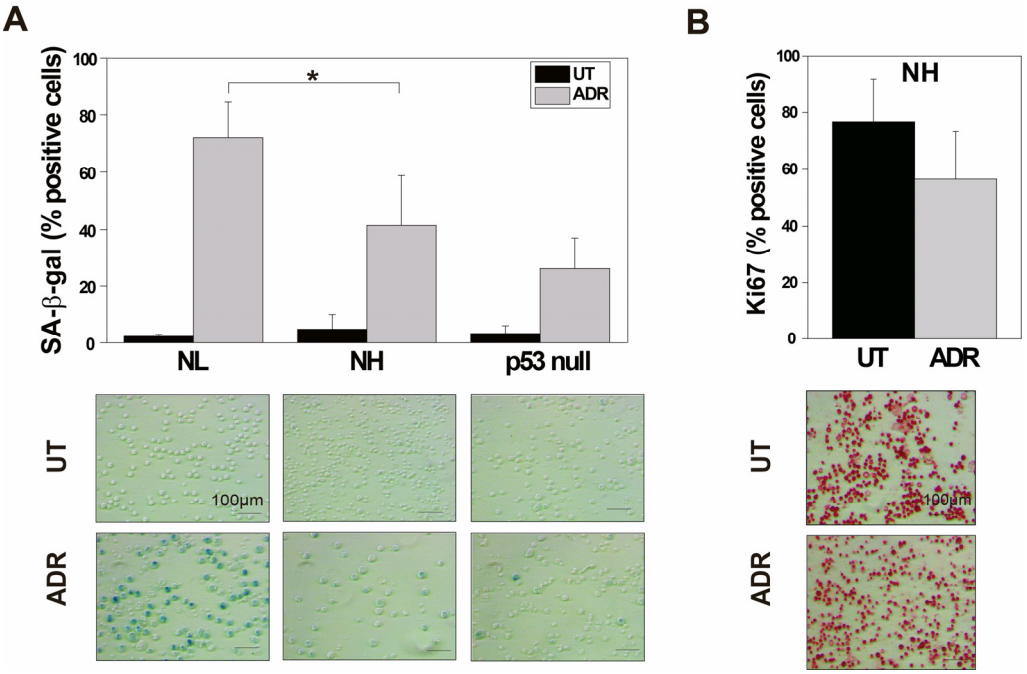

Figure 29: ABC-reminiscent lymphomas show a senescence defect upon treatment. (*A*) Frequencies of SA-β-gal-positive cells in ADR-treated *vs.* untreated (ut) Bcl2-overexpressing NL lymphomas (n = 6), NH lymphomas (n = 6) and p53 null lymphomas (n = 4). Lymphomas were exposed for 5 days to 50 ng/ml ADR *in vitro.* Representative photomicrographs of cytospin preparations are shown underneath the corresponding bars. (*B*) Frequencies of Ki67-positive cells in ADR-treated *vs.* untreated (ut) Bcl2-overexpressing NH lymphomas (n = 6). NH lymphomas were exposed for 5 days to 50 ng/ml ADR *in vitro.* Representative photomicrographs of cytospin preparations are shown underneath the corresponding bars. Note that the number of lymphomas in NL and NH group was expanded according to the NF-κB p65 DNA binding activities.

Although the detailed mechanism still needs to be investigated, there are several possible explanations for this phenotype. Reportedly, numerous genetic

abnormalities in the ABC subtype are rare or absent in the GCB subtype. Among these genetic abnormalities, the *INK4a/ARF* tumor suppressor locus was homozygously or hemizygously deleted in 30% of ABC DLBCL but in only 4% of GCB DLBCL (Lenz et al. 2008c). Since genomic INK4a/ARF deletions directly disable therapy-induced senescence (Schmitt et al. 2002a), analyzing the *INK4a/ARF* defects in NH and NL lymphomas might provide an explanation for the senescence defect phenotype in ABC-reminiscent lymphomas. Another explanation is that instead of hyperactive NF-κB per se, the capability to be further activated upon chemotherapy is crucial for the induction of senescence.

4.3.3 The NF-κB-mediated pro-senescence function contributes treatment outcome in GCB DLBCL with high Bcl2 expression

In contrast to ABC DLBCL, germinal center B-cell-like (GCB) DLBCL present with a much better clinical outcome (Lenz et al. 2008b), although Bcl2 overexpression is common in this subtype as well. Importantly, GCB DLBCL rarely possess activating NF-κB mutations, but frequently (~45%) develop in the context of a t(14;18) translocation that drives *bcl2* overexpression via the immunoglobulin heavy chain locus in an NF-κB-independent fashion, a lesion that is virtually never found in ABC-type DLBCL (Nogai et al. 2011), thereby creating an entirely differently wired "NF-κB/Bcl-2" oncogenic network. When drug-inducible apoptosis is blocked in mouse lymphomas by exogenous Bcl2 overexpression, thereby mimicking the GCB-related t(14;18) translocation, NL (GCB-reminiscent) lymphomas were able to enter TIS (Fig. 29). To test whether higher NF-κB activation levels would further promote senescence induction in these lymphomas, a strongly NF-κB-activating CARD11 (also known as CARMA1 or Bimp3) mutant, the murine homolog of the human CARD11-L244P mutant, was used to modify the NF-κB pathway. Overexpression of CARD11-L251P mutant resulted in increased NF-κB target gene

expression (Fig. 30A; Lenz et al. 2008a).

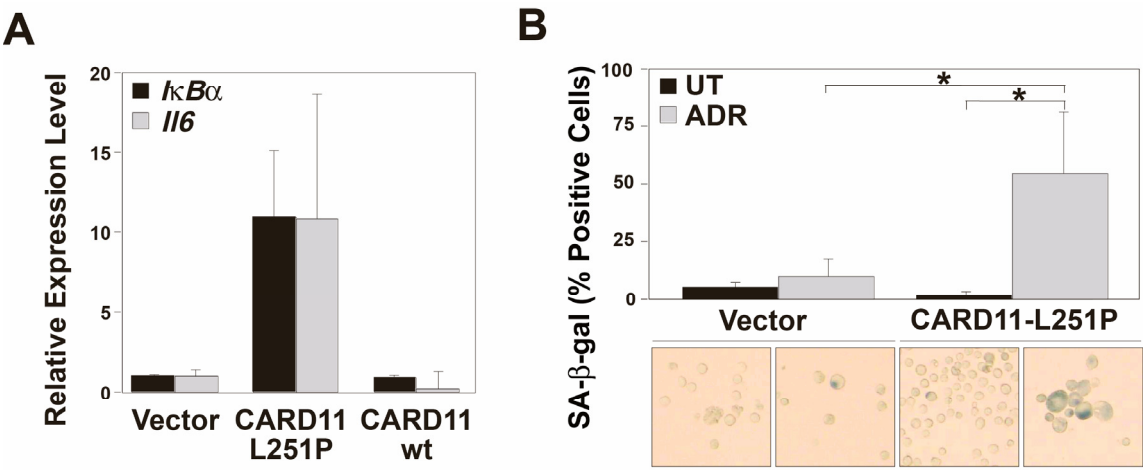

Figure 30: Higher NF-κB activity may contribute to treatment outcome via TIS promotion. (*A*) Enhanced NF-κB target gene expression in response to the oncogenic CARD11-L251P mutant, but not to wild-type (wt) CARD11. RQ-PCR analyses of *IL-6* and *IκBα* transcripts in an Eμ-*myc* control lymphoma stably transduced with the CARD11-L251P mutant, wild-type CARD11 or empty vector-infected for comparison (representative pattern of induction shown for one individual lymphoma out of four tested). (*B*) Frequencies of SA-β-gal-positive cells in Bcl2-overexpressing NL lymphomas ± CARD11-L251P, exposed for 3 days to 50 ng/ml ADR *in vitro* (*n* = 4 matched pairs; representative photomicrographs of cytospin preparations shown underneath the corresponding bars). Note that CARD11-L251P did not induce senescence in the absence of ADR.

While naturally occurring CARD11 mutations are preferentially found in ABC DLBCL, here, such a mutant was used to enhance NF-κB activity in a ‘‘GCB-reminiscent’’ lymphoma cohort, which formed in the absence of highly activated NF-κB and where apoptosis is blocked independently of NF-κB via autochthonous Bcl2 overexpression. Indeed, at an early time, when ADR-exposed Bcl2-engineered NL lymphomas were still largely negative for signs of TIS, a high proportion of the matching, mutant CARD11-overexpressing lymphoma cells already stained positive for SA-β-gal activity (Fig. 30B), suggesting that induced NF-κB activity promotes TIS.

Therefore, higher NF-κB activity mediates a pro-senescence function in Bcl2-overexpressing GCB reminiscent mouse lymphomas. It is reasonable to predict that high NF-κB activity contributes to superior treatment outcome via TIS promotion in *bcl-2*-high-expressing GCB DLBCL.

Suggested by the results in Eμ-*myc* transgenic lymphoma model, we decided to interrogate a large data set of GEP and clinical data after rituximab-CHOP-like standard immunochemotherapy (which includes both ADR and CTX) from 233 DLBCL patients (Lenz et al. 2008b), and asked in the subset of GCB DLBCL patients with high Bcl2 expression (i.e. Bcl2 transcript level above median) whether a previously identified NF-κB gene expression signature consisting of 63 known NF-κB target genes would allow us to stratify two patient cohorts with different clinical outcome (Shaffer et al. 2006). Indeed, as shown in Fig. 31A, Bcl2-overexpressing GCB DLBCL patients with an NF-κB signature expression above median (NH; n = 25) had a significantly superior progression-free survival when compared with the complementary group with lower NF-κB signature expression (n = 24; $P < 0.005$), while such a correlation was not found in patients harboring high Bcl2-expressing lymphomas of the ABC subtype (Fig. 31B) or lymphomas of either subtype with low Bcl2 expression. Notably, multivariant analysis indicated that the NF-κB status in Bcl2-overexpressing GCB DLBCL cases was statistically independent of the International Prognostic Index overall score ($P = 0.3956$), which is used as a clinical standard to predict outcome in lymphoma patients (The International Non-Hodgkin's Lymphoma Prognostic Factors Project 1993).

Taken together, this innovative experimental strategy-termed "cross-species" investigation-led to the identification of a genetically defined and clinically significant subgroup of GCB DLBCL patients who experienced superior treatment outcome if NF-κB signaling was hyperactive, thereby contrasting the well-established association of the ABC subtype with constitutively active NF-κB signaling and poor treatment outcome.

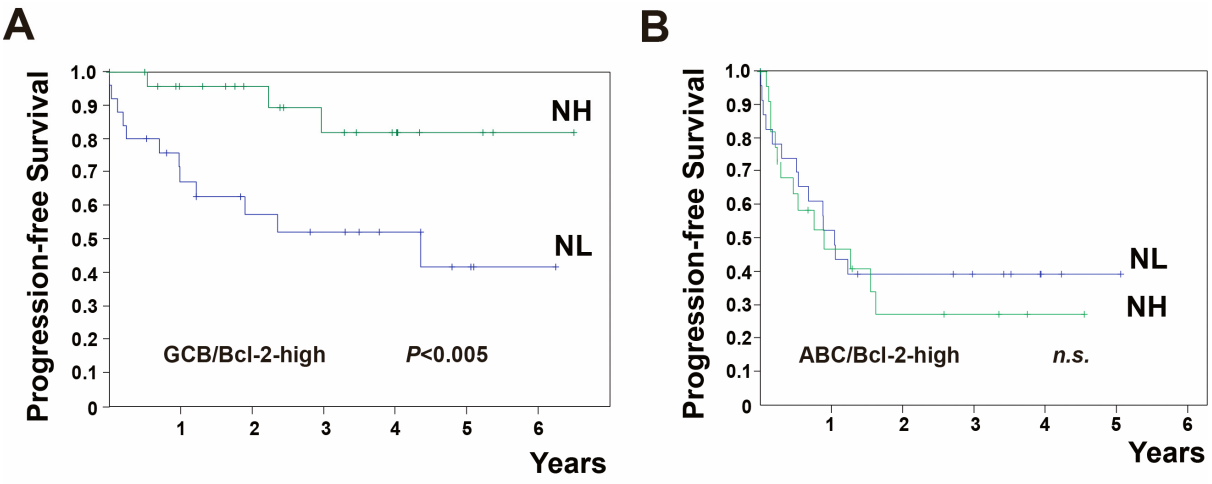

Figure 31: The relation of NF-κB signature and the outcome in DLBCL patients (*A*) Bcl2-high GCB DLBCL patients experience a significantly longer progression-free survival if NF-κB is hyperactive in their lymphomas. Progression-free survival of the 49 R-CHOP-like-treated GCB DLBCL patients from a total of 233 patients (as reported by Lenz et al. (Lenz et al. 2008b)) with an above median *bcl2* expression by microarray based transcriptome analysis of their lymphomas at diagnosis, and further stratified by a 63-gene signature as either "NF-κB high" (NH, *n* = 25, green) or "NF-κB low" (NL, *n* = 24, blue). All histogram bars indicate mean values ± SDEV. (B) The NF-κB signature fails to stratify the outcome of ABC DLBCL patients with high Bcl2 expression to R-CHOP-like induction therapy. Progression-free survival of the 45 R-CHOP-like-treated ABC DLBCL patients from a total of 233 patients (as reported by Lenz et al. (Lenz et al. 2008b)) with an above median *bcl2* expression by microarray-based transcriptome analysis of their lymphomas at diagnosis, and further stratified by the 63-gene signature as either "NF-κB high" (NH, *n* = 22, green) or "NF-κB low" (NL, *n* = 23, blue).

5 Discussion

5.1 NF-κB's function in cellular senescence

Ever since the identification of senescence as a stable growth arrest with potential implications in aging, its physiological relevance has been expanded as stresses like oncogenes, ionizing radiation or exposure to chemotherapeutic drugs were also found to activate senescence. Similar to apoptosis, cellular senescence has been demonstrated to function as a tumor suppressor mechanism, preventing the accumulation of cells that encountered signaling imbalances and other transforming events. Moreover, senescence also contributes to the outcome of cancer therapy *in vivo* (Schmitt et al. 2002a and Haugstetter et al. 2010).

Activated NF-κB signaling has mostly been linked to treatment resistance, especially when the inability to enter drug-induced apoptosis was measured in short-term assays (Wang et al. 1999). Tumors with constitutive NF-κB activation usually show increased resistance to chemotherapy.

Previous studies linked oncogene-induced senescence to the massive production of a large variety of cytokines, such as interleukins, GM-CSF, bFGF, CXCL-1/-2/-3/-5/-7 and MCP-1. Many of these SASP factors possess NF-κB-binding sites in their promoters. Using Bcl2-overexpressing primary Eμ-*myc* transgenic mouse lymphoma cells, we revealed a dramatic induction of non-secreted and secreted NF-κB target genes during TIS, and, importantly, a dependency of the senescent phenotype on functional NF-κB signaling that becomes particularly evident *in vivo*—a finding in full agreement with related work by Chien and colleagues (Chien et al. 2011).

As discussed in the former part of this thesis, therapy-induced senescence is accompanied by a senescence-associated secretory phenotype, as well as NF-κB

activation, which was demonstrated by GSEA of NF-κB target genes, NF-κB nuclear translocation and DNA-binding activity analysis. Our results unveiled that activated NF-κB signaling is a prominent feature of chemotherapy-induced senescence.

Reportedly, NF-κB is a multi-functional transcription factor and involved in many processes like cell survival, growth, stress response, and inflammation. The fact that NF-κB is activated during treatment-induced senescence implies its regulatory role in this process. Indeed, enforced NF-κB activation by mutant Card11 accelerated TIS *in vitro*. However, individual lymphoma reacts differently to NF-κB inhibition *in vitro*. We observed a substantial decline in the percentage of SA-β-gal-positive cells in some lymphomas of the SR cohort compared with controls while in others the uncompromised TIS phenotype was not affected. The incomplete ablation of senescence phenotype *in vitro* suggests that instead of being a linear and essential component of the DDR-initiated senescence pathway, NF-κB operates as a corroborating, collateral relay of the prosenescent DNA damage response. Surprisingly, we observed a much more pronounced impairment of TIS following NF-κB inhibition *in vivo*. The virtual absence of senescence in NF-κB-defective lymphoma cells at a time when NF-κB-competent lymphomas became largely senescent indicates additional, non-cell-autonomous implications of NF-κB signaling in the senescence process. Compared with the *in vitro* situation, the *in vivo* environment is more complex, including paracrine modes of action and crosstalk to other, non-malignant cell types. As recent studies revealed certain secreted factors, such as TGF-beta (Reimann et al. 2010) and IL8 (human) (Acosta et al.2008) as potential senescence inducers, NF-κB is possibly involved in the process of senescence induced by prosenescent factors released by adjacent cells *in vivo*.

The senescence program involves a complex interplay between intracellular and extracellular processes that influence the cell cycle arrest, the tissue microenvironment, and the surveillance of senescent cells by various immune system components. Senescent cells communicate with their environment by secreting

various cytokines and growth factors, and it was reported that the secretory phenotype could reinforce the senescence arrest and mediate cross-talk between senescent cells and other cells within their microenvironment. As a major regulator of SASP, NF-κB is involved not only in the stabilizing cell cycle arrest but also in promoting immune cell clearance (Chien et al, 2011). Chien and colleagues demonstrated that disruption of the SASP through NF-κB inhibition promotes chemoresistance of lymphomas mainly through a failure to engage the senescence response and to trigger immune clearance of the senescent cells. Consequently, animals harboring lymphomas with suppressed NF-κB show early relapse and poor survival post-therapy. Given the large number of genes regulated by NF-κB, it is quite possible that NF-κB functions as a tumor suppressor in a microenvironment consisting of senescent cells, factors secreted by senescent cells and non-malignant bystanders, particularly immune cells.

5.2 Dark side of NF-κB—anti-apoptosis

NF-κB regulates important cellular processes ranging from establishment of the immune and inflammatory responses to regulation of cell proliferation or apoptosis through the induction of a large array of target genes. Until now, NF-κB has been considered as an important factor in the tumorigenic process mainly because it exerts strong anti-apoptotic functions in cancer cells. Recent studies have shown that B-cell lymphomas frequently harbor genetic mutations in NF-κB pathway components resulting in constitutive, and presumably oncogenic, NF-κB signaling by establishing a prosurvival phenotype (Staudt et al, 2010). Numerous studies have demonstrated that inhibition of NF-κB by different means increased sensitivity of cancer cells to the apoptotic action of diverse effectors such as TNFα, chemo-, or radiotherapies (Wang et al. 1996; Jung et al. 2001; Smirnov et al. 2001). From these studies emerged the concept that NF-κB blockade could be combined to conventional therapies in order to increase therapy efficiency. Although our results demonstrate an essential role for NF-κB in the induction of cellular senescence in a genetically defined model scenario,

the net impact of NF-κB on treatment outcome in natural tumors is much more difficult to assess.

Human DLBCL can be divided into at least two subtypes according to their gene-expression profiling: ABC DLBCL and GCB DLBCL. Compared to GCB, the ABC subtype exhibits constitutive activation of the NF-κB pathway and presents with inferior clinical treatment outcome. The fact that ablation of NF-κB in cell lines derived from ABC DLBCL, but not in GCB DLBCL, led to apoptosis suggests that NF-κB activation plays a critical role in the oncogenic phenotype of ABC DLBCL. Based on human DLBCL data linking the ABC subtype to activating NF-κB lesions and an inferior outcome to standard immunochemotherapy (Lenz et al. 2008b; Compagno et al. 2009), we classified a series of primary Eμ-*myc* transgenic lymphomas with known long-term responses to chemotherapy *in vivo* based on their NF-κB activity levels at manifestation. Reminiscent of GCB-type DLBCL, the group of Eμ-*myc* lymphomas with good clinical outcome was largely composed of lymphomas exhibiting low basal NF-κB activity. Importantly, the group of Eμ-*myc* lymphomas with high NF-κB activity exhibited high Bcl-2 expression, which correlated with chemoresistance. By Bcl-2 inhibition on top of chemotherapy, we were able to demonstrate that high Bcl-2 expression driven by NF-κB is responsible for the chemoresistance in ABC reminiscent group. These results are in accordance with the NF-κB's anti-apoptotic function in the ABC subtype of human diffuse large B-cell lymphoma. More importantly, restoring treatment sensitivity by inhibiting Bcl-2 or NF-κB suggests that NF-κB/Bcl-2 is a potential treatment target in this subgroup.

NF-κB-activating mutations acquired during lymphoma development, as preferentially observed in the ABC subtype of DLBCL, account for the selective vulnerability of these lymphomas to NF-κB inhibitors or shRNAs targeting components of the NF-κB pathway (Davis et al. 2001; Ngo et al. 2006). Since the anti-apoptotic bcl2 gene is a *bona fide* NF-κB target, ABC DLBCLs are genetically determined to depend on an NF-κB-to-Bcl2 signaling module (a linear, two-factor oncogenic network model). The

highly active NF-κB signaling is an ‘‘Achilles’ heel’’ of this group and is an ideal target for cancer therapy.

5.3 Beneficial side of NF-κB—prosenescence

Unlike ABC DLBCL, in which an NF-κB/Bcl2 signaling module mediates chemoresistance, about 45% of the GCB DLBCL subtype express high level of BCL-2 as a consequence of the t(14;18) translocation. Therefore, apoptosis is blocked by BCL-2 independent of the status of NF-κB pathway in GCB DLBCL. Unlike tumors characterized by a broad spectrum of detrimental biological properties directly linked to their constitutively active NF-κB network, tumor types, such as GCB that do not rely on NF-κB signaling as the driving oncogenic force but present with an NF-κB-independent apoptotic block may use the prosenescent potential of NF-κB signaling to execute TIS as an alternative, outcome-improving chemotherapeutic effector mechanism.

Indeed, while NF-κB mediates chemoresistance in ABC DLBCL, NF-κB shows its beneficial function in GCB DLBCL. The GCB- reminiscent Eμ-*myc* lymphomas were used to experimentally explore the contribution of enhanced NF-κB activity to senescence induction after drug-inducible apoptosis was independently blocked by retroviral Bcl2 overexpression (a parallel or independent two-factor alternative of the same oncogenic network players). Lymphomas overexpressing a CARD11mutant, which results in persistent activation of the NF-κB pathway, enter senescence at an early time, when lymphomas with normal NF-κB activity were still largely negative for signs of TIS. This observation suggests that in tumors with apoptosis deficiency, instead of acting as an oncogenic factor, NF-κB plays a positive role in the tumor-suppressive senescence process.

ABC DLBCL has a worse survival after upfront chemotherapy and is characterized by constitutive activation of the antiapoptotic NF-κB pathway, which mediates treatment

resistance. Our investigation in the Eμ-*myc* transgenic lymphoma model confirmed that the NF-κB/Bcl2 signaling module mediates chemoresistance in ABC-reminiscent lymphomas. Since apoptosis is blocked by NF-κB/Bcl2 signaling in ABC-reminiscent lymphomas, one obvious question is whether they are able to make use of the constrictively activated NF-κB pathway and enter senescence upon cancer therapy treatments. Surprisingly, instead of being prone to senescence, ABC-reminiscent (NH) lymphomas displayed a senescence defect in comparison with GCB-reminiscent (NL) lymphomas. Although the detailed mechanism can not be addressed here, one possible explanation is that instead of hyperactive NF-κB per se, the capability to be further activated is crucial for the induction of senescence. Possibly, the NF-κB activity in ABC-reminiscent cells reached such a high level that the cancer therapeutic agents fail to further activate this pathway.

Given the fact that senescence contributes to the outcome of cancer therapy, we asked whether hyperactive NF-κB contributes to treatment outcome in human lymphoma patients. We used the genetic determinants of the TIS-prone scenario—GCB-reminiscent lymphomas with high Bcl2 expression were stratified by the level of NF-κB activity—to interrogate a large GEP set derived from 233 DLBCL patients with known clinical outcome to therapy. Strikingly, we were able to confirm the mechanistic results from the murine lymphoma model in DLBCL-harboring patients. The ‘‘Bcl2 high/NF-κB high’’ GCB DLBCL subgroup of patients presenting with a significantly prolonged survival after therapy underscores a hitherto unknown beneficial association of NF-κB hyperactivation and treatment outcome in lymphoma patients.

5.4 Context-dependency of NF-κB in tumor development

Nuclear translocation and subsequent DNA binding represent critical steps in the

NF-κB pathway activation. However, the functional consequences of NF-κB activation can differ dramatically depending on the nature of the inducer and the cellular context. NF-κB can affect cancer development through the transcriptional activation of genes associated with cell proliferation, apoptosis suppression, angiogenesis, metastasis, tumor promotion and inflammation. Various mouse models of cancer in which IKK/NF-κB activation has been blocked by genetic means have highlighted the key role of NF-κB as a critical promoter of cancers. One of the most documented functions of NF-κB is its ability to promote cell survival through induction of target genes whose products inhibit the apoptotic machinery in both normal and malignant cells. The biochemical and pathophysiologic roles of NF-κB in carcinogenesis are confounded by its tumor suppression activity. In addition to a large volume of circumstantial evidence demonstrating constitutively active NF-κB in many types of cancer, the underlying mechanism of the tumor-promoting effect of NF-κB has been intensively explored. In contrast, how NF-κB or its activation signaling contributes to tumor suppression remains a *terra incognita*.

Our data highlight how oncogenic networks and interdependencies, wired up during tumor development, may regulate the actual functions and even opposing roles of NF-κB in subsequent responses to therapy. NF-κB mutations acquired during lymphoma development, as preferentially observed in the ABC subtype of DLBCL, account for the selective vulnerability of these lymphomas to NF-κB inhibitors or shRNAs targeting components of the NF-κB pathway (Davis et al. 2001; Ngo et al. 2006). Since the anti-apoptotic *bcl2* gene is a *bona fide* NF-κB target, ABC DLBCL are genetically determined to depend on an NF-κB/Bcl2 signaling module, while GCB DLBCL frequently present with bcl2 translocations that uncouple their anti-apoptotic activity from NF-κB upstream control. While ABD DLBCL characterized by a broad spectrum of detrimental biological properties directly linked to the constitutively active NF-κB network, GCB DLBCL present with an NF-κB-independent apoptotic block and use the prosenescent potential of NF-κB signaling to execute TIS as an alternative, outcome-improving chemotherapeutic effector mechanism. Our mouse model

findings obtained in Myc-driven lymphomas engineered to overexpress Bcl2 not only genetically approximate the human Myc/Bcl2 ‘‘double-hit’’ lymphomas frequently found in the GCB subtype of DLBCL, but also more advanced follicular lymphomas, which, in addition to their t(14;18) hallmark lesion, often acquire activating Myc lesions in the course of the disease, and, of note, also do not belong to NF-κB-hyperactivated lymphoma entities (Aukema et al. 2011).

5.5 Apoptosis or senescence: implications for cancer treatment

In the validation and selection of targets for therapeutic intervention in cancer, the mutation or deregulation of a particular target or a pathway in human cancers may indicate of its importance in the malignancy process and the potential use of a drug that acts on that target or pathway. The IKK/NF-κB signaling module is often altered in human cancers. Moreover, tumor cells appear to use NF-κB to achieve resistance to anticancer drugs and irradiation. Therefore, inhibition of NF-κB activation might be a promising option to improve the efficacy of conventional anti-cancer therapies.

However, the relationship between NF-κB and cancer is not simple and cannot be reduced to one grand theory. The complex role for NF-κB in oncogenesis and the context dependency of NF-κB signaling must be taken into account when designing NF-κB–based therapies against cancer. Our study emphasizes the tumor-suppressive role of NF-κB as a regulator of chemotherapy-induced senescence *in vivo*, particularly in tumors with an apoptosis deficiency. Therefore, inhibition of NF-κB signaling might actually reduce chemo-efficacy instead of promoting cell death when apoptosis is defective. Our study underscores the importance of determining the context in which certain NF-κB-mediated functions are preferentially executed. The mouse model and patient-derived data indicate that NF-κB inhibitors should be rather applied to those cancers in which the

tumor-suppressive functions of NF-κB are outweighed by verified NF-κB oncogenic functions. In turn, tumors with an NF-κB signaling predestined to promote senescence in response to DNA-damaging therapies, would rather not qualify as candidates for NF-κB (co)-inhibition. In essence, our findings suggest that we should carefully select, or at least monitor, genetically defined patient subcohorts in which therapeutic interference with the NF-κB pathway may or may not be of clinical benefit (Dunleavy et al. 2009; Ruan et al. 2011).

5.6 Eμ-*myc* transgenic mouse lymphomas—a model for human diffuse large B-cell lymphoma

Human cancer is characterized by substantial heterogeneity, resulting from the acquisition of multiple somatic genetic and epigenetic alterations. Genetically engineered mouse models of human cancer are valuable tools for cancer research, in which genetic alterations can be directed without much complication. In this study, the Eμ-*myc* transgenic lymphoma model was used to elucidate the function of NF-κB in senescence and cancer treatment outcome. Myc is deregulated in various human cancers, such as lymphoma, breast cancer, and prostate cancer. Dysregualtion of the *c-myc* oncogene is a common genetic alteration in non-Hodgkin's lymphoma. In Burkitt's lymphoma, virtually every case involves chromosomal translocation of the *myc* locus to the IgH-J segment (Nesbit et al. 1999), resulting in overexpression of c-Myc in B cells. In addition to rearrangement, nonrandom somatic mutations within the *myc* coding region, which include those providing stabilization to the protein, have been observed. Burkitt-like (or atypical Burkitt) lymphoma and a fraction of diffuse large B-cell lymphoma (DLBCL) also feature Myc deregulation.

The Eμ-*myc* transgenic mouse is a valuable model for human aggressive B-cell non-Hodgkin's lymphomas (B-NHL). Like most cancer models that are initiated by a defined genetic alteration, the development of lymphomas in the Eμ-*myc* mouse

involves the acquisition of additional mutations (Mori et al. 2008), giving rise to some heterogeneity in the resulting tumors, thereby recapitulating a feature of naturally forming cancers. Suggested by the GEP classification of human diffuse large B-cell lymphoma, we classified the primary Eμ-*myc* transgenic lymphomas into a GCB-reminiscent and an ABC-reminiscent group, allowing us to study the opposing role of NF-κB in mouse model, to correlate findings with the human clinical data, and to reveal a clinically relevant group in which NF-κB's beneficial side is unveiled.

Translocation of the *Bcl2* gene, on encoded chromosome band 18q21.3, to *the immunoglobulin* (*IG*) *heavy chain* (*IGH*) gene as t(14;18)(q32;q21.3) results in consistent expression of the Bcl2 protein. *Bcl2* translocation is detected in 70-95% of follicular lymphomas (Weiss et al. 1987) and ~20% of diffuse large B cell lymphomas, whereby t(14;18) translocation are found virtually exclusively in the GCB subtype. *Myc* and *Bcl2* co-activation is also seen in so-called "double-hit (DH) lymphomas". Double-hit lymphomas are defined by a chromosomal breakpoint affecting the *myc*/8q24 locus in combination with another recurrent breakpoint, mainly a t(14;18)(q32;q21) Bcl2-involving translocation. By using the Bcl-2 overexpressing *Myc*-driven B-cell lymphomas, we established a model for therapy-induced senescence. Technically, the Bcl-2 overexpression in *myc* lymphomas blocks apoptosis, thereby allowing senescence to occur throughout the tumor all population. Moreover, this model approximates the situation observed in patients with *bcl2* translocation and aggressive "double-hit" B-cell lymphomas with Myc and Bcl2 translocations.

5.7 Cross-species investigations—a novel approach to unveil clinically relevant patient subgroups

Mouse models in which the various disease phenotypes resemble the spectrum of clinical manifestations in human provide valuable resources to understand molecular

pathogenesis and to test ways to prevent or treat the resulting diseases. Although the data in mouse models are valuable per se, it is important to translate information thereof back into the human condition. Cross-species investigations, which integrate the power of functional studies in mice and the combination of clinical-molecular data in patients, is a novel approach to unveil clinically relevant patient subgroups.

In this thesis, we used mouse models to recapitulate defined genetic determinants of human tumor cohorts, followed by the genetic manipulation and subsequent functional exploration of murine surrogate tumors with the ultimate goal to use mouse-derived mechanistic information for a reassessment of the human data set to gain novel functional insights. Our data illustrate the power of cross-species investigations to redefine clinically relevant patient subcohorts. The cross-species investigation strategy was instrumental in unveiling a genetically defined tumor subset with a distinct NF-κB-dependent responsiveness. The subgroup of human lymphoma patients who benefit from hyperactive NF-κB would not have been identified without the cross-species investigation of primary Eμ-*myc* lymphomas.

5.8 Open questions and outlook

NF-κB is viewed as a candidate target for cancer therapy because of the key role it plays in cancer development and progression. Our study demonstrates that settings exist in which NF-κB stimulates tumor cells to enter senescence during chemotherapy and provides significant therapeutic implications. However, the experimental design in this study did not aim at explaining how precisely NF-κB contributes to senescence. The detailed mechanism and signaling pathways involved still need to be further investigated. Our data suggested that ABC-reminiscent lymphomas have a senescence defect. On one hand, this explains the poor treatment outcome of ABC DLBCL from the perspective of senescence. On the other hand, this unveils the complexity of NF-κB's function in senescence. The detailed mechanisms require further investigation.

Discussion

Our study sheds new light on the context-dependent roles of NF-κB in oncogenesis and therapy. The opposing roles of NF-κB in oncogenesis, promoting tumorigenesis on one hand and mediating therapy-induced senescence on the other, have significant therapeutic implications. First, these findings imply that the use of NF-κB inhibitors in the clinic requires thorough assessment, since NF-κB inhibition could interfere with the cytotoxicity of standard chemotherapy in combination therapies. Second, we observed that treatment-ralated activation of NF-κB in mouse lymphomas with low NF-κB activity enhances therapy-induced senescence; these results provide a rationale for the development of therapeutic strategies that enhance chemosensitivity by activating NF-κB concomitantly with cytotoxic chemotherapy. Third, elucidating the precise mechanisms of NF-κB in oncogenesis versus therapy-induced senescence could lead to the identification of crucial downstream components of NF-κB that mediate chemosensitivity, with the eventual goal of developing strategies to boost senescence in tumors where NF-κB's oncogenic function dominates. The findings provide important new insights into the complexity of NF-κB signaling in cancer cells. Future studies will exploit the development of specific, more effective anticancer therapies that utilize and/or target NF-κB functionalities.

6 Appendix

6.1 Reference

1. Acosta JC, O'Loghlen A, Banito A, et al. Chemokine Signaling via the CXCR2 Receptor Reinforces Senescence. **Cell** 133, 1006-1018 (2008).
2. Adams JM, Harris AW, Pinkert CA, et al. The c-myc oncogene driven by immunoglobulin enhancers induces lymphoid malignancy in transgenic mice. **Nature** 318, 533-538 (1985).
3. Adams PD. Healing and hurting: molecular mechanisms, functions, and pathologies of cellular senescence. **Mol Cell** 36, 2-14 (2009).
4. Alizadeh AA, Eisen MB, Davis RE, et al. Distinct types of diffuse large B-cell lymphoma identified by gene expression profiling. **Nature** 403, 503-511 (2000).
5. Annunziata CM, Davis RE, Demchenko Y, et al. Frequent engagement of the classical and alternative NF-κB pathways by diverse genetic abnormalities in multiple myeloma. **Cancer Cell** 12, 115–130 (2007).
6. Arkan MC, Greten FR. IKK- and NF-κB-mediated functions in carcinogenesis. **Curr Top Microbiol Immunol** 349,159-169 (2011).
7. Aukema SM, Siebert R, Schuuring E, et al. Double-hit B-cell lymphomas. **Blood** 117, 2319-2331 (2011).
8. Baeuerle PA, Henkel T. Function and activation of NF-kappaB in the immune system. **Annu Rev Immunol** 12,141-179 (1994).
9. Bakkenist CJ, Kastan MB. Initiating cellular stress responses. **Cell** 118, 9-17 (2004).
10. Baldwin AS. Control of oncogenesis and cancer therapy resistance by the transcription factor NF-kappaB. **J Clin Invest** 107, 241-246 (2001)
11. Bargou RC, Emmerich F, Krappmann D, et al. Constitutive nuclear factor-kappaB-RelA activation is required for proliferation and survival of Hodgkin's disease tumor cells. **J Clin Invest**. 100, 2961-299 (1997).

12. Bargou RC, Leng C, Krappmann D, et al. High-level nuclear NF-kappa B and Oct-2 is a common feature of cultured Hodgkin/Reed-Sternberg cells. **Blood** 87, 4340-4347 (1996).
13. Bartkova J, Rezaei N, Liontos M, et al. Oncogene-induced senescence is part of the tumorigenesis barrier imposed by DNA damage checkpoints. **Nature** 444, 633-637 (2006).
14. Basseres DS, Baldwin AS. Nuclear factor-kappaB and inhibitor of kappaB kinase pathways in oncogenic initiation and progression. **Oncogene** 25, 6817-6830 (2006).
15. Basseres DS, Ebbs A, Levantini E, et al. Requirement of the NF-κB subunit p65/RelA for K-Ras-induced lung tumorigenesis. **Cancer Res** 70, 3537-3546 (2010).
16. Ben-Neriah Y, Karin M. Inflammation meets cancer, with NF-κB as the matchmaker. **Nat Immunol** 12, 715-723 (2011).
17. Bernard D, Monte D, Vandenbunder B, et al. The c-Rel transcription factor can both induce and inhibit apoptosis in the same cells via the upregulation of MnSOD. **Oncogene** 21, 4392-4402 (2002).
18. Bettermann K, Vucur M, Haybaeck J, et al. TAK1 suppresses a NEMO-dependent but NF-κB-independent pathway to liver cancer. **Cancer Cell** 17, 481–496 (2010).
19. Blais A, Dynlacht BD. E2F-associated chromatin modifiers and cell cycle control. **Curr Opin Cell Biol** 19, 658-662 (2007).
20. Bonizzi G, Karin M. The two NF-kappaB activation pathways and their role in innate and adaptive immunity. **Trends Immunol** 25, 280-288 (2004).
21. Bours V, Bonizzi G, Bentires-Alj M, et al. NF-kappaB activation in response to toxical and therapeutical agents: role in inflammation and cancer treatment. **Toxicology** 153, 27-38 (2000).
22. Boxer LM, Dang CV. Translocations involving c-myc and c-myc function. **Oncogene**. 20, 5595-5610 (2001).
23. Bracken AP, Ciro M, Cocito A, et al. E2F target genes: unraveling the biology. **Trends Biochem Sci** 29, 409-417 (2004).

24. Braig M, Lee S, Loddenkemper C, et al. Oncogene-induced senescence as an initial barrier in lymphoma development. **Nature** 436, 660-665 (2005).
25. Calado DP, Zhang B, Srinivasan L, et al. Constitutive canonical NF-κB activation cooperates with disruption of BLIMP1 in the pathogenesis of activated B cell-like diffuse large cell lymphoma. **Cancer Cell** 18, 580-589 (2010).
26. Campisi J. d'Adda di Fagagna F. Cellular senescence: when bad things happen to good cells. **Nat Rev Mol Cell Biol** 8, 729-740 (2007).
27. Catz SD, Johnson JL, Transcriptional regulation of bcl-2 by nuclear factor kappa B and its significance in prostate cancer. **Oncogene** 20, 7342–7351 (2001).
28. Chang BD, Broude EV, Dokmanovic M, et al. A senescence-like phenotype distinguishes tumor cells that undergo terminal proliferation arrest after exposure to anticancer agents. **Cancer Res.** 59, 3761-3767 (1999).
29. Chien Y, Scuoppo C, Wang X, et al. Control of the senescence-associated secretory phenotype by NF-κB promotes senescence and enhances chemosensitivity. **Genes Dev** 25, 2125-2136 (2011).
30. Ciccia A, Elledge SJ. The DNA damage response: making it safe to play with knives. **Mol Cell** 40, 179-204 (2010).
31. Classon M, Salama S, Gorka C, et al. Combinatorial roles for pRB, p107, and p130 in E2F-mediated cell cycle control. **Proc Natl Acad Sci USA** 97, 10820-10825 (2000).
32. Collado M, Gil J, Efeyan A, et al. Tumour biology: senescence in premalignant tumours. **Nature** 436, 642 (2005).
33. Collado M, Serrano M. Senescence in tumours: evidence from mice and humans. **Nat Rev Cancer** 10, 51–57 (2010).
34. Collado M, Serrano M. The power and the promise of oncogene-induced senescence markers. **Nat Rev Cancer** 6, 472-476 (2006).
35. Compagno M, Lim WK, Grunn A, et al. Mutations of multiple genes cause deregulation of NF-kappaB in diffuse large B-cell lymphoma. **Nature** 459, 717–721 (2009).
36. Coppé JP, Desprez PY, Krtolica A, et al. The senescence-associated secretory

phenotype: the dark side of tumor suppression. **Annu Rev Pathol** 5, 99-118 (2010).

37. Coppé JP, Kauser K, Campisi J, et al. Secretion of vascular endothelial growth factor by primary human fibroblasts at senescence. **J Biol Chem** 281, 29568-29574 (2006).
38. Coppé JP, Patil CK, Rodier F, et al. Senescence-associated secretory phenotypes reveal cell-nonautonomous functions of oncogenic RAS and the p53 tumor suppressor. **PLoS Biol** 6, 2853–2868 (2008).
39. Dajee M, Lazarov M, Zhang JY, et al. NF-κB blockade and oncogenic Ras trigger invasive human epidermal neoplasia. **Nature** 421, 639-643 (2003).
40. Dang CV. c-Myc target genes involved in cell growth, apoptosis, and metabolism. **Mol Cell Biol** 19, 1-11 (1999).
41. Davis RE, Brown KD, Siebenlist U, et al. Constitutive nuclear factor kappa B activity is required for survival of activated B cell-like diffuse large B cell lymphoma cells. **J Exp Med** 194, 1861-1874 (2001).
42. Derheimer FA, Kastan MB. Multiple roles of ATM in monitoring and maintaining DNA integrity. **FEBS Lett** 584, 3675-3681 (2010).
43. Di Micco R, Fumagalli M, Cicalese A, et al. Oncogene-induced senescence is a DNA damage response triggered by DNA hyper-replication. **Nature** 444, 638-642 (2006).
44. Dilley TK, Bowden GT, Chen QM. Novel mechanisms of sublethal oxidant toxicity: Induction of premature senescence in human fibroblasts confers tumor promoter activity. **Exp Cell Res** 290, 38-48 (2003).
45. Dimri GP, Itahana K, Acosta M, et al. Regulation of a senescence checkpoint response by the E2F1 transcription factor and p14 (ARF) tumor suppressor. **Mol Cell Biol** 20, 273-285 (2000).
46. Dimri GP, Lee X, Basile G, et al. A biomarker that identifies senescent human cells in culture and in aging skin in vivo. **Proc Natl Acad Sci USA** 92, 9363-9367 (1995).
47. Di X, Bright AT, Bellott R, et al. A chemotherapy-associated senescence bystander

effect in breast cancer cells. **Cancer Biol Ther** 7, 864-872 (2008).

48. Dunleavy K, Pittaluga S, Czuczman MS, et al. Differential efficacy of bortezomib plus chemotherapy within molecular subtypes of diffuse large B-cell lymphoma. **Blood** 113, 6069-6076 (2009).
49. Emmerich F, Meiser M, Hummel M, et al. Overexpression of I kappa B alpha without inhibition of NF-kappaB activity and mutations in the I kappa B alpha gene in Reed-Sternberg cells. **Blood** 94, 3129-3134 (1999).
50. Franzoso G, Bours V, Park S, et al. The candidate oncoprotein Bcl-3 is an antagonist of p50/NF-κB-mediated inhibition. **Nature** 359, 339-342 (1992).
51. Grivennikov S, Greten FR, Karin M. Immunity, inflammation, and cancer. **Cell** 140, 883-899 (2010).
52. Guttridge DC, Albanese C, Reuther JY, et al. NF-kappaB controls cell growth and differentiation through transcriptional regulation of cyclin D1. **Mol Cell Biol** 19, 5785–5799 (1999).
53. Harley CB, Futcher AB, Greider CW, et al. Telomeres shorten during ageing of human fibroblasts. **Nature** 345, 458-460 (1990).
54. Harvey M, Sands AT, Weiss RS, et al. In vitro growth characteristics of embryo fibroblasts isolated from p53-deficient mice. **Oncogene** 8, 2457-2467 (1993).
55. Haugstetter AM, Loddenkemper C, Lenze D, et al. Cellular senescence predicts treatment outcome in metastasised colorectal cancer. **Br J Cancer** 103, 505-509 (2010).
56. Hayflick L. The limited in vitro lifetime of human diploid cell strains. **Exp Cell Res** 37, 614-636 (1965).
57. Hayflick L, Moorhead PS. The serial cultivation of human diploid cell strains. **Exp Cell Res** 25, 585-621 (1961).
58. Helmrich A, Lee S, O'Brien P, et al. Recurrent chromosomal aberrations in INK4a/ARF defective primary lymphomas predict drug responses in vivo. **Oncogene** 24, 4174-4182 (2005).
59. Heyninck K, Beyaert R. A20 inhibits NF-κB activation by dual ubiquitin-editing functions. **Trends Biochem Sci** 30, 1-4 (2005).

60. Hinata K, Gervin AM, Jennifer Zhang Y, et al. Divergent gene regulation and growth effects by NF-kappa B in epithelial and mesenchymal cells of human skin. **Oncogene** 22, 1955-1964 (2003).
61. Hinz M, Stilmann M, Coel Arslan S, et al. A cytoplasmic ATM-TRAF6-cIAP1 module links nuclear DNA damage signaling to ubiquitin-mediated NF-kappaB activation. **Molecular Cell** 40, 63-74 (2010)
62. Hollstein M, Rice K, Greenblatt MS, et al. Database of p53 gene somatic mutations in human tumors and cell lines. **Nucleic Acids Res** 22, 3551-3555 (1994).
63. Honma K, Tsuzuki S, Nakagawa M, et al. TNFAIP3/A20 functions as a novel tumor suppressor gene in several subtypes of non-Hodgkin lymphomas. **Blood** 114, 2467-2475 (2009).
64. Huang JZ, Sanger WG, Greiner TC, et al. The t(14;18) defines a unique subset of diffuse large B-cell lymphoma with a germinal center B-cell gene expression profile. **Blood** 99, 2285-2290 (2002).
65. Inokuchi S, Aoyama T, Miura K, et al. Disruption of TAK1 in hepatocytes causes hepatic injury, inflammation, fibrosis, and carcinogenesis. **Proc Natl Acad Sci USA** 107, 844-849 (2010).
66. Iqbal J, Neppalli VT, Wright G, et al. BCL2 expression is a prognostic marker for the activated B-cell-like type of diffuse large B-cell lymphoma. **J Clin Oncol** 24, 961-968 (2006).
67. Iyer VR, Eisen MB, Ross DT, et al. The transcriptional program in the response of human fibroblasts to serum. **Science** 283, 83-87 (1999).
68. Jackson SP, Bartek J. The DNA-damage response in human biology and disease. **Nature** 461, 1071-1078 (2009).
69. Jones CJ, Kipling D, Morris M, et al. Evidence for a telomere-independent “clock” limiting RAS oncogene-driven proliferation of human thyroid epithelial cells. **Mol Cell Biol** 20, 5690-5699 (2000).
70. Jung M, Dritschilo A. NF-κB signaling pathway as a target for human tumor radiosensitization. **Semin Radiat Oncol** 11, 346-351 (2001).

71. Kaltschmidt B, Kaltschmidt C, Hofmann TG et al. The pro- or anti-apoptotic function of NF-kappaB is determined by the nature of the apoptotic stimulus. **Eur J Biochem** 267, 3828-3835 (2000).
72. Kamijo T, Zindy F, Roussel MF, et al. Tumor suppression at the mouse INK4a locus mediated by the alternative reading frame product p19ARF. **Cell** 91, 649-659 (1997).
73. Karin M, Cao Y, Greten FR, et al. NF-kappaB in cancer: from innocent bystander to major culprit. **Nat Rev Cancer** 2, 301-310 (2002)
74. Karin M, Greten FR. NF-kappaB: linking inflammation and immunity to cancer development and progression. **Nat Rev Immunol** 5, 749-759 (2005).
75. Kasibhatla S, Genestier L, Green DR. Regulation of fas-ligand expression during activation-induced cell death in T lymphocytes via nuclear factor kappaB. **J Biol Chem** 274, 987-992 (1999).
76. Keats JJ, Fonseca R, Chesi M, et al. Promiscuous mutations activate the noncanonical NF-κB pathway in multiple myeloma. **Cancer Cell** 12, 131-144 (2007).
77. Keller U, Huber J, Nilsson JA, et al. Myc suppression of Nfkb2 accelerates lymphomagenesis. **BMC Cancer** 10, 348 (2010).
78. Kortlever RM, Higgins PJ, Bernards R. Plasminogen activator inhibitor-1 is a critical downstream target of p53 in the induction of replicative senescence. **Nat Cell Biol** 8, 877-884 (2006).
79. Krappmann D, Emmerich F, Kordes U, et al. Molecular mechanisms of constitutive NF-kappaB/Rel activation in Hodgkin/Reed-Sternberg cells. **Oncogene** 18, 943-953 (1999).
80. Krappmann D, Wegener E, Sunami Y et al. The IkappaB kinase complex and NF-kappaB act as master regulators of lipopolysaccharide-induced gene expression and control subordinate activation of AP-1. **Molecular and Cellular Biology** 24, 6488-6500 (2004).
81. Krappmann D, Wulczyn FG, Scheidereit C. Different mechanisms control signal-induced degradation and basal turnover of the NF-kappaB inhibitor

IkappaB alpha in vivo. **EMBO J** 15, 6716-6726 (1996).

82. Krtolica A, Parrinello S, Lockett S, et al. Senescent fibroblasts promote epithelial cell growth and tumorigenesis: a link between cancer and aging. **Proc Natl Acad Sci USA** 98, 12072-12077 (2001).
83. Kuilman T, Michaloglou C, Mooi WJ, et al. The essence of senescence. **Genes Dev** 24, 2463-2479 (2010).
84. Kuilman T, Michaloglou C, Vredeveld LC, et al. Oncogene-induced senescence relayed by an interleukin-dependent inflammatory network. **Cell** 133, 1019-1031 (2008).
85. Kuilman T, Peeper DS. Senescence-messaging secretome: SMS-ing cellular stress. **Nat Rev Cancer** 9, 81-94 (2009).
86. Lam LT, Davis RE, Pierce J, et al. Small molecule inhibitors of IkappaB kinase are selectively toxic for subgroups of diffuse large B-cell lymphoma defined by gene expression profiling. **Clin Cancer Res** 11, 28-40 (2005).
87. Lee S, Schmitt CA. Chemotherapy response and resistance. **Curr Opin Genet Dev** 13, 90-96 (2003)
88. Lenz G, Davis RE, Ngo VN, et al. Oncogenic CARD11 mutations in human diffuse large B cell lymphoma. **Science** 319, 1676–1679 (2008) (a).
89. Lenz G, Wright G, Dave SS, et al. Stromal gene signatures in large-B-cell lymphomas. **N Engl J Med** 359, 2313-2323 (2008) (b).
90. Lenz G, Wright G, Emre NCT, et al. Molecular subtypes of diffuse large B-cell lymphoma arise by distinct genetic pathways. **Proc Natl Acad Sci USA** 105, 13520-13525 (2008) (c).
91. Levine AJ. p53, the cellular gatekeeper for growth and division. **Cell** 88, 323-331 (1997).
92. Lin WW, Karin M. A cytokine-mediated link between innate immunity, inflammation, and cancer. **J Clin Invest** 117, 1175-1183 (2007).
93. Li N, Banin S, Ouyang H, et al. TM is required for IkappaB kinase (IKKk) activation in response to DNA double strand breaks. **J Biol Chem** 276, 8898-8903 (2001).
94. Lowe SW, Sherr CJ. Tumor suppression by Ink4a-Arf: progress and puzzles. **Curr**

Opin Genet Dev 13, 77-83 (2003).

95. Luedde T, Beraza N, Kotsikoris V, et al. Deletion of NEMO/IKKgamma in liver parenchymal cells causes steatohepatitis and hepatocellular carcinoma. **Cancer Cell** 11, 119-132 (2007).
96. Maeda S, Kamata H, Luo JL, et al. IKKβ couples hepatocyte death to cytokine-driven compensatory proliferation that promotes chemical hepatocarcinogenesis. **Cell** 121, 977-990 (2005).
97. Mallette FA, Gaumont-Leclerc MF, Ferbeyre G. The DNA damage signaling pathway is a critical mediator of oncogene-induced senescence. **Genes Dev** 21, 43-48 (2007).
98. Martin AG, Trama J, Crighton D, et al. Activation of p73 and induction of Noxa by DNA damage requires NF-kappa B. **Aging** 1, 335-349 (2009).
99. Michaloglou C, Vredeveld LC, Soengas MS, et al. BRAFE600-associated senescence-like cell cycle arrest of human naevi. **Nature** 436, 720-724 (2005).
100. Mori S, Rempel RE, Chang JT, et al. Utilization of pathway signatures to reveal distinct types of B lymphoma in the Eμ-myc model and human diffuse large B-cell lymphoma. **Cancer Res** 68, 8525-8534 (2008).
101. Narita M, Nunez S, Heard E, et al. Rb-mediated heterochromatin formation and silencing of E2F target genes during cellular senescence. **Cell** 113, 703-716 (2003).
102. Neri A, Chang CC, Lombardi L, et al. B cell lymphoma-associated chromosomal translocation involves candidate oncogene lyt-10, homologous to NF-κB p50. **Cell** 67, 1075-1087 (1991).
103. Nesbit CE, Tersak JM, Prochownik EV. MYC oncogenes and human neoplastic disease. **Oncogene** 18, 3004-3016 (1999).
104. Ngo VN, Davis RE, Lamy L, et al. A loss-of-function RNA interference screen for molecular targets in cancer. **Nature** 441, 106-110 (2006).
105. Ngo VN, Young RM, Schmitz R, et al. Oncogenically active MYD88 mutations in human lymphoma. **Nature** 470, 115-119 (2011).
106. Nogai H, Dorken B, Lenz G. Pathogenesis of non-Hodgkin' s lymphoma. **J**

Clin Oncol 29, 1803-1811 (2011).

107. Nyman H, Adde M, Karjalainen-Lindsberg ML, et al. Prognostic impact of immunohistochemically defined germinal center phenotype in diffuse large B-cell lymphoma patients treated with immunochemotherapy. **Blood** 109, 4930-4935 (2007).

108. Parrinello S, Samper E, Krtolica A, et al. Oxygen sensitivity severely limits the replicative lifespan of murine fibroblasts. **Nat Cell Biol** 5, 741-747 (2003).

109. Popivanova BK, Kitamura K, Wu Y, et al. Blocking TNF-alpha in mice reduces colorectal carcinogenesis associated with chronic colitis. **J Clin Invest** 118, 560-570 (2008).

110. Prasad S, Ravindran J, Aggarwal BB. NF-kappaB and cancer: how intimate is this relationship. **Mol Cell Biochem** 336, 25-37 (2010).

111. Rebbaa A, Zheng X, Chou PM, et al. Caspase inhibition switches doxorubicin-induced apoptosis to senescence. **Oncogene** 22, 2805-2811 (2003).

112. Reimann M, Lee S, Loddenkemper C, et al. Tumor stroma-derived TGF-beta limits myc-driven lymphomagenesis via Suv39h1-dependent senescence. **Cancer Cell** 17, 262-272 (2010).

113. Reinhardt HC, Yaffe MB. Kinases that control the cell cycle in response to DNA damage: Chk1, Chk2, and MK2. **Curr Opin Cell Biol** 21, 245-255 (2009).

114. Riley T, Sontag E, Chen P, et al. Transcriptional control of human p53-regulated genes. **Nat Rev Mol Cell Biol** 9, 402-412 (2008).

115. Rodier F, Coppé JP, Patil CK, et al. Persistent DNA damage signalling triggers senescence-associated inflammatory cytokine secretion. **Nat Cell Biol** 11, 973-979 (2009).

116. Rosenwald A, Wright G, Chan WC, et al. The use of molecular profiling to predict survival after chemotherapy for diffuse large-B-cell lymphoma. **N Engl J Med** 346, 1937-1947 (2002).

117. Rosenwald A, Wright G, Leroy K, et al. Molecular diagnosis of primary mediastinal B cell lymphoma identifies a clinically favorable subgroup of diffuse large B cell lymphoma related to Hodgkin lymphoma. **J Exp Med** 198, 851-862

(2003).

118. Rovillain E, Mansfield L, Caetano C, et al. Activation of nuclear factor-kappa B signalling promotes cellular senescence. **Oncogene** 30, 2356-2366 (2011).

119. Ruan J, Martin P, Furman RR, et al. Bortezomib plus CHOP-rituximab for previously untreated diffuse large B-cell lymphoma and mantle cell lymphoma. **J Clin Oncol** 29, 690-697 (2011).

120. Ruland J, Mak TW. From antigen to activation: specific signal transduction pathways linking antigen receptors to NF-kappaB. **Semin Immunol** 15, 177-183 (2003).

121. Ryan KM, Ernst MK, Rice NR, et al. Role of NF-kappaB in p53-mediated programmed cell death. **Nature** 404, 892-897 (2000).

122. Schmitt CA. Cellular senescence and cancer treatment. **Biochim Biophys Acta** 1775, 5-20 (2007).

123. Schmitt CA, Fridman JS, Yang M, et al. A senescence program controlled by p53 and p16INK4a contributes to the outcome of cancer therapy. Cell 109, 335-346 (2002) (a).

124. Schmitt CA, McCurrach ME, de Stanchina E, et al. INK4a/ARF mutations accelerate lymphomagenesis and promote chemoresistance by disabling p53. **Genes Dev** 13, 2670-2677 (1999).

125. Schmitt CA, Rosenthal CT, Lowe SW. Genetic analysis of chemoresistance in primary murine lymphomas. **Nat Med** 6, 1029-1035 (2000).

126. Schmitt CA, Lowe SW. Apoptosis and chemoresistance in transgenic cancer models. **J Mol Med** 80,137-46 (2002) (b).

127. Schneider A, Martin-Villalba A, Weih F et al. NF-kappaB is activated and promotes cell death in focal cerebral ischemia. **Nat Med** 5, 554-559 (1999).

128. Schon M, Wienrich BG, Kneitz S, et al. KINK-1, a novel small-molecule inhibitor of IKKbeta, and the susceptibility of melanoma cells to antitumoral treatment. **J Natl Cancer Inst** 100, 862-875 (2008).

129. Sears R, Leone G, DeGregori J, et al. Ras enhances Myc protein stability. **Mol Cell** 3, 169-179 (1999).

130. Seitz CS, Lin Q, Deng H, et al. Alterations in NF-κB function in transgenic epithelial tissue demonstrate a growth inhibitory role for NF-κB. **Proc Natl Acad Sci USA** 95, 2307-2312 (1998).

131. Sen R, Baltimore D. Multiple nuclear factors interact with the immunoglobulin enhancer sequences. **Cell** 46, 705-716 (1986).

132. Serrano M, Lin AW, McCurrach ME, et al. Oncogenic ras provokes premature cell senescence associated with accumulation of p53 and p16INK4a. **Cell** 88, 593-602 (1997).

133. Shaffer AL, Rosenwald A, Staudt LM. Lymphoid malignancies: the dark side of B-cell differentiation. **Nat Rev Immunol** 2, 920-932 (2002).

134. Shaffer AL, Wright G, Yang L, et al. A library of gene expression signatures to illuminate normal and pathological lymphoid biology. **Immunol Rev** 210, 67-85 (2006).

135. Shaffer AL, Young RM, Staudt LM. Pathogenesis of human B cell lymphomas. **Annu Rev Immunol** 30, 565-610 (2012)

136. Sheehy AM and Schlissel MS. Overexpression of RelA Causes G1 Arrest and Apoptosis in a Pro-B Cell Line. **J Biol Chem** 274, 8708-8716 (1999).

137. Sherr CJ. Divorcing ARF and p53: an unsettled case. **Nat Rev Cancer** 6, 663-673 (2006).

138. Shelton DN, Chang E, Whittier PS, et al. Microarray analysis of replicative senescence. **Curr Biol** 9, 939-945 (1999).

139. Smirnov AS, Ruzov AS, Budanov AV. High constitutive level of NF-kappaB is crucial for viability of adenocarcinoma cells. **Cell Death Differ** 8, 621-630 (2001).

140. Staudt, LM. Oncogenic activation of NF-κB. **Cold Spring Harb Perspect Biol** 2, a000109 (2010)

141. Staudt LM, Dave S. The biology of human lymphoidmalignancies revealed by gene expression profiling. **Adv Immunol** 87, 163-208 (2005).

142. Stehlik C, de Martin R, Kumabashiri I, et al. Nuclear factor (NF)-kappaB-regulated X-chromosome-linked iap gene expression protects endothelial cells from tumor necrosis factor alpha-induced apoptosis. **J Exp Med**

188, 211-216 (1998).

143. Stilmann M, Hinz M, Arslan SC, et al. A nuclear Poly (ADP-ribose)-dependent signalosome confers DNA damage induced IκB kinase activation. **Mol Cell** 36, 365-378 (2009).

144. Subramanian A, Tamayo P, Mootha VK, et al. Gene set enrichment analysis: a knowledgebased approach for interpreting genome-wide expression profiles. **Proc Natl Acad Sci** 102, 15545-15550 (2005).

145. Sun L, Deng L, Ea CK, et al. The TRAF6 ubiquitin ligase and TAK1 kinase mediate IKK activation by BCL10 and MALT1 in T lymphocytes. **Mol Cell** 14, 289-301 (2004)

146. Tamatani M, Che YH, Matsuzaki H, et al. Tumor necrosis factor induces Bcl-2 and Bcl-x expression through NFkappaB activation in primary hippocampal neurons. **J Biol Chem** 274, 8531-8538 (1999).

147. te Poele RH, Okorokov AL, Jardine L, et al. DNA damage is able to induce senescence in tumor cells in vitro and in vivo. **Cancer Res** 62, 1876-1883 (2002).

148. Tu S, Bhagat G, Cui G, et al. Overexpression of interleukin-1beta induces gastric inflammation and cancer and mobilizes myeloid-derived suppressor cells in mice. **Cancer Cell** 14, 408-419 (2008).

149. Uetsuka H, Haisa M, Kimura M, et al. Inhibition of inducible NF-kappaB activity reduces chemoresistance to 5-fluorouracil in human stomach cancer cell line. **Exp Cell Res** 289, 27-35 (2003).

150. Viatour P, Merville MP, Bours V, et al. Phosphorylation of NF-kappaB and IkappaB proteins: implications in cancer and inflammation. **Trends Biochem Sci** 30, 43-52 (2005).

151. Vousden KH, Lu X. Live or let die: the cell's response to p53. **Nat Rev Cancer** 2, 594-604 (2002).

152. Vousden KH, Prives C. Blinded by the light: the growing complexity of p53. **Cell** 137, 413-431 (2009).

153. Wajapeyee N, Serra RW, Zhu X, et al. Oncogenic BRAF induces senescence and apoptosis through pathways mediated by the secreted protein IGFBP7. **Cell**

132, 363-374 (2008).

154. Wang CY, Mayo MW, Korneluk RG, et al. NF-κB antiapoptosis: induction of TRAF1 and TRAF2 and c-IAP1 and c-IAP2 to suppress caspase-8 activation. **Science** 281, 1680-1683 (1998).

155. Wang CY, Cusack JC Jr, Liu R, et al. Control of inducible chemoresistance: enhanced anti-tumor therapy through increased apoptosis by inhibition of NF-κB. **Nat Med** 5, 412-417 (1999).

156. Wang CY, Mayo MW, Baldwin AS Jr. TNF-α and cancer therapy-induced apoptosis: potentiation by inhibition of NF-kappaB. Science 274, 784-787 (1996).

157. Weiss LM, Warnke RA, Sklar J, et al. Molecular analysis of the t(14;18) chromosomal translocation in malignant lymphomas. **N Engl J Med** 317, 1185-1189 (1987)

158. Wertz IE, O'Rourke KM, Zhou H, et al. De-ubiquitination and ubiquitin ligase domains of A20 downregulate NF-κB signalling. **Nature** 430, 694-699 (2004).

159. Wilson WH, Dunleavy K, Pittaluga S, et al. Phase II study of dose-adjusted EPOCH and rituximab in untreated diffuse large B-cell lymphoma with analysis of germinal center and post-germinal center biomarkers. **J Clin Oncol** 26, 2717-2724 (2008).

160. Wright G, Tan B, Rosenwald A, et al. A gene expression-based method to diagnose clinically distinct subgroups of diffuse large B cell lymphoma. **Proc Natl Acad Sci USA** 100, 9991-9996 (2003).

161. Wu ZH, Shi Y, Tibbetts RS, et al. Molecular linkage between the kinase ATM and NF-kappaB signaling in response to genotoxic stimuli. **Science** 311, 1141-1146 (2006).

162. Xue W, Zender L, Miething C, et al. Senescence and tumour clearance is triggered by p53 restoration in murine liver carcinomas. **Nature** 445, 656-660 (2007).

163. Yamamoto K, Arakawa T, Ueda N, et al. Transcriptional roles of nuclear factor kappa B and nuclear factor-interleukin-6 in the tumor necrosis factor alpha-dependent induction of cyclooxygenase-2 in MC3T3-E1 cells. **J Biol Chem**

270, 31315-31320 (1995).

164. Yang J, Splittgerber R, Yull FE, et al. Conditional ablation of Ikkβ inhibits melanoma tumor development in mice. **J Clin Invest** 120, 2563-2574 (2010).

165. Zhou H, Wertz I, O'Rourke K, et al. Bcl10 activates the NF-kappaB pathway through ubiquitination of NEMO. **Nature** 427, 167-171 (2004).

166. Zhu L, Fukuda S, Cordis G, et al. Anti-apoptotic protein surviving plays a significant role in tubular morphogenesis of human coronary arteriolar endothelial cells by hypoxic preconditioning. **FEBS Lett** 508, 369-374 (2001).

6.2 Abbrevations

ABC	Activated B-cell–like
ADR	Adriamycin
ATM	Ataxia telangiectasia mutated
bp	Base pair
Bcl2	B cell lymphoma 2
BSA	Bovine serum albumin
cDNA	Complementary DNA
CTX	Cyclophosphamide
dH_2O	Deionized water
DAPI	4', 6-diamidino-2-phenylindole
DDR	DNA damage response
DEPC	Diethylpyrocarbonate
DMEM	Dulbecco´s modified Eagle medium
dNTP	2'-deoxy nucleoside-5'-triphosphate
DLBCL	Diffuse large B-cell lymphoma
DMSO	Dimethylsulfoxid
DNA	Desoxyribonucleic acid
DNase	Deoxyribonuclease
DTT	Dithiothreitol
E. coli	*Escherichia coli*
EDTA	Ethylendiamintetraacetat = Titriplex III
FCS	Fetal calf serum
GCB	Germinal-center B-cell-like
GFP	Green-fluorescent protein
H3K9	Lysin 9 of Histone H3
H3K9met3	Tri-methylated Lysine 9 of Histone H3
HEPES	N-2-hydroxyethylpiperazin-N'-2-ethanesulfonic acid
IF	Immunofluorescence
IκB	Inhibitor of NF-κB
IKK	IκB Kinase
IL-1 α	Interleukin-1 alpha

IL6	Interleukin 6
IMDM	Iscove's modified Dulbecco's medium
IRES	Internal ribosomal entry site
kb	Kilobase
MEF	Mouse embryonic fibroblasts
mRNA	Messenger ribonucleicacid
MSCV	Murine stem cell virus
NF-κB	Nuclear Factor κB
NP-40	Nonidet P-40
PAGE	Polyacrylamid-gel electrophoresis
PBS	Phosphate buffered saline
PCR	Polymerase chain reaction
PFA	Paraformaldehyde
pfu	Plaque-forming unit
PVDF	Poly vinylidene difluoride
Rb	Retinoblastoma protein
RNA	Ribonucleic acid
RNase	Ribonuclease
rpm	Rotations per minute
RT	Room temperature
SASP	Senescence-associated secretory phenotype
SA-β-Gal	Senescence-associated β-galactosidase
SDS	Natriumdodecylsulfat
SR	NF-κB super repressor
TAE	Tris-acetate-EDTA
TEMED	N,N,N´,N´-Tetramethylethylendiamin
TIS	Therapy-induced senescence
TNFα	Tumor necrosis factor-alpha
Tris	Tris (hydroxymethyl) aminomethane
Triton X-100	Octylphenoldecaethylenglycolether
Tween 20	Polyoxyethylensorbitanmonolaurat
X-Gal	5-bromo-4-chloro-3-indolyl β-D-galactoside

7 Acknowledgements

I would like to express my sincere gratitude to Prof. Clemens Schimtt for providing me the opportunity to work on this PhD project, offering a good working condition and supervising my PhD project constantly. I am grateful to the whole Schmitt group for their kindness and help. I want to say thank you to Dr. Soyoung Lee and Dr. Sujuan Ji, who helped me to finish this project in such a short time. I want to thank Anna Meis for the German translations. I want to say thank you to Jing Du and Yong Yu for their kindness help all the time.

My PhD project is a well-cooperated project. I am grateful to Prof. Claus Scheidereit and Dr. Michael Hinz for their help and advice from the perspective of NF-κB experts. I would like to thank the group of Prof. Georg Lenz for the cooperation in analyzing the clinical data. I want to express my gratitude to my doctor father Prof. Dr. Achim Leutz, my PhD committee members Prof. Thomas Sommer and Dr. Michal Or-Guil for their most valuable suggestions.

I also want to say thank you to Ms. Pamela Glowacki and the Charité International Cooperation (ChIC), Ms. Sylvia Sibilak, Ms. Annet Schledz and the Graduate Office at MDC, and Embassy of the People's Republic of China in Germany. Their help made my life abroad much easier.

Last, I want to express my deeply gratitude to my family. For so many years they loved me, helped me and supported me but ask for nothing. I want to say thank you to my mother, an ordinary person but a great mother. For months, I cannot but be grieved whenever I realized that you have left me forever. I was so lucky to have you with me in the last 27 years. I will cherish your love, your instructions and the memory deeply in my heart. I hope that one day when you look back to this world, you can be proud of me.

8 Publications

Jing H*, Kase J*, Dörr JR, Milanovic M, Lenze D, Grau M, Beuster G, Ji S, Reimann M, Lenz P, Hummel M, Dörken B, Lenz G, Scheidereit C, Schmitt CA and Lee S.
(*Equal contribution)
Opposing roles of NF-kappa B in anti-cancer treatment outcome unveiled by cross-species investigations.
Genes Dev 25, 2137-2146 (2011).

Yang X, **Jing H**, Zhao K, Sun R, Liu Z, Ying Y, Ci L, Kuang Y, Huang F, Wang Z, Fei J. Functional imaging of Rel expression in inflammatory processes using bioluminescence imaging system in transgenic mice.
PLoS One 8, e57632. doi: 10.1371/journal.pone.0057632 (2013)

Jing H, Kuang Y, Wang L, Mao J, and Fei J.
Generation of conditional simian virus 40 large T antigen gene transgenic mouse model.
Journal of Tongji University 33, 29-33 (2009).

9 Selbständigkeitserklärung

Hiermit erkläre ich, die vorliegende Arbeit selbständig ohne fremde Hilfe verfasst und nur die angegebene Literatur verwendet zu haben. Alle aus anderen Quellen oder indirekt übernommenen Daten und Konzepte sowie Ergebnisse aus Kooperationsprojekten sind unter Angabe der Referenz gekennzeichnet.

Außerdem erkläre ich hiermit, dass ich mich nicht anderweitig um einen entsprechenden Doktorgrad beworben habe.

Die dem Promotionsverfahren zugrunde liegende Promotionsordnung vom 09.06.2011 ist mir bekannt.

Berlin, 10.09.2012 Hua Jing

10 Summary

Utilizing the Eμ-*myc* transgenic mouse lymphoma model, I showed in this thesis that therapy-induced senescence presents with and depends on active NF-κB signaling, whereas NF-κB simultaneously promotes resistance to apoptosis. By cross-species comparison of transcriptome data and clinical data from lymphoma patients, Bcl2-overexpressing germinal center B-cell-like DLBCL was identified as a clinically relevant subgroup with significantly superior outcome when NF-κB is hyperactive. These results demonstrate the context-dependent role of NF-κB signaling in cancer therapy. These findings suggest that we should carefully select, or at least monitor, genetically defined patient subcohorts in which therapeutic interference with the NF-κB pathway may or may not be of clinical benefit.

Resümee

In der vorliegenden Arbeit konnte ich unter Verwendung des Eμ-myc transgenen Mauslymphommodells zeigen, dass therapie-induzierte Seneszenz mit aktiviertem NF-κB Signalweg verbunden ist und davon abhängt, während NF-κB gleichzeitig Resistenz gegenüber Apoptose vermittelt. Durch einen „Cross-species”-Vergleich von Transkriptom- und Patientendaten wurden Bcl2-überexprimierende Keimzentrums-B-Zell-DLBCL als klinisch relevante Gruppe identifiziert, welche nach NF-κB-Hyperaktivierung signifikant besser auf Therapie ansprach. Diese Ergebnisse zeigen eine kontext-spezifische Rolle des NF-κB Signalwegs unter Chemotherapie. Die Daten suggerieren, dass wir genetisch definierte Patientengruppen, in denen therapeutische Interventionen im NF-κB Signalweg einen klinischen Vor- beziehungsweise Nachteil darstellen könnten, genau beobachten und gegebenenfalls selektieren sollten.